# MAGNETIC MANIPULATION OF CELLS FOR TISSUE ENGINEERING AND DIAGNOSTIC APPLICATIONS

**A Thesis Submitted to**
**the Graduate School**
**İzmir Institute of Technology**
**in Partial Fulfillment of the Requirements for the Degree of**

**DOCTOR OF PHILOSOPHY**

**in Bioengineering**

**by**
**İlayda ÖZKAN**

**January 2025**
**İZMİR**

We approve the thesis of **İlayda ÖZKAN**

**Examining Committee Members:**

**Assoc. Prof. Hüseyin Cumhur TEKİN**
Department of Bioengineering
Izmir Institute of Technology

**Asst. Prof. Dr. Yavuz OKTAY**
Department of Medical Biology
Dokuz Eylul University

**Assoc. Prof. Sinan GÜVEN**
Department of Medical Biology
Dokuz Eylul University

**Asst. Prof. Dr. Deniz Tanıl YÜCESOY**
Department of Bioengineering
Izmir Institute of Technology

**7/2/2025**

**Prof. Dr. Engin ÖZÇİVİCİ**
Supervisor, Department of Bioengineering
Izmir Institute of Technology

**Asst. Prof. Dr. Ceyda ÖKSEL KARAKUŞ**
Head of the Department of Bioengineering

**Prof. Dr. Mehtap EANES**
Dean of the Graduate School of
Engineering and Sciences

# ACKNOWLEDGEMENTS

I would like to express my deep and sincere gratitude to my supervisor Prof. Dr. Engin ÖZÇİVİCİ, for his guidance, academic and mental support, encouragement, patience, and understanding throughout my doctoral education.

I am grateful to my esteemed committee members Assoc. Prof. Dr. Hüseyin Cumhur TEKİN, Dr. Yavuz OKTAY, Assoc. Prof. Dr. Sinan GÜVEN and Dr. Deniz Tanıl YÜCESOY for their mentorship throughout my research. I also thank Assoc. Prof. Dr. Gülistan MEŞE ÖZÇİVİCİ and Assoc. Prof. Dr. Özden YALÇIN ÖZUYSAL for their helpful guidance. I am also grateful to Dr. Betül ALDEMİR DİKİCİ for her valuable support and contribution.

I would like to thank my teammates and dear friends Müge ANIL İNEVİ, Öykü SARIGİL, Meryem Azra YILDIRIM, Ece İNAL, and Zehra Elif GÜNYÜZ, for their continuous support and kind help. I am also thankful to my labmates, Meltem GÜZELGÜLGEN, Hüsniye BÜYÜKÇAKIR, and Eda EFE for their kind help and contributions. I would also like to thank Ece SÖNMEZLER from Izmir Biomedicine and Genome Center, and Prof. Dr. Volkan SEYRANTEPE and Dr. Seçil AKYILDIZ DEMİR with whom we worked collaboratively, for their help and contributions.

I would like to specially thank The Scientific and Technological Research Council of Turkey (TUBITAK) for providing me the opportunity to conduct a part of my thesis in University College Dublin (Ireland) with a scholarship under "2214/A International Research Fellowship Programme for PhD Students" in the Tissue Engineering Field (Application No: 1059B142300595). I am also very grateful to Prof. Dr. Dimitrios Zeugolis for giving me the opportunity to collaborate and for his mentorship. I also thank Andrea ROSSONI and Lefki CHANIOTAKI for their valuable help.

I would like to express my deepest gratitude and love to my beloved family members, Seray ÖZKAN, Funda ÖZKAN, and Oktay ÖZKAN, for their unconditional love and support for my whole life and throughout this journey. Last but not least, words are not enough to express my gratefulness to my dearest Efe KIZILKAYA for his enormous support and love.

# ABSTRACT

## MAGNETIC MANIPULATION OF CELLS FOR TISSUE ENGINEERING AND DIAGNOSTIC APPLICATIONS

In the context of this thesis, the magnetic levitation technique based on the negative magnetophoresis principle was used for two different approaches. Firstly, the magnetic levitation system was employed as bioprinting method to create scaffold-free three-dimensional tissue models. The first approach focused on developing and improving scaffold-free heterogeneous three-dimensional spheroid models that can better resemble the *in vivo* tissue. Heterogenous breast cancer spheroids were obtained in the single-ring magnet-based levitation system with various conformations. The effect of different cell loading parameters in the localization of two cell types in the spheroid structure was examined. Additionally, the macromolecular crowding method was integrated to enhance the accumulation of extracellular matrix, improving the *in vivo*-like nature of the scaffold-free spheroid models created by magnetic levitation. Secondly, the thesis explored the use of magnetic levitation for diagnostic purposes in neurodevelopmental disorders. Investigation of the relationship between the volumetric mass density and neural pathological conditions was carried out using the fibroblasts, and the neural progenitor cells and induced pluripotent stem cells acquired from fibroblasts isolated from patients with rare neurodevelopmental disorders and healthy subjects. Furthermore, the study investigated how the single cell density is affected in lysosomal storage diseases using primary neuroglial cells isolated from mouse models with different types of lysosomal storage disorders. In this thesis, potential of magnetic levitation as a rapid, cost-effective, and safe technique for both tissue engineering applications and cell-based diagnostic studies was demonstrated.

# ÖZET

## DOKU MÜHENDİSLİĞİ VE TANI UYGULAMALARINDA HÜCRELERİN MANYETİK MANİPÜLASYONU

Bu tez kapsamında, negatif magnetoferez prensibine dayalı manyetik levitasyon tekniği, iki farklı yaklaşım için kullanılmıştır. İlk olarak, manyetik levitasyon sistemi, doku iskelesiz üç boyutlu doku modelleri oluşturmak için bir biyofabrikasyon yöntemi olarak kullanılmıştır. İlk yaklaşımda, *in vivo* dokuyu daha iyi taklit edebilen, üç boyutlu heterojen küresel modeller geliştirmek ve iyileştirmek amaçlanmıştır. Tek halka mıknatıs tabanlı levitasyon sisteminde çeşitli konfigürasyonlarda heterojen meme kanseri küreleri elde edilmiştir. İki farklı hücre tipinin lokalizasyonunda sferoid yapı içerisindeki farklı hücre yükleme parametrelerinin etkisi incelenmiştir. Ek olarak, hücre dışı matriks birikimini artırarak, manyetik levitasyon ile oluşturulan doku iskelesiz sferoid modellerin *in vivo* yapıyı taklit edebilme kapasitesini artırmak için makromoleküler kalabalıklaştırma yöntemi entegre edilmiştir. İkinci olarak, nörogelişimsel bozukluklarda teşhis amaçlı olarak manyetik levitasyonun kullanımı araştırılmıştır. Araştırmada, sağlıklı bireylerden ve nörogelişimsel bozukluğu olan bireylerden elde edilen fibroblastlar, sinir progenitör hücreleri ve indüklenmiş pluripotent kök hücreler arasındaki farkı belirlemek amacıyla hücrelerin özkütle profilleri analiz edilmiştir. Ayrıca, farklı tipte lizozomal depo hastalıklarının hücre özkütlesi üzerindeki etkisi fare modellerinden izole edilen primer nöroglial hücreler kullanılarak incelenmiştir. Bu tezde, hem doku mühendisliği uygulamaları hem de hücre bazlı tanı çalışmalarında hızlı, maliyet etkin ve güvenli bir yöntem olarak manyetik levitasyon tekniğinin potansiyeli gösterilmiştir.

# TABLE OF CONTENTS

APPENDICES

# LIST OF FIGURES

**Figure** **Page**

**Figure** **Page**

**Figure** **Page**

**Figure** **Page**

# LIST OF TABLES

# CHAPTER 1

# INTRODUCTION TO MAGNETIC LEVITATION

Biochemical reactions and cellular events, such as differentiation (Maric, Maric, and Barker 1998), apoptosis (Wyllie and Morris 1982), alterations in the amount of specific intracellular products or organelles (Gowrishankar et al. 2015; Braak et al. 1989), changes in cellular ultrastructural elements (Compagnucci et al. 2016) can cause persistent or temporary changes in the inherent properties of cells. The detection of these changes and investigation of the relationship between the cellular events they originate from, have a considerable implication for understanding disease models and mechanisms, stem cells commitment and differentiation processes, cell heterogenicity studies, and drug testing and dose-response relationships.

Cell manipulation plays a significant role in diagnostics, cell biology studies and tissue engineering applications. There are various methodologies for single cell detection and sorting and isolation, guiding and spatial positioning in 2D and 3D culture of different types of cells, or cells with different biological or morphological properties in the same population. In these studies, manipulation on cells are achieved using five distinct types of external forces which are either mechanical (Davis et al. 2006), electrical (Graham, Messerli, and Pethig 2012; Hondroulis et al. 2013), acoustic (Petersson et al. 2007), optical (M. M. Wang et al. 2005; Wojdyla, Raj, and Petrov 2012; Chiou, Ohta, and Wu 2005; X. Wang et al. 2011) or magnetic forces (Lehmann et al. 2006; Okochi et al. 2009; Bratt-Leal et al. 2011; Ino, Okochi, and Honda 2009).

Magnetic levitation is one of the magnetic force-based cell manipulation techniques (Qian et al. 2013). Magnetic force-based manipulation of cells can be applied by means of the magnetophoresis principle. Magnetophoresis is the process of movement of particles in a viscous medium under applied magnetic field and occurs in the existence of magnetic gradient (Irimia 2015). Magnetic levitation protocols are categorized as positive and negative magnetophoresis based on the magnetic nature of the application (Figure 1). While magnetic particles move through the diamagnetic medium in positive

magnetophoresis methods, in contrast diamagnetic particles move through the magnetized medium in studies that use negative magnetophoresis (Munaz, Shiddiky, and Nguyen 2018). Most of the cells are intrinsically diamagnetic particles, which means they are not attracted to magnetic forces in nature. Diamagnetic materials are magnetized in the opposite direction of applied magnetic fields, and for most cells this constitutes a very weak repulsive force from the magnetic gradient. In order to manipulate these diamagnetic particles through magnetization, a system must possess either a high magnetic field or significant magnetic gradients (Wonhee Lee, Tseng, and Carlo 2017; Hirota et al. 2004; Zborowski and Chalmers 2015). This can be achieved by either increasing the magnetic field strength or increasing the difference in the magnetic susceptibility of the medium and the cells. While strong magnets like electromagnets and superconductors can generate high magnetic fields, they are of the impractical, expensive and may adversely affect cell viability (L. Zhang et al. 2017). Alternatively, permanent magnets can be employed in conjunction with magnetic labeling particles in the positive magnetophoresis principle or with magnetic solutions (paramagnetic solutions or ferrofluids) in the negative magnetophoresis principle to manipulate the cells. Ferromagnetic or paramagnetic materials become magnetic when exposed to an external magnetic field (Irimia 2015) and thereby increasing the magnetic susceptibility of the surrounding medium.

In the positive magnetophoresis, cells become magnetized either by internalization or by labeling with magnetic particles and they migrate to the high magnetic field regions (Robert et al. 2011; Pamme and Wilhelm 2006; Guryanov et al. 2019). On the other hand, the cells are repulsed from high magnetic fields regions and move towards to the lower magnetic field regions in negative magnetophoresis and there are no magnetic particles internalized by or label the cells (Kose et al. 2009; Krebs et al. 2009) (Figure 1). Therefore, it eliminates the disadvantages of positive magnetophoresis such as difficulty of standardization of magnetic nanoparticles internalized by the cells, long and labor-intensive experimental steps. Also, it decreases the potential cytotoxicity of the label particles on the cell viability since it is a contactless method.

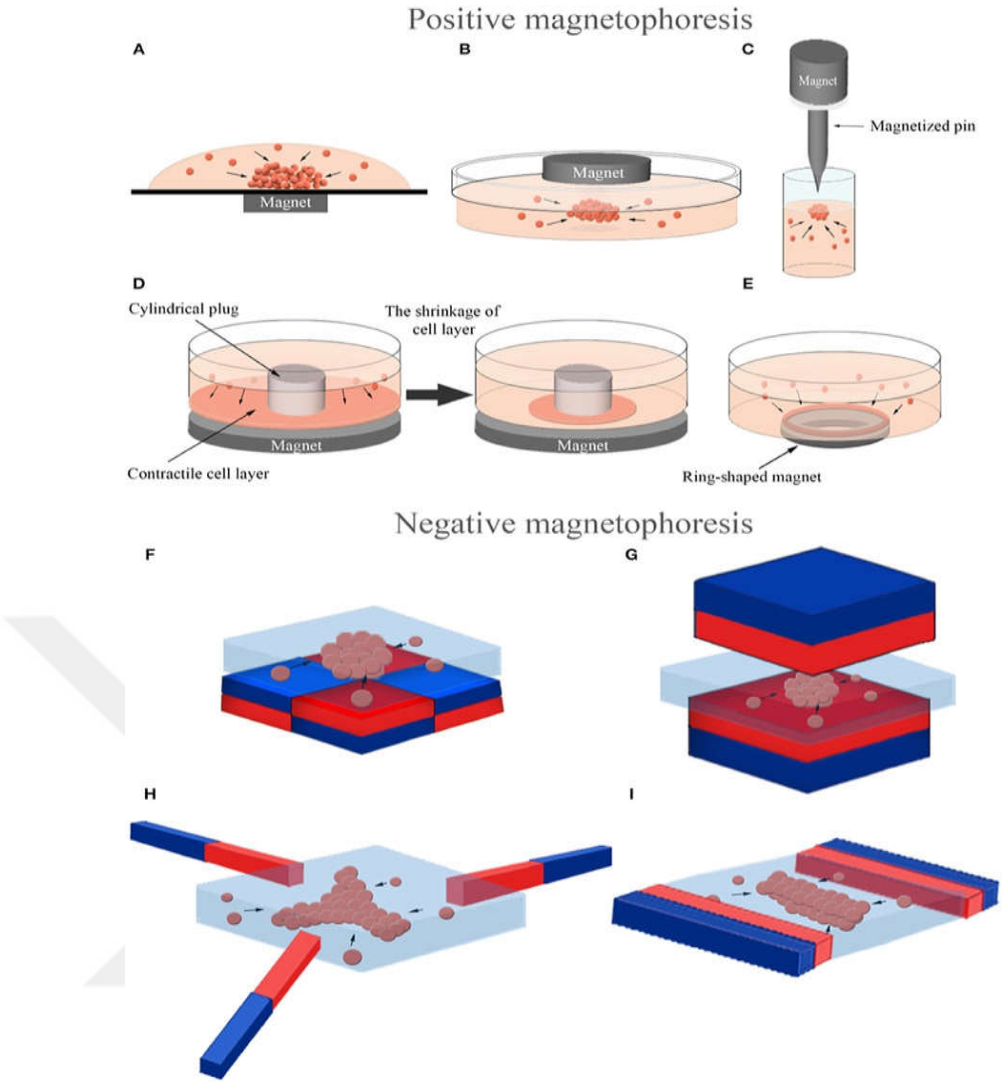


Figure 1. Magnetic force-based manipulation of magnetically labeled cells (positive magnetophoresis) and label-free diamagnetic cells (negative magnetophoresis). 3D assembly of magnetically labeled cells into a spheroid by a magnet (a) under the culture chamber, (b) on the top of the culture chamber and (c) by a magnetized pin beneath the magnet to concentrate the magnetic field for attracting cells in a focused direction. 3D assembly of magnetically labeled cells into a ring-shaped structure (d) using a cylindrical plug and a magnet under it to accumulate contractile cells around the plug and (e) using a ring-shaped magnet. 3D assembly of label-free diamagnetic cells into (f, g) spheroid, (h) three-pointed star and (i) rectangular bar in a magnetic liquid with different configurations of magnets to produce a spatially varying field along the culture chamber (The north poles: red, the south poles: blue) (Source: Yaman et al. 2018).

This method enables distinguishing cells based on their volumetric mass or magnetic properties. Each cell levitates at unique positions due to differences in their volumetric mass density or magnetic susceptibility, which directly influence the buoyancy and magnetic force acting on them. A novel magnetic levitation strategy was developed to distinguish cells based on their dynamic density or magnetic properties that can be changed during a response to a stimulus, over time, and that can vary between cell types or cells in the same population. This method incorporated a paramagnetic solution to increase the medium's magnetic susceptibility (Tasoglu et al. 2015).

This strategy was later applied to investigate density changes in individual cells throughout the differentiation process of bone marrow stem cells into lipid accumulating adipocytes (Sarigil et al. 2019). In this work, a paramagnetic medium containing the cells was introduced into a microcapillary channel positioned between two neodymium magnets. The same poles of these magnets faced the microcapillary (Figure 2a), generating a magnetic field gradient (Figure 2c). and the cells were then subjected to opposing buoyancy and magnetic forces which were balanced at some point. The cells were levitated at certain positions according to their volumetric mass density and difference between the magnetic susceptibility of the surrounding medium and the cells. It was shown that the increasing concentration of the $Gd^{3+}$ solution in the medium provided increased density detection range and resolution (Figure 2d, 2e). Magnetic levitation has been successfully employed in various applications, including density-based profiling of different types of cancer cells and blood cells, enabling the detection of circulating tumor cells in blood samples (Durmus et al. 2015). Additionally, it has been used for density profiling and sorting of lipid accumulating subpopulations during the differentiation of human induced pluripotent cells (hiPSCs) into cardiomyocytes (Puluca et al. 2020). Furthermore, it has been applied to guide the assembly of ex situ generated spheroids (Tocchio et al. 2018), contactless biofabrication of self-assembling 3D structures and long-term co-culture of bone marrow derived stem cells with adipogenic osteoblast cells and with breast cancer cells (Anil-Inevi et al. 2019; 2018).

The magnetic levitation method based on negative magnetophoresis, utilizing the magnetic field gradient generated between two permanent magnets with opposing poles, faces limitations such as the small sample culture volume within the microcapillary and difficulties in manipulating the culture medium during density-based detection and 3D culture applications. The size of the resulting cellular construct is an important parameter

in drug testing, disease modeling and biofabrication of biological structures for tissue engineering applications.

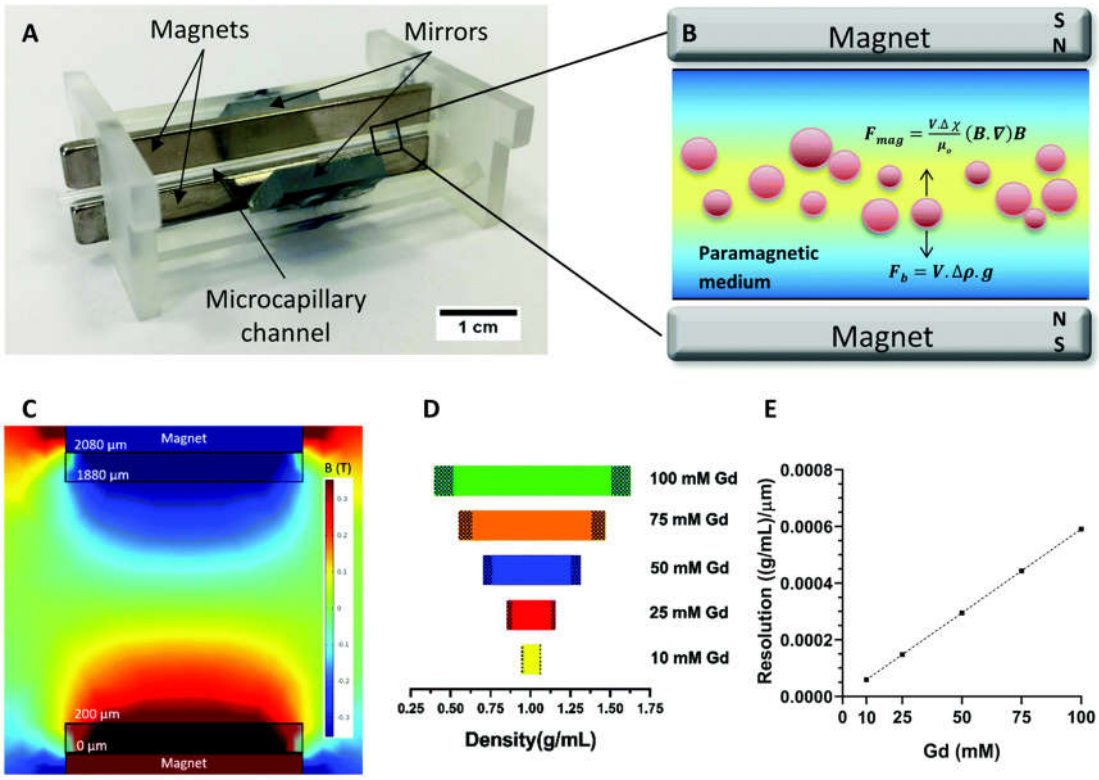


Figure 2. Magnetic levitation setup and working principle. (a) Structure of magnetic levitation device composed of two neodymium magnets, microcapillary channel and two mirrors placed at 45°. (b) Forces acting on cells at equilibrium position in the device; where Fmag: magnetic force, Fb: buoyancy force, V: cell volume, $\Delta\chi$ : magnetic susceptibility difference between paramagnetic medium and cell, μ0: permeability of free space, B: magnetic induction, Δρ: density difference between paramagnetic medium and cell, g: gravitational acceleration. (c) Cross-sectional representation of the magnetic induction between magnets. Shaded areas are not accessible because of capillary wall thickness. (d) The range of single cell density values that can be measured with the microfluidic setup with respect to used $Gd^{3+}$ concentrations based on the computational model. (e) Density resolution of the levitation system with respect to $Gd^{3+}$ concentrations based on the computational model (Source: Sarigil et al. 2019).

A newly developed platform employing two ring magnets has enabled the levitation of larger objects (Ge and Whitesides 2018; C. Zhang et al. 2020) and tissue constructs (Parfenov et al. 2020) compared to the microcapillary system. However, the use of two axial magnets in these methods restricts physical access and manipulation of the culture medium. To address these limitations, a new magnetic levitation system was developed.

This novel magnetic levitation setup, consisting of a single ring-shaped magnet and a culture tube, facilitates the construction of 3D biological structures while preserving cell viability (Figure 3). This configuration mitigates the limitations and disadvantages associated with systems using two ring-shaped magnets and a microcapillary. The system's applicability for transferring and renewing of the cell culture media, as well as its suitability for culturing diverse cell types in 3D without the need for any scaffold material (Anil-Inevi et al. 2021), was demonstrated.

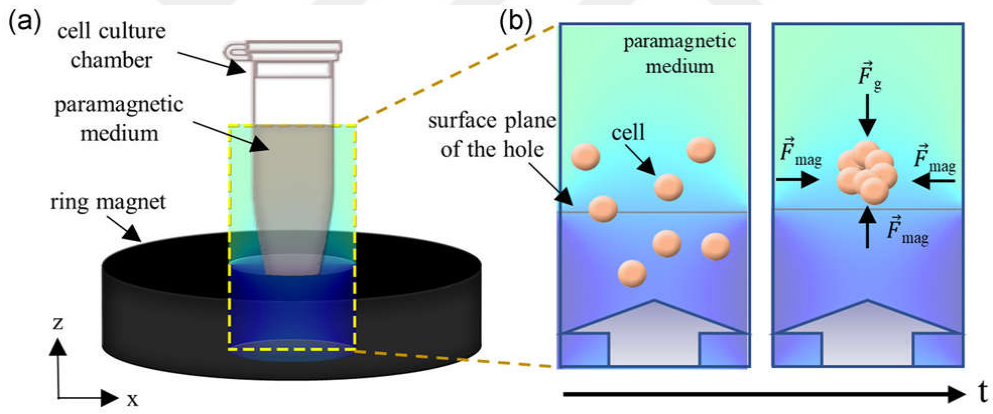


Figure 3. Magnetic force-guided levitation and self-assembly. (a) Illustration of magnetic levitation system. Cell culture chamber is positioned on the ring magnet with the bottom of the chamber attached to the hole of the magnet. (b) Schematic representation of the cellular aggregation. The block arrows in the illustration represent upward magnetic induction (Source: Anil-Inevi et al. 2021).

To investigate tissue functions and repair or replace the damaged or diseased tissues and organs, researchers have developed both scaffold-based and scaffold-free artificial tissue models that mimic the 3D *in vivo* environment. These models are often

constructed using autologous (Attiogbe et al. 2023; Vapniarsky et al. 2015; Maughan et al. 2017), allogenic (Quint et al. 2012; Augello et al. 2007; Peretti et al. 2000), or xenogeneic cells (Sun et al. 2007; Massaro et al. 2021; Jung, Seol, and Chang 2017), along with bioactive factors. A variety of tissue engineering techniques exist for producing these artificial tissue models. Among these, the contactless nature of the magnetic levitation technique offers a significant advantage as a bioprinting method. This is because it minimizes the potential risks of negative mechanical effects on cell viability. Furthermore, the elimination of scaffolds in this system allows for unhindered 3D cell-cell interactions, creating a substantial advantage for tissue engineering studies.

This doctoral dissertation focused on three primary objectives: First, we aimed to develop a scaffold-free, layered pre-invasive breast cancer model that closely resembles the *in vivo* structure using a single ring magnet-based magnetic levitation technique. Second, we sought to improve the model by increasing extracellular matrix accumulation withing scaffold-free spheroid models through the integration of the macromolecular crowding method with magnetic levitation. Finally, we investigated the volumetric mass density differences in primary cells isolated from patients and animal models of neurodevelopmental disorders using a microcapillary-based magnetic levitation method, exploring its potential as a diagnostic tool.

# CHAPTER 2

# BIOFABRICATION OF SCAFFOLD-FREE BREAST CANCER SPHEROID MODELS USING MAGNETIC LEVITATION

## 2.1. Introduction to Cancer Tissue Engineering and Spheroid Models

The life span of people has increased over time due to the advancements in technology and scientific developments. Nonetheless, the aging process inevitably leads to the deterioration and dysfunction of tissues and organs, consequently diminishing quality of life. Tissue engineering has emerged as a cutting-edge alternative to address these challenges. By creating functional tissue constructs to repair damaged tissue or by studying therapeutic approaches on disease models, tissue engineering offers to extend lifespan and improve the quality of life for many individuals.

While numerous definitions of tissue engineering have been proposed to date, the field has evolved rapidly, leading to a dynamic understanding of its scope and changes in the definitions over the years. Tissue engineering is a multidisciplinary field that gathers life sciences and engineering principles under a single roof to develop constructs that can repair, regenerate, or replace damaged tissue using cells, biomaterials, and biochemical cues. Leveraging advancements in 3D bioprinting, organoid technology, gene editing, synthetic and computational biology, and personalized medicine approaches, tissue engineering aims to create *in vitro* models that accurately mimic the *in vivo* physiology of tissues. These models serve as valuable alternatives to animal models in disease biology, drug testing, and regenerative therapy research (Hoffman et al. 2020; Liu et al. 2022; Post et al. 2022; Fonseca et al. 2020; Chaudhary and Chakraborty 2022; Shopova et al. 2023; Lam et al. 2023; Chaicharoenaudomrung, Kunhorm, and Noisa 2019; Kang et al. 2021; El Harane et al. 2023; Ranjbarnejad et al. 2022; Chen et al. 2023; Grath and

Dai 2019; Armstrong and Stevens 2019; Maresca et al. 2023; Bedir et al. 2020; J. Huang et al. 2021; Marques et al. 2023; Bardini and Di Carlo 2024).

In light of technological advances, tissue engineering has developed with different techniques emerging in various fields. In addition to their significant contributions to therapeutic research against numerous diseases and regenerative medicine, tissue engineering methods play a major role in advancing our understanding of cancer mechanisms and developing novel treatments (Marques et al. 2023; Hockney et al. 2023; Shukla et al. 2022; Abuwatfa, Pitt, and Husseini 2024).

Cancer is one of the leading causes of death globally. According to the World Health Organization (WHO) approximately 20 million new cancer cases and 9.7 million cancer-related deaths were reported in countries that participated in the survey in 2022 (World Health Organization (WHO) 2024). This significant global health burden has driven extensive research efforts over decades to elucidate the underlying biology of cancer and develop therapeutic strategies.

In the field of cancer research, conventional approaches encompass both *in vitro* and *in vivo* techniques. Conventional 2D *in vitro* studies utilizing immortalized cancer cell lines in the cell culture plates often fail to reflect the complex tumor structure and stroma found in the human body. This limitation arises from the lack of heterogeneity and absence of crucial microenvironmental signals (Martinez-Pacheco and O'driscoll 2021; Tan, Ling, and Fischbach 2021). Conversely, xenograft animal models, while valuable for preclinical studies, present several drawbacks. They are costly to maintain, require complex experimental procedures, and exhibit physiological differences from humans, thereby limiting the predictive value of the results (Martinez-Pacheco and O'driscoll 2021) and raising ethical concerns.

Tumor cells in 2D *in vitro* culture need to alter their behavior compared to their natural 3D microenvironment because of the absence of crucial factors such as of cell-ECM interactions, complex series of biochemical signals, molecular gradients, natural orientation of cell surface receptors, and polarization of the cells and facing resistance from ECM. Lack of these factors impact cellular characteristics, leading to differences in gene expression, cell-cell interactions, drug response, differentiation, proliferation, tumorigenesis and metastasis profiles, and mechanical behavior (Habanjar et al. 2021; Fontoura et al. 2020; Abbas et al. 2023; Manduca et al. 2023; Xie et al. 2024; Abuwatfa, Pitt, and Husseini 2024). This results in the failure of 2D models in predicting the efficacy of potential anticancer therapeutics in pre-clinical trials (Barbosa et al. 2022).

In the field of tissue engineering, significant efforts have been made to create functional tissue and organ replacements to restore the damaged parts of the body. These tissue engineering technologies have also been applied to cancer research to investigate carcinogenesis (Barbier et al. 2024), angiogenesis (Verbridge, Chandler, and Fischbach 2010), metastasis (Katti and Jasuja 2024), and develop drug delivery systems (Cai et al. 2021) and therapeutics on cancer cells (Mi et al. 2023). To enhance the success of pre-clinical studies, functional and biologically relevant 3D cell culture models that more accurately reflect the tumor structure and its functions have been developed.

3D tumor models combine the simplicity and high control of 2D cultures and the biological complexity of *in vivo* systems to offer a more realistic view of tumor dynamics. These models offer several advantages: the ability to better reflect the *in vivo* tumor structure and microenvironment, the inclusion of multiple non-tumor cells to mimic the intercellular interactions (Jubelin et al. 2022; Manduca et al. 2023), the simulation of the nutrient, pH, and oxygen gradients (Manduca et al. 2023) and barriers within the tumor tissue (J. Y. Lee and Chaudhuri 2021), recapitulation of gene expression profiles and rate of proliferation (Fontoura et al. 2020). These features make them essential tools for cancer therapy research within the fields of tissue engineering and personalized medicine.

Current 3D cell culture platforms for modeling the tumor microenvironment are primarily established using scaffold-based or scaffold-free approaches. Scaffold-based methods utilize hydrogels derived from cross-linking of natural and synthetic polymers (Casey et al. 2017; Sepantafar et al. 2017; Katz and West 2022; Sievers et al. 2023; Worthington, Pochan, and Langhans 2015; Shu et al. 2024; Mosquera et al. 2022; W. Li et al. 2019; Asadi et al. 2024) , decellularized tissue ECM (Ferreira et al. 2021; Dunne et al. 2014; Jin et al. 2019; Tamayo-Angorrilla et al. 2022; Lv et al. 2021), and microfluidic incorporated polymers (Lewis and Gerecht 2016; T. Song et al. 2023; J. M. Lee et al. 2017). These scaffolds provide mechanical support and surface for cell attachment, as ECM does for the cells *in vivo* to enable studying on cancer biology or therapeutic strategies. Cells are either seeded or embedded within these scaffold materials. A wide range of biomaterials have been employed in cancer research, including natural sources like proteins (e.g., collagen (Redmond et al. 2021), gelatin (Y. Wu et al. 2023; Peter et al. 2019), fibronectin (Mahmoodi et al. 2022), silk (Gangrade and Mandal 2020)) and polysaccharides (e.g., hyaluronic acid (Demirel et al. 2024; Suo et al. 2019), alginate (Kletzmayr et al. 2020), chitosan (Xu et al. 2019; Le et al. 2021)) as well as synthetic biomaterials (e.g., PEG (Z. Wang et al. 2023; Livingston et al. 2019; Pradhan et al. 2017),

PCL (Rabionet et al. 2017; Palamà et al. 2017; Rabionet, Puig, and Ciurana 2020), PLA (Rabionet et al. 2017; Palamà et al. 2017; Rabionet, Puig, and Ciurana 2020).Various conventional techniques have been utilized to fabricate different forms of scaffolding for tissue engineering, including gas foaming (Angeloni et al. 2017; Manavitehrani et al. 2019), freeze-drying (Auvinen et al. 2019; Campbell et al. 2017), solvent casting and particulate leaching (Kolathupalayam Shanmugam et al. 2020; 2023; Rakib Hasan Khan et al. 2022; Obayemi et al. 2020), thermal induced phase separation (Lombardo et al. 2019), and electrospinning (Rabionet, Puig, and Ciurana 2020; Sadeghi et al. 2023; Ricci et al. 2023; Nelson et al. 2014; Y. Wang et al. 2017). Besides, rapid prototyping techniques, including stereolithography, solvent-based extrusion free-forming, selective laser sintering, bioprinting, and fused deposition modeling overcome the limitations in the conventional techniques by enabling spatial manipulation and control of biomaterials during scaffold fabrication (Eltom, Zhong, and Muhammad 2019). 3D bioprinting technologies, in particular, allow for the dimensional control and patterning of biomaterials, cells, and biochemical factors that mimic the tumor microarchitecture (Shukla et al. 2022). However, scaffold-based cell culture models also present several challenges. Variability between batches in natural biomaterials, insufficient bioactivity, and formation of byproducts from degradation of synthetic biomaterials, reduced mechanical strength, instability and difficulty of controlling the structure of hydrogels, immunogenicity concerns, and complexity of decellularized matrices can all pose limitations (Abuwatfa, Pitt, and Husseini 2024). Furthermore, despite their numerous advantages, 3D scaffold-based cell cultures face challenges such as such as scaffold material constraints, uneven cell seeding and distribution, limited oxygen and nutrient diffusion throughout the scaffold, scaffold degradation and stability concerns, difficulties in achieving tumor complexity, the high cost of equipment, and time-consuming fabrication processes.

In contrast to scaffold-based cultures, scaffold-free models leverage the capability of forming intercellular adhesions and the self-aggregate into 3D structures without the need for external support. Various cancer cell types can assemble into 3D cellular aggregates in the form of spheroids in non-adherent environments, where they secrete and deposit their own ECM over time (Costa et al. 2016; Santini, Rainaldi, and Indovina 2000; de Araújo et al. 2024). In these models, tumor cells are not in contact with a scaffold material; therefore, they are in close contact with the other cells, fostering a more physiologically relevant environment. 3D tumor spheroids are valuable models for

studying on cancer biology, initiation, metastasis, and evaluating potential therapeutics. They closely resemble the *in vivo* avascular tumor architecture, characterized by their spatial organization and physiological cell-ECM and cell-cell interactions, gradients of soluble factors, pH, and oxygen (Costa et al. 2016). A variety of cell types, including cancer cell lines, primary tumor cells (Kondo et al. 2011; Qureshi-Baig et al. 2016), and cancer stem cells (Quereda et al. 2018; Raghavan et al. 2017), can be used to generate spheroids. Tumor spheroids are generally classified into four types which are multicellular tumor spheroids (MCTS), tumorospheres, tissue-derived tumor spheres (TDTS), and organotypic multicellular spheroids (OMS) (Weiswald, Bellet, and Dangles-Marie 2015) . Widely employed methods for generation of scaffold-free 3D tumor spheroids include the hanging drop method (Ganguli et al. 2021), forced floating method (ultra-low attachment plates) (Close et al. 2018), liquid overlay method (Jubelin et al. 2023), agitation-based techniques (Clémence et al. 2017), pellet culture (Dhandapani et al. 2023), micro-molding (Guo et al. 2019), microfluidics (Tevlek et al. 2023), bioprinting using magnetic levitation (Mishriki et al. 2019; Dzamukova et al. 2015; Jaganathan et al. 2014; Türker, Demirçak, and Arslan-Yildiz 2018; Anil-Inevi et al. 2020; 2021; 2018; Sarigil et al. 2021). Several limitations are associated with these scaffold-free generation methods. In hanging drop, forced floating, liquid overlay, and micro-molding methods, the range of cell types suitable for spheroid formation is limited, and achieving consistent spheroid size and shape can be challenging. In agitation-based methods and pellet culture, together with the inconsistency of the spheroid structure, gravitational forces and sheer stress act on the cells, which can be harmful to their viability in the long term. Furthermore, creating scaffold-free spheroids using microfluidic systems is often costly and labor-intensive, requiring technical expertise. Additionally, the variety of cell types compatible with microfluidic channels is limited, and the throughput of these methods is lower than that of other methods.

The concept of magnetic manipulation can be achieved through two approaches, as described in the first chapter: positive and negative magnetophoresis. In positive magnetophoresis, cells are magnetized by incorporating magnetic nanoparticles, inducing movement from regions of lower magnetic field strength towards regions of a higher field strength one. On the other hand, negative magnetophoresis involves suspending cells in a paramagnetic medium or ferrofluids, which exhibit higher magnetic susceptibility than the cells themselves. This differential magnetic susceptibility generates a magnetic force that drives the cells to move towards a weaker magnetic field and to form aggregates

when they subjected to a magnetic field gradient. This method offers a valuable approach for for creating cell aggregates or spheroids without the adverse effects of labeling on cells and time-consuming experimental steps.

Previously, it was shown that magnetic levitation of cells could be applied using two axial ring magnets (Ge and Whitesides 2018). However, the presence of two magnets within the environment poses challenges, including difficulties in manipulating the cell culture difficult and limits the working volume. On the other hand, the single magnet in the newly developed ring magnetic levitation system eliminates these disadvantages (Anil-Inevi et al. 2021). This system incorporates ring shaped magnets with holes on their center. The magnetic field strength decreases towards the center of this hole. As time passes, the cells levitate and stably gather on the local minimum magnetic field above the magnet hole. At this equilibrium point, the cells interact with each other and form stable spheroid-like structures (Figure 4). The point where the cells are stably positioned is the equilibrium point determined by their volumetric mass density (see Appendix).

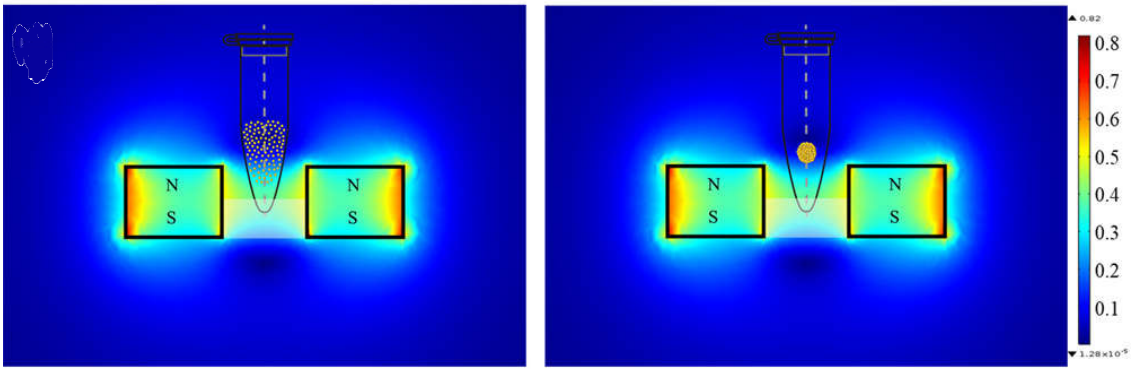


Figure 4. Representation of cellular aggregation on the simulation of magnetic flux density norm around the ring magnet (Source: Anil-Inevi et al. 2021).

The tumor microenvironment, encompassing the extracellular matrix and neighboring healthy cells, plays a pivotal role in shaping the behavior of cancer cells. Significant research has demonstrated the substantial impact of normal cells on cancer biology, including their ability to expel oncogene-transformed epithelial cells and suppress the growth of breast cancer cells in co-culture (Spink et al. 2006; Hogan et al. 2011). Beyond cellular diversity, the spatial organization of cells within the three-

dimensional tumor structure is a key determinant of the tumor characteristics. In normal breast tissue, epithelial and myoepithelial cells are confined within a basement membrane layer, separating them from the surrounding fibrous and adipose tissue (Figure 5) (Bahcecioglu et al. 2020). However, in cancer, the functions of the healthy cells become disrupted.

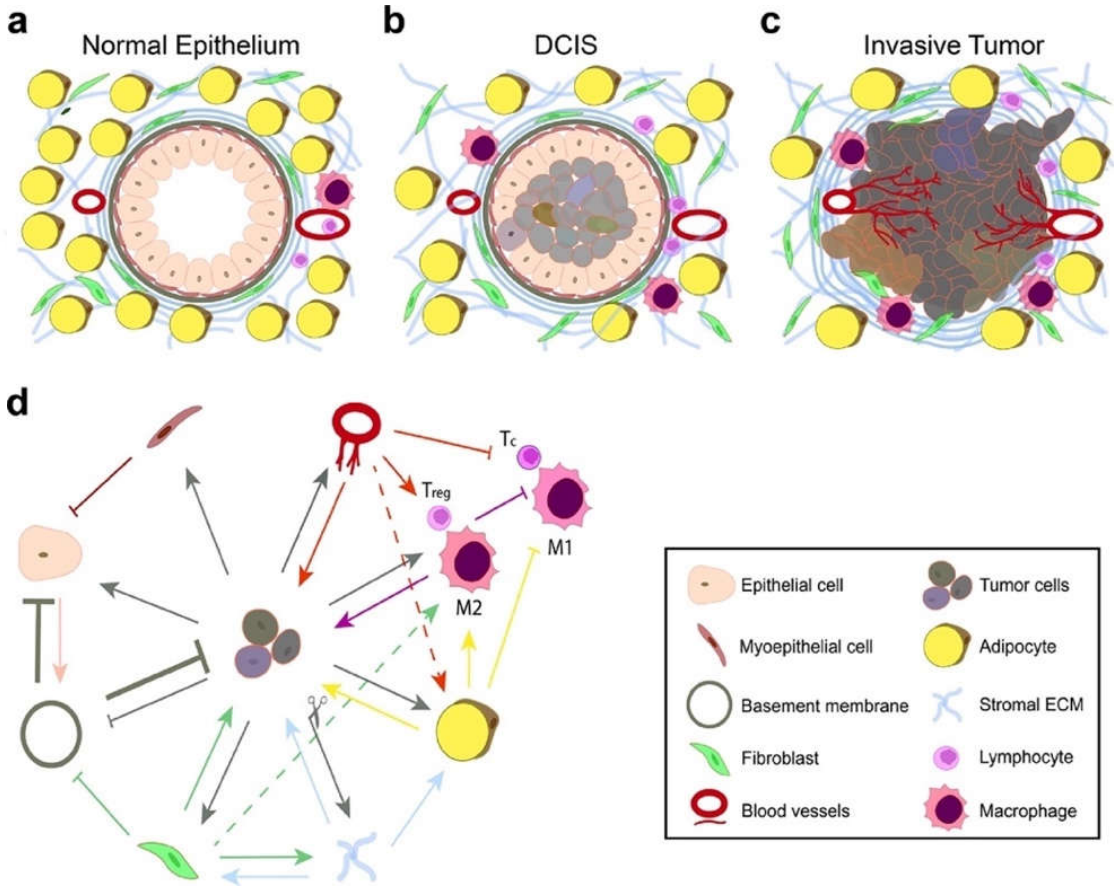


Figure 5. Interactions between cells and ECM lead to alteration of normal epithelium towards the tumor. (a) Normal epithelium, (b) ductal carcinoma in situ (DCIS), and (c) invasive tumor. (d) Simplified illustration of the network of interactions between cells and the ECM. Crosstalk between the tumor cells, stromal cells (fibroblasts and adipocytes), immune cells (regulatory (Treg) and cytotoxic (Tc) T cells, and type 1 (M1) and type 2 (M2) macrophages), and the endothelial cells alters the microenvironment (Source: Bahcecioglu et al. 2020).

In ductal carcinoma in situ, an early form of breast cancer, which is one of the most prevalent cancer types, the transition to an invasive phenotype is associated with the detachment of abnormal cells from the normal epithelial cell layer and their subsequent migration into surrounding tissue (Cowell et al. 2013). It was shown in a study that the presence of the breast epithelial cells in co-culture with breast cancer cells, can induce an invasive and metastatic phenotype in the tumor cells (M.-H. Lee et al. 2015).

In the light of these findings, the utilization of three-dimensional heterogeneous cell culture models is vital for comprehending the progression of breast cancer, studying molecular changes, and evaluating potential treatments. However, creating a completely symmetrical layered structure presents significant challenges. Therefore, our goal was to develop a heterogenous three-dimensional layered model of breast cancer by surrounding the breast cancer cell cluster, formed using magnetic levitation, with breast epithelial cells.

## 2.2. Methods

### 2.2.1. Cell Culture

MDA-MB-231$^{dsRed}$ (breast cancer cell line, ATCC) cells were cultured in Dulbecco's modified Eagle medium (Gibco) supplemented with 10% fetal bovine serum (FBS) and 1% penicillin/streptomycin (P/S). MCF-10A$^{eGFP}$ (breast epithelial cell line, ATCC) cells were cultured in DMEM/F-12 medium supplemented with 5% Donor Horse Serum, 1% P/S, 20 ng/mL EGF, 0.5 µg/mL hydrocortisone (Sigma, H0888), 100 ng/mL Cholera Toxin and 10 µg/mL insulin. Within this period, the cells were incubated in the incubator at 37°C, 5% CO2. The growth mediums were refreshed every other day, and the cells were passaged when they reached 90% confluency by using trypsin to detach the cells.

### 2.2.2. Single Ring Magnet-Based Magnetic Levitation of Cells

The cells were detached with 0.25% trypsin-EDTA solution when the culture reached 90% confluency. Following centrifugation and removal of the supernatant, the cells were resuspended to $10^6$ cells/ml in the culture medium with various $Gd^{3+}$ concentrations (100, 150, and 200 mM). A total of 200 µl of cell suspension was loaded into the cell culture tube, and the culture tube was placed in the hole of the ring magnet. The cells were levitated in the magnetic levitation system and were incubated for 24 h at 37°C, 5% $CO_2$. The spheroids were photographed after 24 h of culture by a mobile phone equipped with a ×15 micro focal length lens (Baseus) for short-distance focusing. Additionally, they were visualized under a confocal microscope (Leica DMI8 confocal microscope).

### 2.2.3. Microcapillary-Based Magnetic Levitation of Cells

Cells were suspended in $Gd^{3+}$ containing 50 µl paramagnetic medium and were loaded into a microcapillary channel. They were repulsed from the region of high magnetic field (i.e., close to the magnets) to the region of low magnetic field (i.e., middle region of cell culture chamber in the vertical direction) owing to the difference between the magnetic susceptibility of cells and the surrounding medium. After about 10 min, cells stopped moving and came to an equilibrium position in the microcapillary channel according to their volumetric mass densities. Magnetic levitation images were observed under an inverted microscope (Olympus IX-83). Images were analyzed using Image J software to investigate the levitation profiles of cells.

### 2.2.4. Heterogenous Co-culture of Cells in Magnetic Levitation Setup

MDA-MB-231$^{dsRed}$ cells were loaded into the cell culture tube with varying cell and $Gd^{3+}$ concentrations with a total of 200 µl of cell suspension. After determined time of culture of MDA-MB-231$^{dsRed}$ cells, which is at the core of the layered cell aggregate, half of the cell suspension (100 µl) was withdrawn with a pipette. It was replaced by 100 µl cell suspension containing the MCF-10A$^{eGFP}$ cells with varying cell concentration in the presence of the same $Gd^{3+}$ concentration as the other half of the culture media. The cells were co-cultured at 37°C, with 5% $CO_2$ for the determined culture time.

### 2.2.5. Cell Viability Experiments

MDA-MB-231$^{dsRed}$ and MCF-10A$^{eGFP}$ cells were seeded at a starting concentration of $10^4$ cells/well in a 96-well plate and cultured for 4h, 24 h and 48 h. The cells were exposed to different $Gd^{3+}$ concentrations of (0, 100, 150 and 200 mM) and cell viability was measured at 4$^{th}$, 24$^{th}$ and 48$^{th}$ hour with thiazolyl blue tetrazolium bromide (MTT) assay. 0.5 mg/ml of MTT reagent (Amresco) was added to each well and the plates were incubated at 37 °C for 3 h in the dark. The media was removed, 100 µl of DMSO was subsequently added to each well and colorimetric measurements were performed at 570 nm with a reference wavelength of 690 nm (Thermo Scientific Multiskan Go).

### 2.2.6. Statistical Analysis

Results were expressed as mean ± standard deviation for each experiment. Each experiment had at least 3 samples in each repetition. In cases where statistical comparisons need to be made, the differences between groups were measured by ANOVA test, 5% was considered as the significance limit.

## 2.3. Results and Discussion

In order to determine the optimum $Gd^{3+}$ concentration to be used in the biofabrication of three-dimensional heterogeneous structures, both cell types were cultured at a constant cell concentration ($1x10^6$ cells/ml), using varying $Gd^{3+}$ concentrations (100 mM, 150 mM, and 200 mM). Cells were visualized using a standard camera after 2 and 24 hours of culture. The spherical structures formed by the cells were observed, and the effects of culture time and $Gd^{3+}$ concentration on the formed structures were investigated. Spheroid like structures were observed in both MDA-MB-$231^{dsRed}$ and MCF-$10A^{eGFP}$ after 2 hours of levitation culture. A $Gd^{3+}$ concentration of 100 mM was found to be optimal for levitating the cells and facilitating the formation of three-dimensional structures through self-assembly. As expected, in the absence of a paramagnetic solution (0 mM $Gd^{3+}$), cells did not levitate and settled at the bottom of the culture chamber.

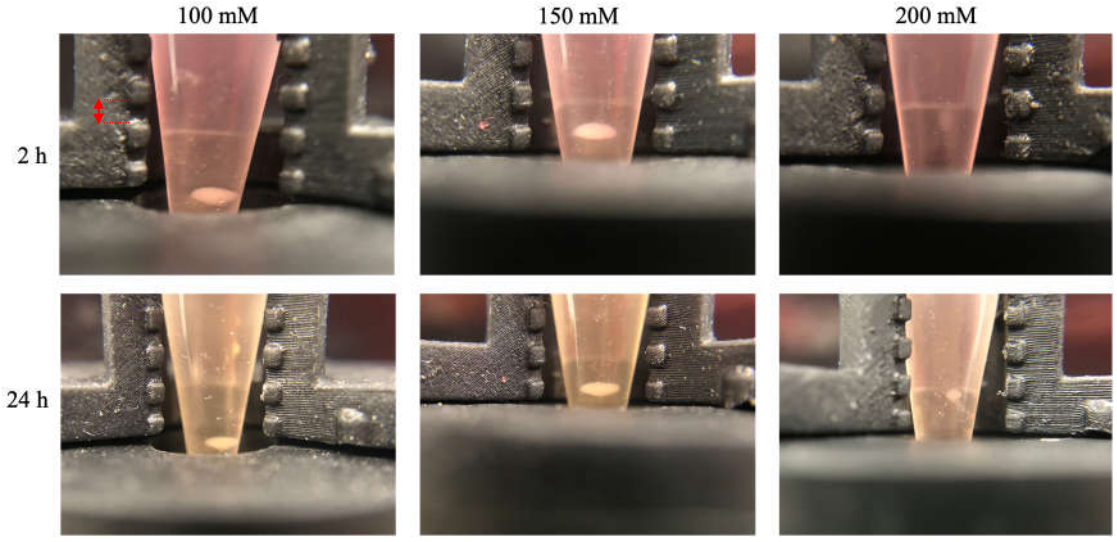


Figure 6. Magnetic levitation images of MDA-MB-$231^{dsRed}$ cells cultured with single ring magnet-based levitation system (100, 150, and 200 mM $Gd^{3+}$, $10^6$ cells/ml) after 2 and 24 h of culture. n=3. Each vertical scale: 1 mm

After 24 hours of culture, the cells were photographed, and it was observed that the MDA-MB-231$^{dsRed}$ cells were stable with only slight flattening on the cellular assembly (Figure 6). On the other hand, MCF-10A$^{eGFP}$ cells exhibited instability after 24 hours of culture, with cell clusters gravitating to the bottom of the culture tube in all samples (Figure 7).

The levitation experiment was repeated at 150 mM and 200 mM $Gd^{3+}$ concentrations in order to determine the maximum time that MCF-10A$^{eGFP}$ cells can be cultured without gravitating in the levitation system. Cells were photographed after 2 hours and 5 hours of culture. The three-dimensional structures formed after 2 hours remained stable for up to 5 hours (Figure 8). However, the cell sedimentation was observed after 24 h of culture. Therefore, it was concluded that the MCF10A$^{eGFP}$ cells can be cultured for up to 5 hours in the formation of a heterogenous cell culture model.

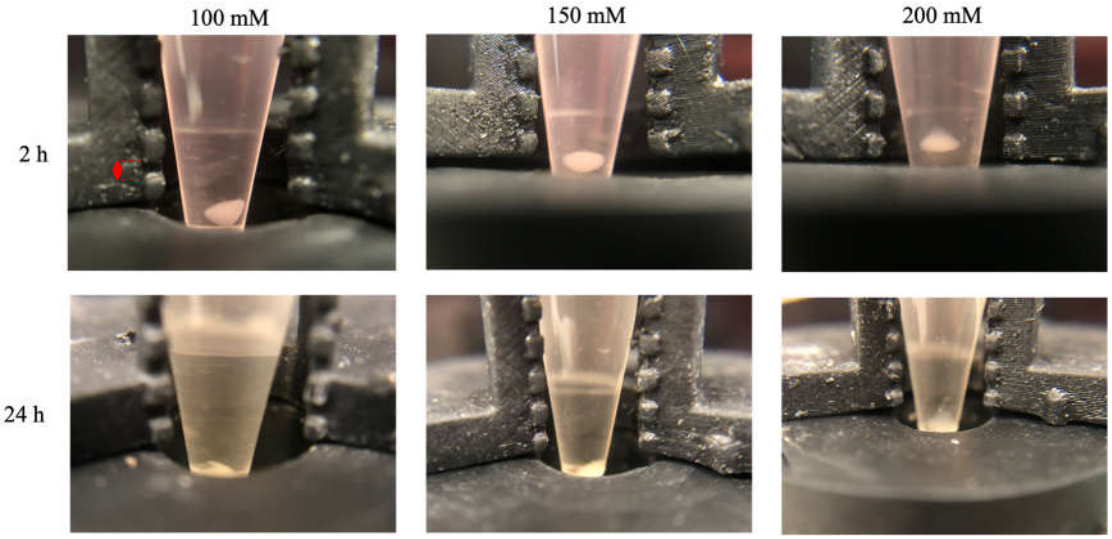


Figure 7. Magnetic levitation images of MCF-10A$^{eGFP}$ cells cultured with single ring magnet-based levitation system (100, 150, and 200 mM $Gd^{3+}$, $10^6$ cells/ml) after 2 and 24 h of culture. n=3. Each vertical scale: 1mm

MTT assay was conducted to examine the effect of the $Gd^{3+}$ on the cell viability, which might have contributed to the gravitation of 3D aggregates, formed by MCF-10A$^{eGFP}$ cells, after 24 hours. Analysis revealed that the increased $Gd^{3+}$ concentration at the 4$^{th}$ hour time point did not cause a significantly affect the viability of either cell line.

No statistically significant changes in cell in viability was observed for either cell type with increasing $Gd^{3+}$ concentration until a reduction in viability was noted at 200 mM $Gd^{3+}$ after 24 hours. However, lower cell viability rates were observed in MCF-10A$^{eGFP}$ cells compared to the control group, with increasing $Gd^{3+}$ concentrations at 48 h. In contrast, MDA-MB-231$^{dsRed}$ cell viability remained relatively stable until a decrease was observed at 200 mM concentration, similar to the 24-hour time point (Figure 9).

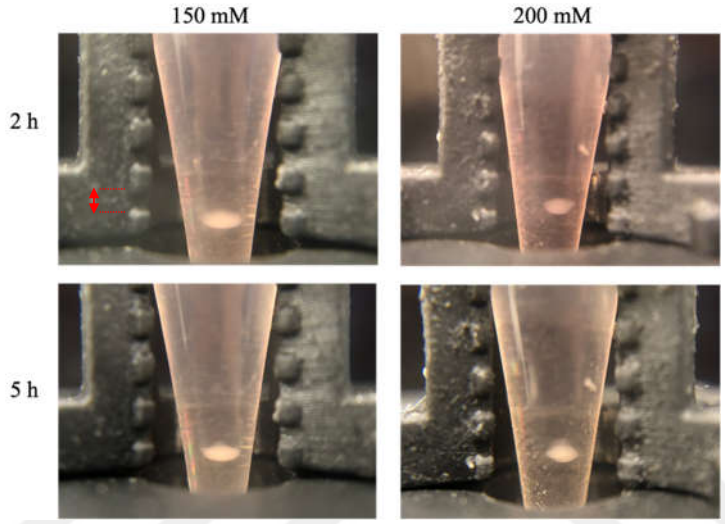


Figure 8. Magnetic levitation images of MCF-10A$^{eGFP}$ cells at 150 mM and 200 mM $Gd^{3+}$ concentrations after 2 and 5 hours of levitation culture. n=3. Each vertical scale: 1 mm.

When MCF-10A$^{eGFP}$ cells were cultured at 100 mM $Gd^{3+}$ concentration for 24 and 48 hours, an increase in cell viability was observed compared to the 4-hour time point. This finding suggests that $Gd^{3+}$ induced toxicity is not the primary reason for gravitation of the cells in the levitation system. In addition, the inability of MCF-10A$^{eGFP}$ mammary epithelial cells, which are anchorage-dependent (Ishikawa et al. 2015), to adhere to any surface in the levitation system may contribute to structural and functional changes within the cells. These changes could potentially alter the physical properties of the cells or increase membrane permeability, allowing $Gd^{3+}$ ions to enter the cells and contribute to their gravitation in the system. Following the biofabrication of the three-dimensional MDA-MB-231$^{dsRed}$ cell aggregates, MCF-10A$^{eGFP}$ cells were introduced in

the levitation system to establish a co-culture model. This approach was intended to facilitate intercellular attachment between the two cell types.

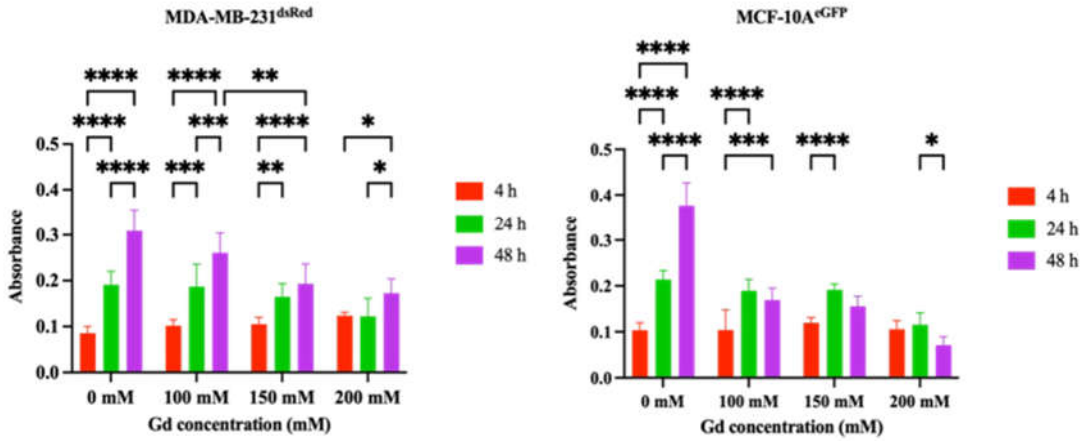


Figure 9. Absorbance values after 4 hours, 24 hours, and 48 hours of culture of MDA-MB-231$^{dsRed}$ and MCF- 10A$^{eGFP}$ cells at 0 mM, 100 mM, 150 mM, and 200 mM $Gd^{3+}$ concentrations. n=3.

To determine the optimum concentration for the three-dimensional culture, MDA-MB-231$^{dsRed}$ cells, intended to occupy the inner core of the heterogenous structure, were levitated at varying concentrations ($5x10^5$ cells/ml, $2.5x10^5$ cells/ml, $1.25x10^5$ cells/ml and $5x10^4$ cells/ml) with 100 mM $Gd^{3+}$ (Figure 10). Notably, three-dimensional structures were observed with macroscopic imaging after 24 hours of levitation culture even at the lower cell concentrations ($1.25x10^5$ cells/ml and $5x10^4$ cells/ml). Following this observation, we decided to use these low cell concentrations to minimize potential viability loss due to the decreased nutrient and oxygen diffusion within the 3D cell structure.

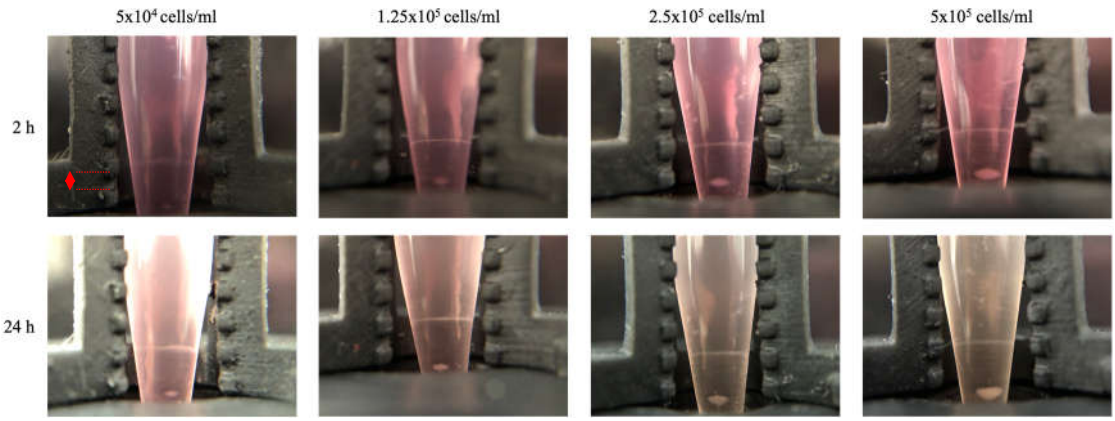


Figure 10. Magnetic levitation images of MDA-MB-231$^{dsRed}$ cells at different cell concentrations (5x10$^5$ cells/ml, 2.5x10$^5$ cells/ml, 1.25x10$^5$ cells/ml, and 5x10$^4$ cells/ml) with 100 mM $Gd^{3+}$ after 2 and 24 hours of culture. n=3. Each vertical scale: 1 mm.

MDA-MB-231$^{dsRed}$ cells were cultured in the levitation system for 24 hours at pre-determined cell concentrations (1.25x10$^5$ cells/ml and 5x10$^4$ cells/ml) in the presence of $Gd^{3+}$ (100 mM). Following this period, half of the cell culture medium was replaced with the MCF-10A$^{eGFP}$ cell suspension at identical cell and $Gd^{3+}$ concentrations. The cells were subsequently co-cultured for an additional 4 hours and the resulting 3D heterogeneous cell structures were photographed (Figure 11). Our observations revealed that the formed 3D heterogeneous cell structures remained levitated and exhibited an increase in size compared to the aggregates formed by MDA-MB-231$^{dsRed}$ cells after the initial 24-hour culture period.

Following the culture period, the spheroids were transferred to Petri dish for imaging and subsequent examination using confocal microscopy (Figure 12). Analysis revealed that the absence of the intended core-shell cell structure, with the MDA-MB-231$^{dsRed}$ cells inside and MCF-10A$^{eGFP}$ cells outside, was due to the inability of the cellular structures to maintain their integrity, resulting in dispersion during the transfer phase. Although the cells remained suspended for 28 hours during the culture period, they were unable to form robust and stable structures with sufficient mechanical strength for transfer and manipulation.

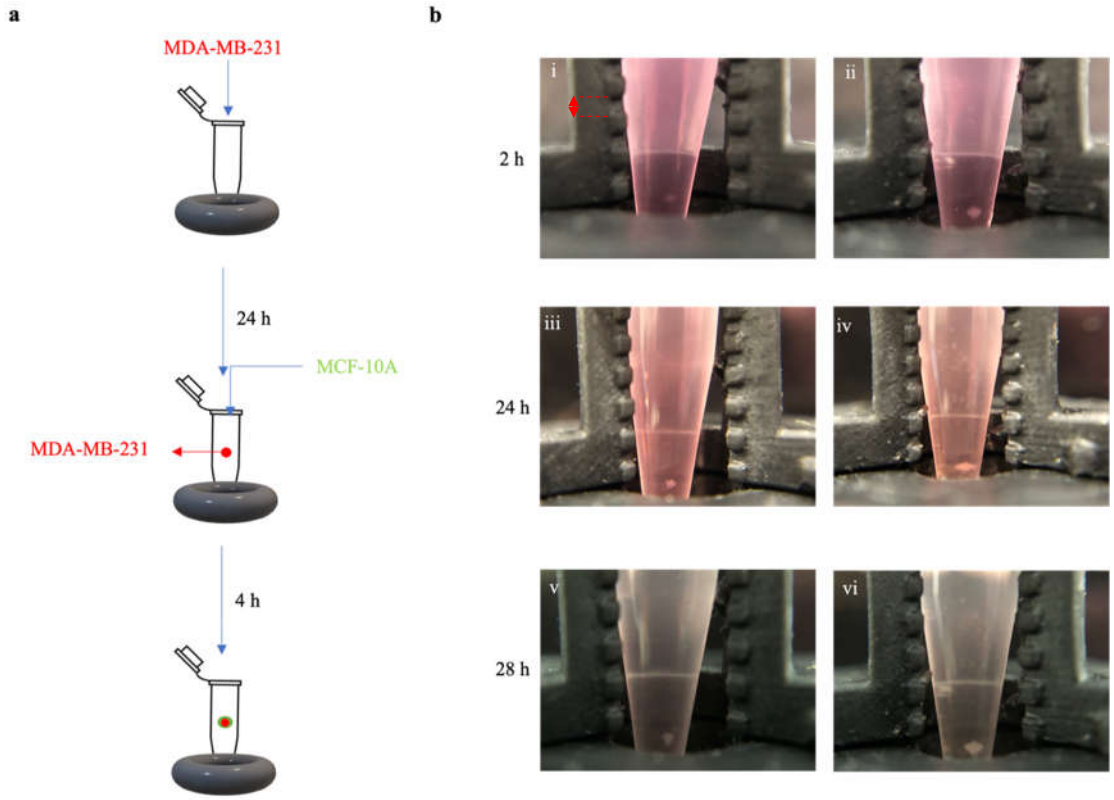


Figure 11. Schematic representation of the experiment (a), Magnetic levitation images of MDA-MB-231$^{dsRed}$ cells after 2 h and 24 h of culture at different cell concentrations (b) ($5x10^4$ cells/ml (i and iii) and $1.25x10^5$ cells/ml (ii and iv)). Images of heterogeneous spheroids at the end of the culture time after the addition of MCF-10A$^{eGFP}$ cells ($5x10^4$ cells/ml (v) and $1.25x10^5$ cells/ml (vi)) to the system. n=3. Each vertical scale:1 mm.

To evaluate the long-term stability of these heterogenous structures over extended culture periods, the experiment was repeated for a total of 48 hours culture time and images were captured at designated time points (Figure 13). Upon observation, the spheroids were found to remain stable after 48 hours, exhibiting an increase in volume for both cell concentrations. This observation indicates the successful formation of 3D heterogeneous spheroids.

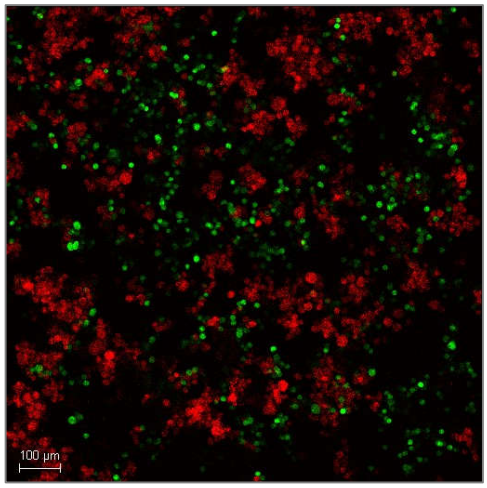


Figure 12. Confocal microscope image of MDA-MB-231$^{dsRed}$ and MCF-10A$^{eGFP}$ cells cultured in a levitation system for 28 hours. Scale bar: 100 µm.

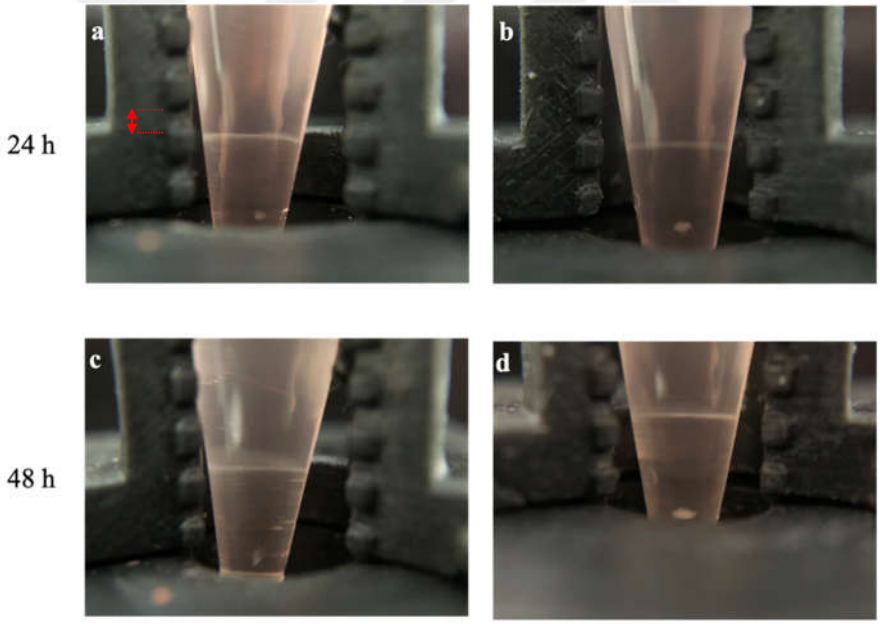


Figure 13. Magnetic levitation images of MDA-MB-231$^{dsRed}$ spheroids after 24 h of culture (a, b) and images of heterogeneous spheroids after adding MCF-10A$^{eGFP}$ cells into the levitation culture (c, d). MDA-MB-231$^{dsRed}$ cell concentration: $5x10^4$ cells/ml (a) and $1.25x10^5$ cells/ml (b), MCF-10A$^{eGFP}$ cell concentration: $5x10^4$ cells/ml (c) and $1.25x10^5$ cells/ml (d). n=3. Each vertical scale: 1 mm.

The lack of gravitational movement in MCF-10A$^{eGFP}$ cells after 24 hours is attributed to the establishment of intercellular interactions with the MDA-MB-231$^{dsRed}$ cells. These interactions likely contributed to the stability of the anchorage dependent MCF10A$^{eGFP}$ cells within the levitated position for an extended duration.

While the cells remained stable within the levitation system, they lacked the necessary compactness for successful transfer onto a culture dish for subsequent confocal microscopy analysis. To address this limitation, an investigation was conducted to assess the impact of incorporating $Ca^{2+}$ into the culture medium on cell-cell interactions within the single-ring magnetic levitation system. This approach was expected to enhance cell-cell adhesion (S. A. Kim et al. 2011) and promote the formation of more manageable, compact structures.

The impact of $Ca^{2+}$ on the formation of more tightly packed cellular assemblies was investigated by levitating cells in a ring magnetic levitation system with a culture medium containing 3 mM and 5 mM $CaCl_2$ (Figure 14). When spheroids were transferred to the petri dish, they exhibited increased stability and compactness compared to previous trials. Confocal microscopy was employed to examine the morphology and localization of MDA-MB-231$^{dsRed}$ and MCF-10A$^{eGFP}$ cells co-cultured at a 1:1 ratio within the magnetic levitation system in the presence of 3 mM $Ca^{2+}$ (Figure 15) and 5 mM $Ca^{2+}$ (Figure 16), Analysis of the confocal images, specifically the merged channels (Figure 14c, Figure 15c), revealed both cell types' spatial distribution and co-localization within the spheroid structure. This is depicted in the images, where MDA-MB-231$^{dsRed}$ cells are labeled in red, MCF-10A$^{eGFP}$ cells in green, and the merged channels illustrate the composite spheroid structure. The scale bar provided in the images measures 200 μm, offering a reference for evaluating the size and density of the spheroidal aggregates formed under these culture conditions.

Confocal imaging analysis revealed that the concentration of MCF-10A$^{eGFP}$ cells was insufficient to fully encapsulate the MDA-MB-231$^{dsRed}$ cell clusters at every depth level, attributable to the 1:1 cell loading ratio. In order to create a core-shell structure, the concentration of MDA-MB-231$^{dsRed}$ cells was kept the same ($1.25x10^5$ cells/ml) or reduced by half ($6.25x10^4$ cells/ml), while the concentration of MCF-10A$^{eGFP}$ cells was doubled ($2.5x10^5$ cells/ml) to achieve cell loading ratios of 1:2 and 1:4 (Figure 17).

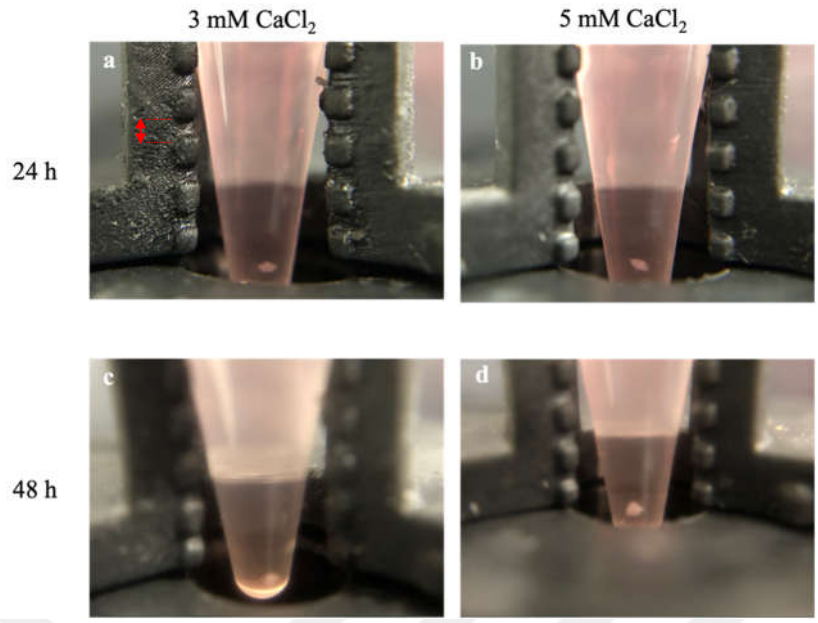


Figure 14. Magnetic levitation images of MDA-MB-231$^{dsRed}$ cell clusters (1.25x10$^5$ cells/ml) after 24 h of culture in the presence of 3 and 5 mM $CaCl_2$ (a,b). Images of heterogeneous spheroids after adding MCF-10A$^{eGFP}$ cells (1.25x10$^5$ cells/ml) into the levitation system with 3 and 5 mM $CaCl_2$ (c,d), with cell 1:1 cell loading ratio in the presence of 100 mM $Gd^{3+}$ . n=3.

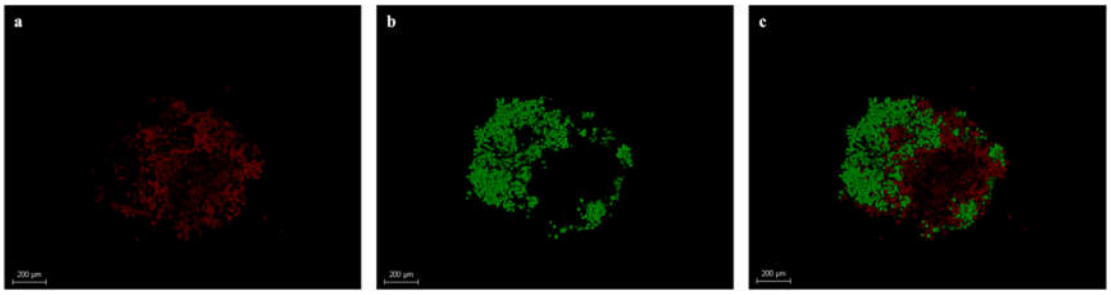


Figure 15. Confocal microscope images of MDA-MB-231$^{dsRed}$ (a) and MCF-10A$^{eGFP}$ (b) cells (1:1) cultured in the levitation system for 48 hours with 3 mM $Ca^{2+}$ and 100 mM $Gd^{3+}$. Merged channels showing both cell types in the spheroid structure together (c). n=3. Scale bar: 200 µm.

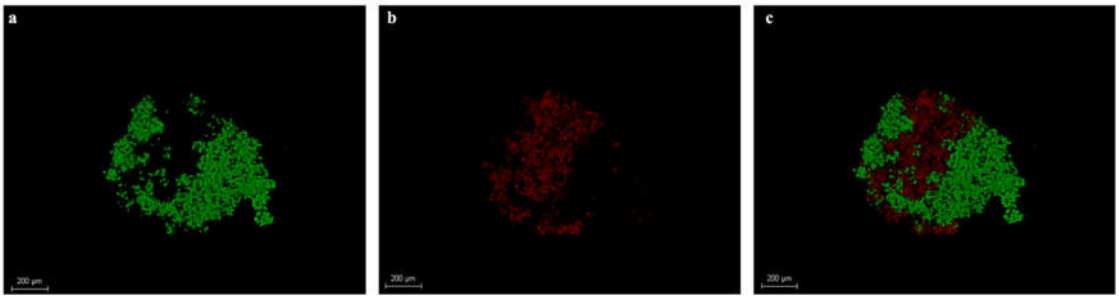


Figure 16. Confocal microscope images of MDA-MB-231$^{dsRed}$ (a) and MCF-10A$^{eGFP}$ (b) cells (1:1) cultured in the levitation system for 48 hours with 5 mM $Ca^{2+}$ 100 mM $Gd^{3+}$. Merged channels showing both cell types in the spheroid structure together (c). n=3. Scale bar: 200 µm.

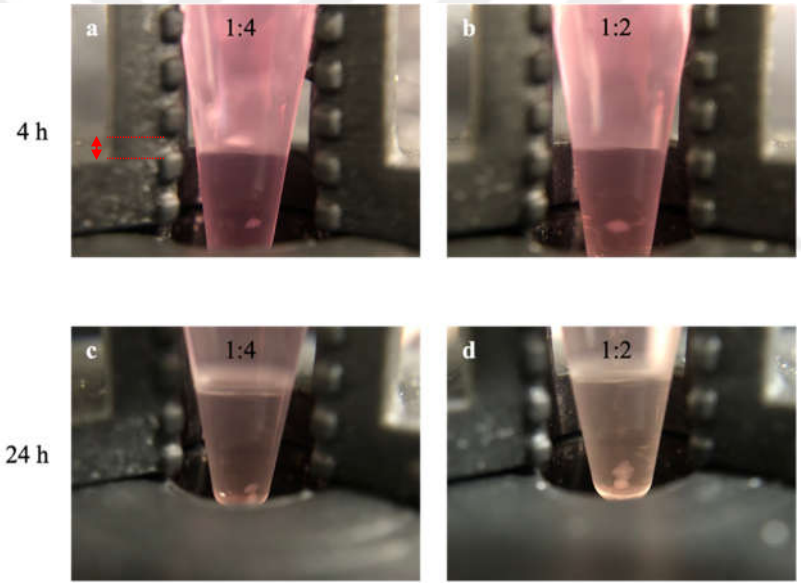


Figure 17. Magnetic levitation images of MDA-MB-231$^{dsRed}$ and MCF-10A$^{eGFP}$ cells cultured with single ring magnet-based levitation system in the presence of 5 mM $CaCl_2$ and 100 mM $Gd^{3+}$. Cell loading ratios: 1:4 and 1:2, respectively. MDA-MB-231$^{dsRed}$ cell concentration: $6.25x10^4$ cells/ml (a) and $1.25x10^5$ cells/ml (b), MCF-10A$^{eGFP}$ cell concentration in co-culture: $2.5x10^5$ cells/ml (c and d). Total cell concentration: $3.125x10^5$ cells/ml (c) and $3.75x10^5$ cells/ml (d). n=3. Each vertical scale: 1 mm.

MDA-MB-231$^{dsRed}$ cells were levitated for 4 hours, followed by the addition of MCF-10A$^{eGFP}$ cells. Despite the increased stability of the cells after the transfer phase, the expected core-shell structure was not observed. Instead, two adjacent cell clusters were noted (Figure 17c, Figure 17d). This could be attributed to inadequate mixing of the cell solutions during the addition of the MCF-10A$^{eGFP}$ solution to the system or to intercellular interactions among the MDA-MB-231$^{dsRed}$ cells.

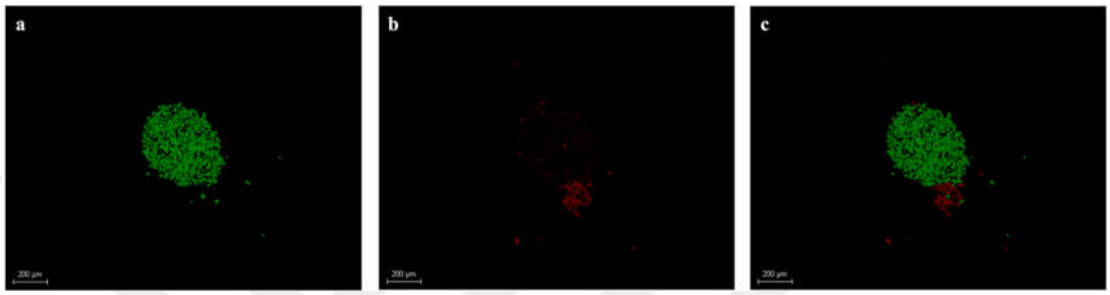


Figure 18. Confocal microscope images of MDA-MB-231$^{dsRed}$ (a) and MCF-10A$^{eGFP}$ (b) cells (1:4) cultured in the levitation system for 28 hours with 5 mM $Ca^{2+}$ and 100 mM $Gd^{3+}$. Merged channels showing both cell types in the spheroid structure together (c). Scale bar: 200 µm.

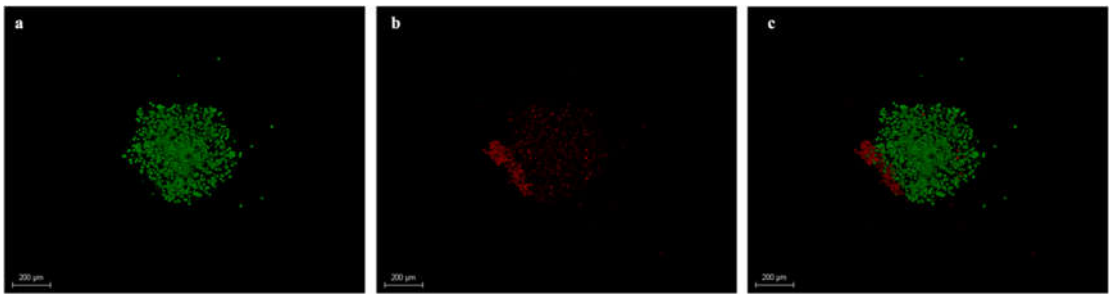


Figure 19. Confocal microscope images of MDA-MB-231$^{dsRed}$ (a) and MCF-10A$^{eGFP}$ (b) cells (1:2) cultured in the levitation system for 28 hours with 5 mM $Ca^{2+}$ and 100 mM $Gd^{3+}$. Merged channels showing both cell types in the spheroid structure together (c). Scale bar: 200 µm.

However, confocal images of one of the two spheroids in each sample showed that MCF-10A$^{eGFP}$ cells were able to cover the outer surface of the MDA-MB-231$^{dsRed}$ cells (Figure 18 and Figure 19). Nevertheless, the number of MDA-MB-231$^{dsRed}$ cells was quite low as they were primarily present in the other spheroid.

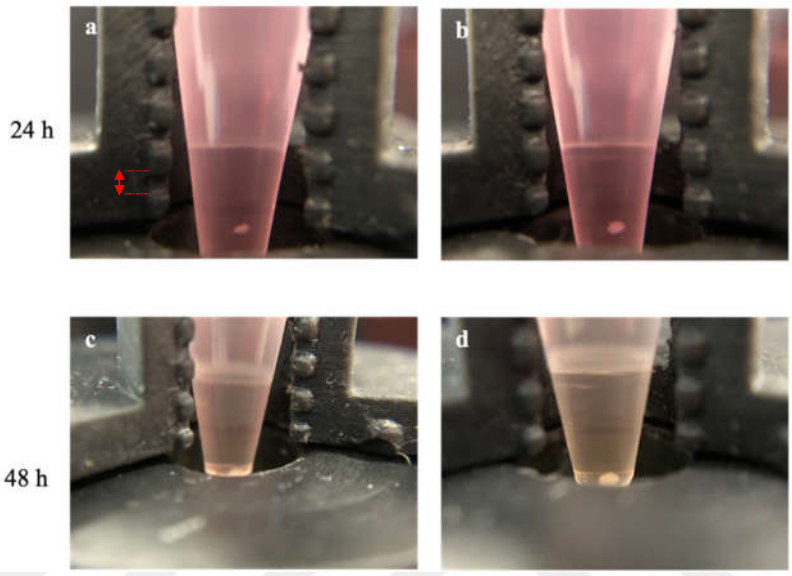


Figure 20. Magnetic levitation images of MDA-MB-231$^{dsRed}$ and MCF-10A$^{eGFP}$ cells cultured with single ring magnet-based levitation system in the presence of 5 mM $CaCl_2$ and 100 mM $Gd^{3+}$ with a cell loading ratio of 1:4. MDA-MB-231$^{dsRed}$ cell concentration: 5 x$10^4$ cells/ml (a) and 1x$10^5$ cells/ml (b), MCF-10A$^{eGFP}$ cell concentration in co-culture: 2x$10^5$ cells/ml (c) and 4x$10^5$ cells/ml (d). Total cell concentration: 2.5x$10^5$ cells/ml (c) and 5x$10^5$ cells/ml (d). n=3. Each vertical scale: 1 mm.

In order to create compact and layered single spheroids, we employed two different total cell concentrations for both types of cells, at the same cell loading ratio (1:4). After culturing MDA-MB-231$^{dsRed}$ cells for 24 hours, MCF-10A$^{eGFP}$ cells were introduced to the culture medium. This time, careful attention was paid to ensure that the mixing was done properly. The cells were then co-cultured for an additional 24 hours, resulting in the formation of single spheroids (Figure 20). However, a layered structure was not evident this time. Instead, each cell type appeared to be clustered among itself (Figure 21).

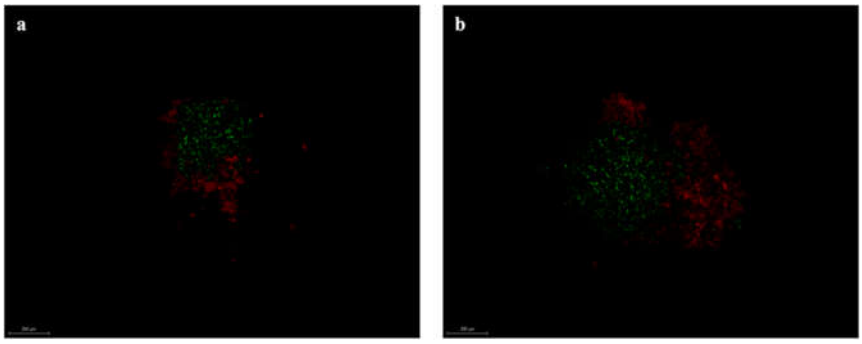


Figure 21. Confocal microscope images of MDA-MB-231$^{dsRed}$ and MCF-10A$^{eGFP}$ cells cultured in the levitation system for 48 hours in the presence of 5 mM $Ca^{2+}$ and 100 mM $Gd^{3+}$ with 1:4 cell loading ratio. Total cell concentration: 2.5x$10^5$ cells/ml (a) and 5x$10^5$ cells/ml (b) Scale bar: 200 μm.

To investigate the impact of cell loading order, first, MCF-10A$^{eGFP}$ cells were cultured, and after 24 hours, MDA-MB-231$^{dsRed}$ cells were introduced to the culture medium with a cell loading ratio of 4:1, respectively. The cells were co-cultured for additional 24 hours (Figure 22).

In the first experiment, it was observed that a significantly low number of MCF-10A$^{eGFP}$ cells was observed within the spheroid (Figure 22a). On the other hand, in the second experiment, MCF-10A$^{eGFP}$ cells appeared to remain viable and present within the spheroid after 48 hours, while MDA-MB-231$^{dsRed}$ cells were predominantly located at the outer sites of the spheroids. This was what we aimed for this experiment by putting MDA-MB-231$^{dsRed}$ cells in the system after MCF-10A$^{eGFP}$ spheroids were formed. Nonetheless, upon observing the second levitation photograph, (Figure 22b a blurry region was noted on the upper side of the spheroid potentially indicating the presence of cells that failed to integrate into the spheroid structure. Although the spheroid was intact, it gravitated to the bottom of the culture tube. This observation suggests that a portion of the MDA-MB-231$^{dsRed}$ cells may have attached to MCF-10A$^{eGFP}$ cells within the spheroid, contributing to their gravitation together. The second experiment was not reproducible because the result was similar to the first experiment when we applied the same order of cell loading again (Figure 22c).

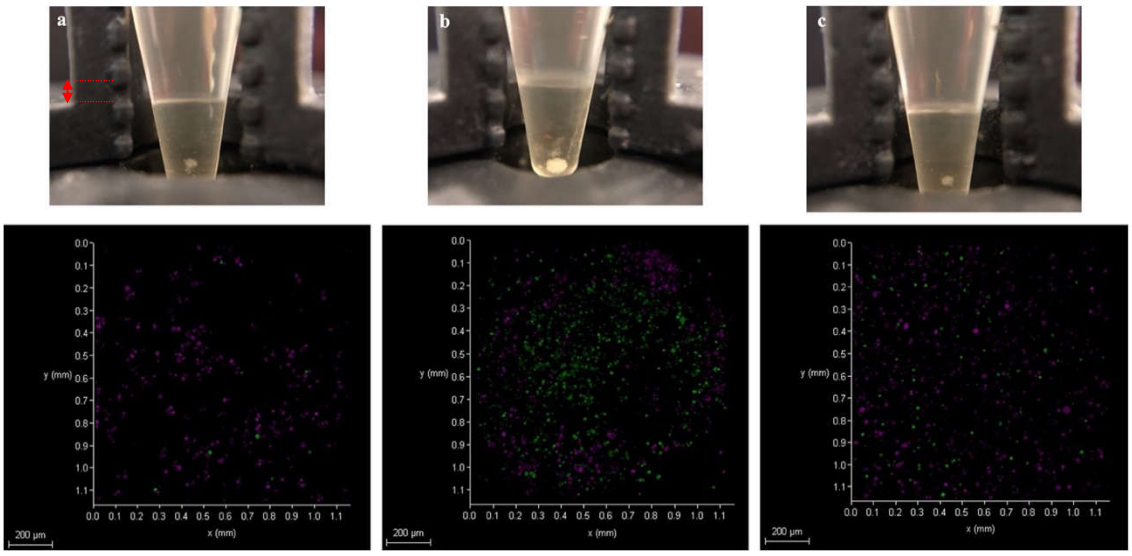


Figure 22. Confocal microscope images of MCF-10A$^{eGFP}$ and MDA-MB-231$^{dsRed}$ cultured in the levitation system for 48 hours in the presence of 5 mM $Ca^{2+}$ and 100 mM $Gd^{3+}$ with a 4:1 cell loading ratio, respectively. Total cell concentration: 5x10$^5$ cells/ml (a, b, c). n= 3. Magenta: MDA-MB-231$^{dsRed}$, green: MCF-10A$^{eGFP}$. Scale bar: 200 µm.

To investigate spatial distribution of two cell types within a spheroid structure when co-cultured from the outset, the cells were mixed and introduced into the levitation culture at different cell loading ratios (1:1, 1:2, and 1:4). The cells were cultured for 24 and 48 hours (Figure 23). Subsequently confocal microscopy was employed to analyze spatial distribution of the two cell types within the spheroids (Figure 24).

Irrespective of culture duration or cell loading ratio, each cell type exhibited a strong tendency to cluster with cells of the same origin. This observation was attributed to differences in volumetric mass densities and, consequently, levitation heights of the two cell types.

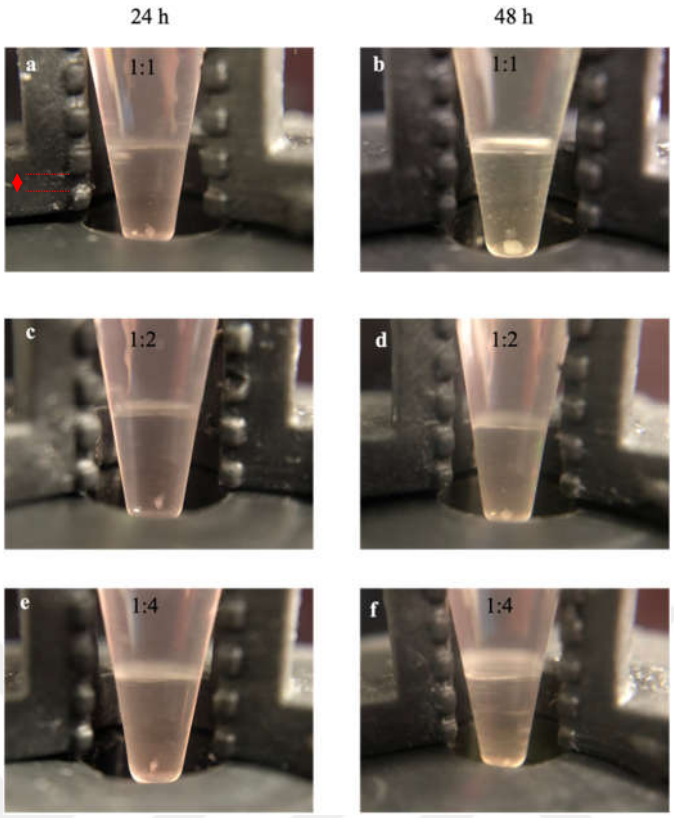


Figure 23. Magnetic levitation images of MDA-MB-231$^{dsRed}$ and MCF-10A$^{eGFP}$ cells cultured with single ring magnet-based levitation system for 24 (a,c,e) and 48 (b,d,f) hours in the presence of 5 mM $CaCl_2$ and 100 mM $Gd^{3+}$. Cell loading ratios: 1:1 (a,b) , 1:2 (c,d) , 1:4 (e,f). Total cell concentration: 5x$10^5$ cells/ml. n=3. Each vertical scale: 1 mm.

To investigate this further, microcapillary magnetic levitation was carried out with MCF-10A$^{eGFP}$ and MDA-MB-231$^{dsRed}$ cells to detect any differences in their single-cell densities, in the presence of 25 mM $Gd^{3+}$ (Figure 25). The results demonstrated that MDA-MB-231$^{dsRed}$ cells exhibited significantly higher average levitation heights compared to MCF-10A$^{eGFP}$ cells (Figure 26, Table 1). These finding suggests that within the magnetic levitation system, MDA-MB-231$^{dsRed}$ cells preferentially occupy the upper regions of the formed spheroids.

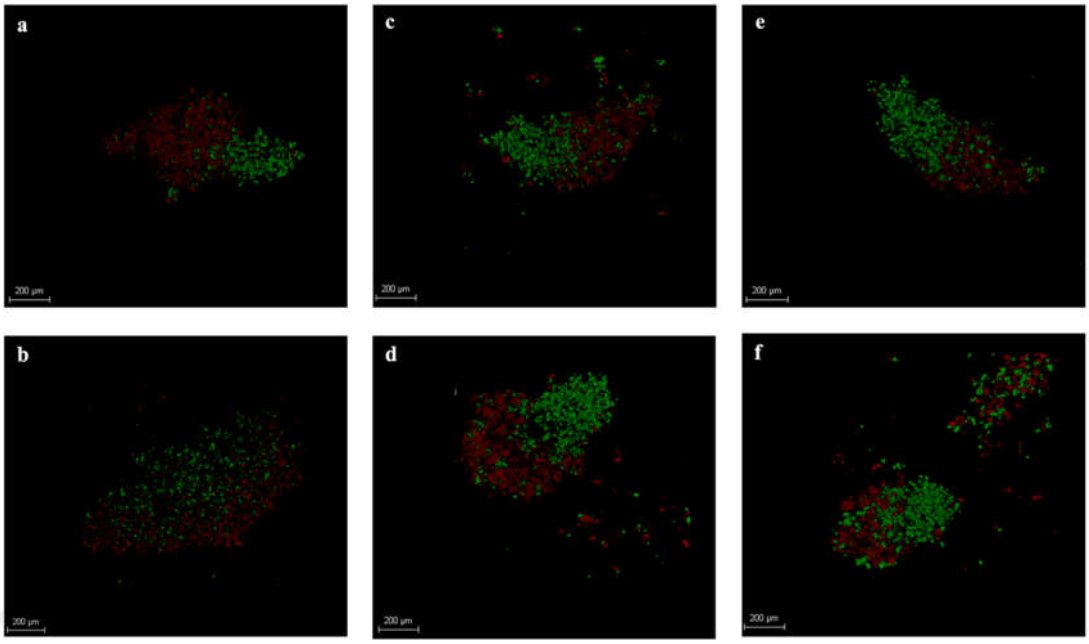


Figure 24. Confocal microscope images of MDA-MB-231$^{dsRed}$ and MCF-10A$^{eGFP}$ cells cultured in the levitation system for 24 (a,c,e) and 48 hours (b,d,f) in the presence of 5 mM $Ca^{2+}$ and 100 mM $Gd^{3+}$. Cell loading ratios: 1:1 (a,b) , 1:2 (c,d) , 1:4 (e,f). Total cell concentration: $5x10^5$ cells/ml. Scale bar: 200 µm.

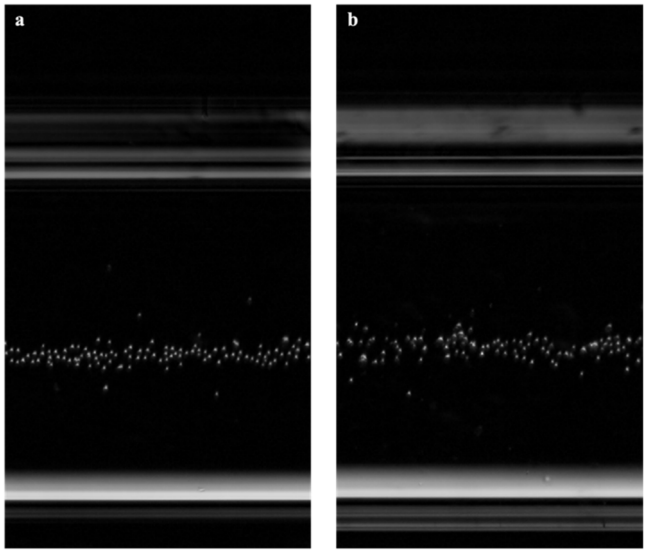


Figure 25. Levitation micrographs of MCF-10A$^{eGFP}$ (a) and MDA-MB-231$^{dsRed}$ cells (b) in the presence of 25 mM $Gd^{3+}$. n=3.

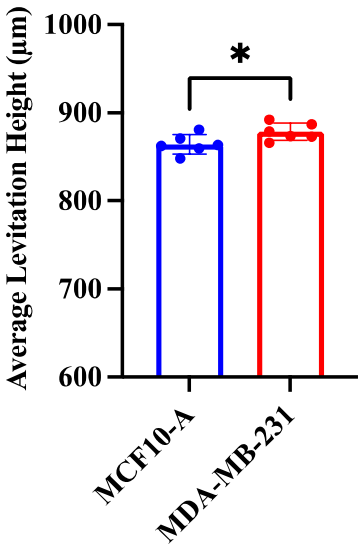


Figure 26. Levitation profiles of the MCF-10A$^{eGFP}$ and MDA-MB-231$^{dsRed}$ cells in the presence of 25 mM $Gd^{3+}$. n=3. * indicates a statistically significant difference ($p<0.05$) between the two groups.

Table 1. Analysis of levitation profiles of the MCF-10A$^{eGFP}$ and MDA-MB-231$^{dsRed}$ cells.

| | Mean | Minimum | Maximum | Range | Std Dev | Skew | CoV(%) |
|---|---|---|---|---|---|---|---|
| MCF-10A | 864.3 | 848.1 | 880.9 | 32.79 | 11.03 | 0.133 | 1.28% |
| MDA-MB-231 | 878.4 | 865.8 | 892.3 | 26.46 | 9.743 | 0.3345 | 1.11% |

To further investigate cell positioning, the cells were co-cultured from the beginning for 48 hours at a 1:4 cell loading ratio. After 48 hours, spheroids seemed to be localized on the bottom of the culture tube, but they were compact and stable (Figure 27). Formed spheroids were transferred onto an agarose surface to examine their behavior in long-term culture in the absence of attachment. Confocal microscopy was employed to monitor cell behavior at different time points (Day 0,1,2 and 5) (Figure 28).

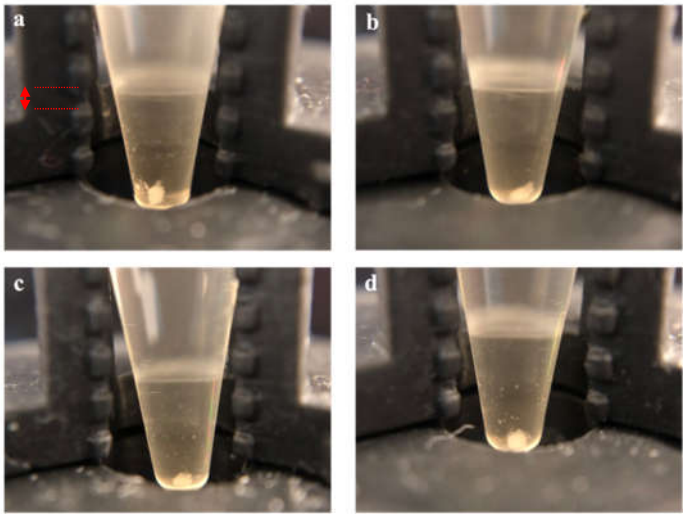


Figure 27. Magnetic levitation images of MDA-MB-231$^{dsRed}$ and MCF-10A$^{eGFP}$ cells cultured with single ring magnet-based levitation system in the presence of 5 mM $CaCl_2$ and 100 mM $Gd^{3+}$. Cell loading ratio: 1:4 (a,b,c,d). Total cell concentration: $5x10^5$ cells/ml. n=4. Each vertical scale: 1 mm.

Observations revealed that MDA-MB-231$^{dsRed}$ cells exhibited proliferative activity and migrated towards the regions occupied by MCF-10A$^{eGFP}$ cells within the spheroid structure. This finding aligns with a previous studies demonstrating that MCF10A$^{eGFP}$ cells enhance the invasive and protrusive properties of MDA-MB-231$^{dsRed}$ cells through interactions between integrins on the cancer cells and laminin proteins secreted by normal breast epithelial MCF10A$^{eGFP}$ cells (M.-H. Lee et al. 2015).

As days go by, MCF-10A$^{eGFP}$ cell viability appear to decline, as evidenced by a decrease in their fluorescence signal. In contrast, MDA-MB-231$^{dsRed}$ breast cancer cells, which are not dependent on the attachment to a surface, remained viable and continued to proliferate, as observed in the confocal images. By day five, a significant reduction in the number of viable MCF-10A$^{eGFP}$ cells was observed, highlighting their dependence on attachment to a surface for sustained proliferation.

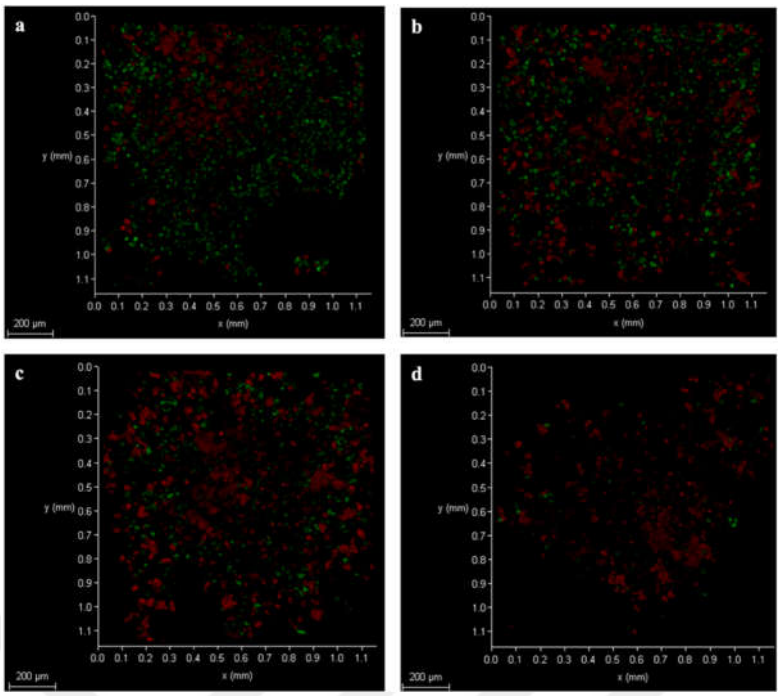


Figure 28. Confocal microscope images of MDA-MB-231$^{dsRed}$ and MCF-10A$^{eGFP}$ spheroids on agarose gel at day 0 (a), day 1 (b), day 2 (c), and day 5 (d). [$CaCl_2$] = 5 mM and [$Gd^{3+}$] =100 mM. Cell loading ratio: 1:4. Total cell concentration: 5x$10^5$ cells/ml. n=4. Scale bar: 200 µm.

## 2.4. Conclusions

Various magnetic manipulation techniques based on positive and negative magnetophoresis have been employed to biofabricate cellular assemblies that model different tissues. Positive magnetophoresis, which involves internalizing or labeling cells with magnetic nanoparticles, has been utilized in biofabrication of self-assembled spheroids and cellular aggregates (Souza et al. 2010; Daquinag, Souza, and Kolonin 2012; J. A. Kim et al. 2013; W. R. Lee et al. 2011; Ho et al. 2013; Gaitán-Salvatella et al. 2021; Mejía-Cruz et al. 2019). As mentioned before, the positive magnetophoresis method presents several limitations, including potential risk to cell viability due to the presence of labeling particles, the requirement for lengthy experimental procedures, and the inability to accurately mimic *in vivo* tissue environments due to the presence of exogenous magnetic particles. In contrast, negative magnetophoresis technique, which

does not require the use of any labeling tools, offers a faster, more cost-effective, and safer alternative for cell manipulation. This technique has been successfully utilized in the fabrication of cellular assemblies and spheroids using various cell types (Akiyama and Morishima 2011; Abdel Fattah et al. 2016; Tocchio et al. 2018; Parfenov et al. 2018; Anil-Inevi et al. 2020; 2021; 2019; 2018; Sarigil et al. 2021; Onbas and Arslan Yildiz 2021; Türker, Demirçak, and Arslan-Yildiz 2018; Moncal, Yaman, and Durmus 2022; Parfenov et al. 2020).

In this study we attempted to create a core-shell structure to mimic the *in vivo* ductal breast carcinoma structure without any extra force or guidance and any scaffold material, in a single ring magnet-based levitation system. As in the microcapillary based levitation method, regardless of the cell loading order, the same type of cells grouped among themselves. Unlike the microcapillary-based methods, where elongated, string-like cellular structures are typically formed due to the elongated shape and parallel positioning of the magnets, the ring magnet levitation system enabled the formation of more-spheroid like aggregates. Furthermore, the diameter of the spheroids was tunable and bigger compared to those generated using microcapillary system. Also, the ease of manipulating the culture medium within the system was makes this approach well-suited for subsequent tissue engineering and cell biology experiments.

# CHAPTER 3

# IMPROVING THE SCAFFOLD-FREE SPHEROID MODELS BY UTILIZING THE MACROMOLECULAR CROWDING METHOD

## 3.1. Introduction to the Role of Extracellular Matrix in Tissue Models

The acellular environment surrounding within the cells in tissues is termed as the extracellular matrix (ECM). The ECM is a comprehensive and three-dimensional molecular network built by structural and functional proteins. This intricate network plays a crucial role in regulating various cell functions through physiological and biochemical signals. Defects or irregularities in the structure and function of ECM can lead to a variety of disease conditions, including cancer (Fernandes et al. 2009; Urciuolo, Imparato, and Netti 2023; Hogan et al. 2011; Pathak and Kumar 2012).

Structural proteins, proteoglycans, glycosaminoglycans, cell adhesion molecules, and signaling molecules such as growth factors and cytokines compose the 3D fibrillar network of the ECM (Yong, Oh, and Kim 2020). This intricate structure reserves a lot of biomechanical and biochemical factors specific to each tissue and organ (Karamanos et al. 2021). Besides, ECM composition varies according to circumstances such as disease, aging, and some external influences (Urciuolo, Imparato, and Netti 2023; Frantz, Stewart, and Weaver 2010). A dynamic bidirectional communication exists between cells and the ECM. Cells continuously modify the spatial structure and composition of the ECM through processes such as degradation, synthesis, and biochemical alterations. Therefore, the ECM is considered to be a dynamic and responsive environment (Hansen et al. 2015; Doyle, Nazari, and Yamada 2022).

The extracellular matrix is an important element in regulating homeostasis in tissues under normal circumstances and regulating the changes under pathological

conditions by providing biochemical and biomechanical signals to cells. Furthermore, the ECM plays a significant role in the remodeling of cells for adaptation to a new state by mechanoregulation processes (Humphrey, Dufresne, and Schwartz 2014). Fibroblasts are a diversity of cells in charge of providing different aspects to specific tissues or organs by producing a variety of ECM molecules to form a connective tissue. Fibroblasts synthesize a variety of ECM components including collagens, fibronectin, laminin, elastin, glycosaminoglycans, proteoglycans, hyaluronic acid, growth factors and cytokines, which are assembled in different combinations to regulate the function of the surrounding tissue and organ in which they are located (Plikus et al. 2021).

Fibroblasts are stromal cells that typically reside in a quiescent state under normal conditions. In response to tissue repair and wound healing processes, they are induced to differentiate into contractile myofibroblasts (Gabbiani, Ryan, and Majno 1971), which exhibit increased ECM production and proliferation (Hinz et al. 2012). Following healing, myofibroblasts revert to fibroblast form (Plikus et al. 2021). However, in fibrotic diseases or during tumor initiation and progression, fibroblasts undergo uncontrolled activation and produce vast amounts of ECM proteins (Hebert et al. 2020). Thus, this uncontrolled activation has led to consideration of cancer as a kind of "wound that does not heal" (Dvorak 2015). Non-mutant cells in the tumor microenvironment that lack markers for epithelial, endothelial, specialized mesenchymal, or immune cells are considered cancer-associated fibroblasts (CAFs). Notably, CAFs constitute a significant portion of the tumor microenvironment, comprising approximately 80 % of the stromal compartment. CAFs engage in continuous reciprocal communication with cancer cells (Truffi, Sorrentino, and Corsi 2020). In addition to producing structural proteins, CAFs also secrete mitogenic growth factors (Balkwill, Capasso, and Hagemann 2012), playing a crucial role in regulating angiogenesis, tumor progression, metastasis, and response to anti-cancer treatments along with the other non-mutant cells in the tumor stroma.

Cells and their ECM cannot be viewed as separate entities, as they are interconnected and work together. For this reason, in *in vitro* studies, it is crucial to provide an extracellular environment that will allow cells to perform their specific functions properly. Conventional 2D and 3D scaffold-based *in vitro* models, utilizing synthetic or natural materials, fail to fulfill this task adequately. Although they provide mechanical support to the cells, they lack the complex signalling cascades found in the natural ECM (Rozario and DeSimone 2010).

To overcome the limitations related to immunological incompatibility and failure to fully represent the ECM structure, several strategies have been implemented. These include decellularizing natural tissues and organs to obtain native-like ECM (Solarte David et al. 2022; Assunção et al. 2020) and inducing somatic cells to produce ECM specific to the tissue or pathological condition (Urciuolo et al. 2016). Another approach is to produce ECM without decellularization; by culturing the stromal cells on 2D plates into cell sheets by their self-assembling ability (Roy et al. 2020) or by immobilizing the stromal cells onto microbeads suspended in a bioreactor to induce the assembly of a connective microtissue (Brancato et al. 2017). Although these strategies recapitulate the ECM composition quite successfully, they require a considerable amount of time to produce ECM. Furthermore, the amount of ECM generated may not be sufficient for constructing a 3D structure. For instance, the cell sheets have approximately 20 µm thickness, necessitating stacking to achieve reasonable dimensions (Tsiapalis and Zeugolis 2021). Additionally, decellularization processes often involve the use of chemical agents, which can potentially disrupt the structure and activity of macromolecules within the ECM.

It is well-established that the tissue-specific extracellular matrix regulates cell functioning through biological signals and leads to pathological conditions if not properly regulated (Insua-Rodríguez & Oskarsson, 2016; Keller et al., 2021). Therefore, extracellular matrix accumulation is an important limiting factor in the formation of 3D *in vitro* models. In their natural environment, cells synthesize and secrete a multitude of macromolecules, creating a densely populated extracellular milieu. In contrast, the dilute nutrient media typically used in *in vitro* cultures cannot replicate this crowded extracellular environment (Habanjar et al., 2021; Hoarau-Véchot et al., 2018). Therefore, strategies aimed at improving and accelerating natural production and accumulation of ECM should be prioritized in tissue engineering studies.

## 3.2. Introduction to the Macromolecular Crowding Method

Recent studies have demonstrated that the “macromolecular crowding” method significantly accelerates and increases the accumulation of tissue-specific extracellular matrix proteins while preserving the phenotypic properties of cells in *in vitro* culture

(Garnica-Galvez et al. 2021; Graceffa and Zeugolis 2019; Korntner et al. 2023; Rampin et al. 2022; Ryan et al. 2023; Shologu et al. 2022; Tsiapalis et al. 2021; Djalali-Cuevas et al. 2019). The principle of macromolecular crowding is underpinned by the second law of thermodynamics. Due to the of steric hindrance and the chemical interactions, molecules within a confined system cannot occupy the same position at the same time and thus exert an exclusionary effect on each other. When a specific macromolecule is introduced into to the system, decreases the volume of possible locations where the molecules can be found, leading to a decrease in system (Sharp 2015). As the concentration of macromolecules added to the environment increases, the system tends to increase entropy by maximizing molecular interactions and expanding the available volume (Kuznetsova et al. 2015; Minton 2006; Ralston 1990). This principle can be illustrated by considering the fate of pro-collagen, a water-soluble precursor of collagen. In a crowded extracellular environment, the increased frequency of molecular encounters facilitates the interaction between pro-collagen and proteases, leading to efficient conversion into water-insoluble collagen, a key component of the extracellular matrix. In contrast, in an external environment where molecules are sparse, the probability of encountering procollagen and proteases is significantly lower, increasing the likelihood of procollagen inactivation or degradation before conversion to collagen can occur, therefore decreasing the accumulation of collagen in the extracellular environment (Figure 29) (Tsiapalis and Zeugolis 2021).

*In vitro* culture studies with different cell types have demonstrated that various macromolecular crowding agents including carrageenan, dextran, polyethylene glycol and Ficoll, significantly increase the accumulation of tissue-specific extracellular matrix proteins (Tsiapalis and Zeugolis 2021). Among these, carrageenan protein has been shown to be the agent that plays the fastest and most effective role in increasing extracellular matrix accumulation due to its negative charge and polydispersity (Gaspar, Fuller, and Zeugolis 2019; Satyam et al. 2014)

Previous studies have demonstrated that macromolecular crowding (MMC), increased the ECM accumulation on several types of fibroblasts, particularly when carrageenan used as the macromolecular crowding agent (Shologu et al. 2022; Gaspar, Fuller, and Zeugolis 2019; Djalali-Cuevas et al. 2024; Tsiapalis and Zeugolis 2021; Kumar et al. 2015; Satyam et al. 2014). Furthermore, it has been shown that when breast cancer cells cultured on the dECM derived from different types of fibroblasts exposed to MMC exhibit increased expression of markers specific to the breast cancer cells and

enhanced drug resistance. These findings suggest that macromolecular crowding provides more relevant *in vitro* 3D models for assessing the pharmacological properties of the tumor cells (Shologu et al. 2022). Notably, in a previous study, macromolecular crowding using Ficoll and Dextran was shown to increase the ECM deposition in mesenchymal stem cell spheroids grown on methylcellulose hydrogels (Chiang et al. 2021).

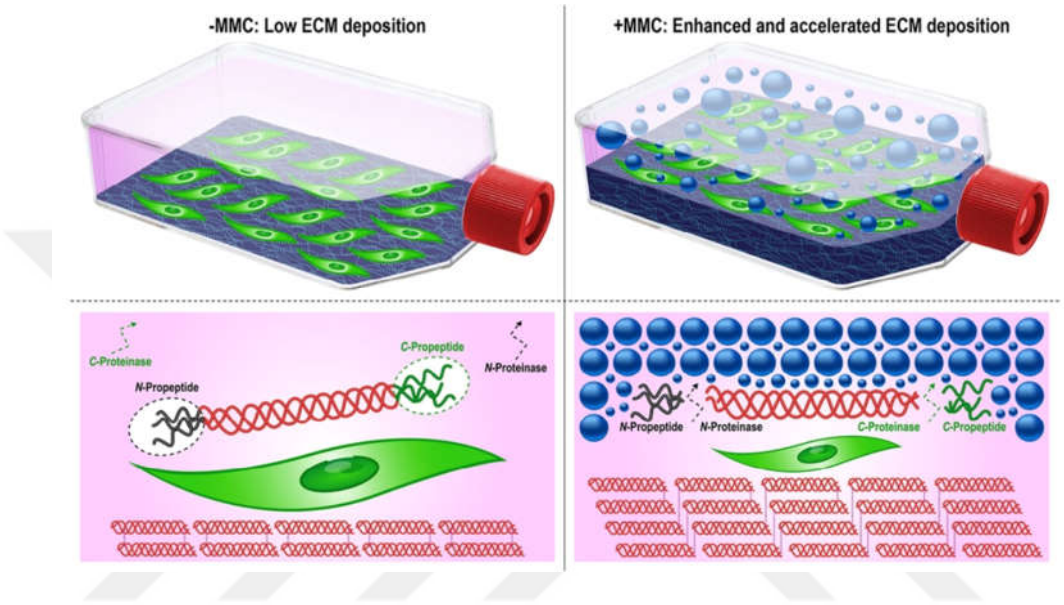


Figure 29. In a dilute cell culture medium (-MMC), N- and C-proteinases are inactivated, and water-soluble procollagen dissolves before interacting, resulting in low collagen deposition (left). In crowded cell cultures (+MMC), the diffusion of procollagen and proteinases is restricted, thus the interactions of molecules with each other increase and collagen accumulation increases and accelerates (right) (Source: Tsiapalis and Zeugolis 2021).

The influence of the macromolecular crowding method on a 3D scaffold-free spheroid model has yet to be evaluated. This section of the thesis aimed to evaluate the application of the macromolecular crowding method, which has been shown to enhance the extracellular matrix accumulation, on scaffold-free spheroid models formed by magnetic levitation technique. It was hypothesized that MMC method would be effective in generating improved 3D spheroid models that more closely resemble the *in vivo* tissue. Fibroblasts and breast cancer cells were selected as model cell types for this application.

## 3.3. Methods

### 3.3.1. Cell Culture and Macromolecular Crowding

WS1, HDFa and MDA-MB-231$^{dsRed}$ cells were expanded in Dulbecco's modified Eagle's high glucose medium containing 10% FBS and 1% P/S. During this process, the cells were stored in a standard incubator (37°C, 5% $CO_2$). When they grew enough to reach the confluency of 70-80% they were passaged by removing them with trypsin. For 2D application of macromolecular crowding, WS1 cells were seeded in 24-well plates at 25,000 cells/cm$^2$ and they were allowed to be attached onto the surface by leaving them for 24 hours in the basal medium. After the cells adhered, the culture medium was replaced on alternate days with macromolecular crowding medium, which contains 100 µM L-ascorbic acid 2-phosphate (AA) in control (-MMC) and MMC-treated (+MMC) groups. +MMC culture medium additionally had 50 µg/ml carrageenan.

### 3.3.2. Magnetic Levitation of Cells

WS1, HDFa and MDA-MB-231$^{dsRed}$ cells in the paramagnetic media were transferred to the tubes (transparent PCR tubes) where magnetic levitation would take place, with the cell concentration and $Gd^{3+}$ concentration specified in the relevant experimental design. The tubes to be used in the magnetic levitation mechanism were fixed with their midpoints at the hole of the ring magnet. They were imaged with a standard camera and the images were recorded for analysis. As time goes by, the cell aggregates formed a stable position above the local bottom magnetic field on the magnet hole. In co-culture studies, it was planned to obtain stable three-dimensional spheroid-like structures in levitation culture with MDA-MB-231$^{dsRed}$ and HDFa cells. During the experiment, cells were stored in a standard incubator (37°C, 5% $CO_2$) along with all components of the levitation apparatus. The images obtained were used for morphological analysis of the structures formed.

### 3.3.3. Cell Metabolic Activity Assessment

Metabolic activity analysis of cells was performed using alamarBlue® analysis. First, 10% alamarBlue® solution was prepared in Hanks' Balanced Salt Solution (HBSS). Then spheroids were washed with HBSS and 200 µl of the alamarBlue® solution was added to the wells that contain the spheroids. As a negative control, alamarBlue® solution alone added to the wells. The spheroids were incubated for 3 hours at 37ºC, 5% $CO_2$. After 3 hours, 100 µl of cell solutions with alamarBlue® and controls were transffered to a 96-well plate. Absorbance values were read at 550 nm and 595 nm, and the percentage of the alamarBlue® reduced by the cells was calculated.

### 3.3.4. Application of Macromolecular Crowding on Three-Dimensional Spheroid Cultures

After the spheroids cultured for 24 hours, they were transferred into U-bottom 96 well plates (BIOFLAT™) and macromolecular crowding medium was added to the wells. The macromolecular crowding medium was renewed every other day during the determined culture period, as previously explained.

### 3.3.5. Quantification of Collagen Amount in 2D and Spheroid Cultures

At the end of the culture period, the collagen amount in the samples was analyzed. The amount of collagen Type-I was quantified by SDS-PAGE for 2D culture of WS1 fibroblasts by following the protocol described previously (Capella-Monsonís et al. 2018). For immunofluorescence analysis of 2D fibroblast cell layers, the cell layers were washed with 1X PBS 3 times for 5 min each, fixed with 3% paraformaldehyde (PFA) for 20 min, washed with PBS 3 times for 5 min each, and then blocked with 3 % bovine serum albumin (BSA) and incubated overnight at 4 ◦C with the mouse monoclonal

primary antibody for Collagen type-I (Santacruz SC-59772). Next day, the cell layers were washed with PBS 3 times for 5 min each, and they were incubated with FITC labeled secondary antibody (donkey anti- mouse IgG (1:500, ThermoFisher Scientific, A21202) at room temperature for 30 min. After that, the cell layers were washed 3 times for 5 min each with PBS again and nuclei staining was done by Hoecht staining. The layers were washed with PBS again 3 times for 5 min each and imaging was done with an Olympus IX73P1F microscope. The images were analyzed by using the Image J software.

For the HDFa and MDA-MB-231$^{dsRed}$ spheroids, images were acquired on an Olympus CKX 53 inverted microscope and analyzed with ImageJ software. Collagen amount in the spheroids was quantified by the Sirius Red staining protocol. First, the spheroids were washed with PBS 3 times and fixed with 3% paraformaldehyde (PFA) for 20 min. Then they were washed again with PBS 3 times. After washing, 200 µl of 1 w/v% Sirius Red solution (Direct Red 80 powder dissolved in picric acid) was added on each spheroid and incubated for 30 min at room temperature. Following the incubation, the spheroids were washed with dd$H_2O$ for the required times to have a clear solution. 200 µl of destaining solution (NaOH:MeOH (1:1)) was added on spheroids and incubated for 30 min at room temperature. 150 µl of the solution was transferred to a 96-well plate, and the absorbances were read at 405 nm.

### 3.3.6. Statistical Analysis

Results were expressed as mean ± standard deviation for each experiment. Each experiment had at least 3 samples in each repetition. In cases where statistical comparisons need to be made, the differences between groups were measured by ANOVA test, 5% was considered as the significance limit.

## 3.4. Results and Discussion

To establish a baseline for evaluating the impact of macromolecular crowding method on 3D spheroid cultures, a 2D *in vitro* culture model using WS1 human skin

fibroblasts was employed. This experiment focused on analyzing the effect of macromolecular crowding on the deposition of ECM deposition in WS1 cells. ECM deposition (Col-I) was assessed at 4,6 and 8 days after the initiation of culture.

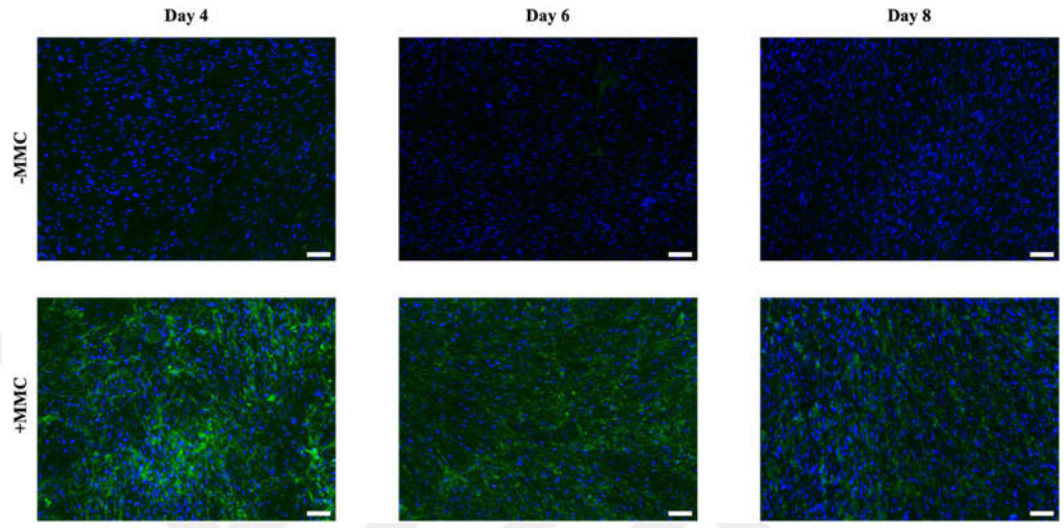


Figure 30. Fluorescent micrographs of WS1 skin fibroblasts after immunofluorescence staining for Col-I after 4,6 and 8 days in culture with (50 µg/ml carrageenan) and without the MMC medium. Collagen type I: green. Hoechst 33342 Fluorescent stained nuclei: blue. n = 3. Scale bar: 100 µm.

Fluorescent immunostaining analysis revealed that macromolecular crowding (+MMC) significantly enhanced collagen type I deposition, compared to control (-MMC) samples at each time point (Figure 30).

Analysis revealed that macromolecular crowding significantly increased collagen deposition (green signal) in the MMC groups. Concomitantly, a reduction in cell spreading was observed compared to the non-crowded controls. This observation was attributed to the accumulation of collagen layers within the extracellular environment of the cells, which likely exerted spatial constraints on cell spreading (Figure 31). Subsequent fluorescent intensity analysis confirmed that Col-I deposition in WS1 culture was significantly increased ($p < 0.05$) by macromolecular crowding at all time points (Figure 32).

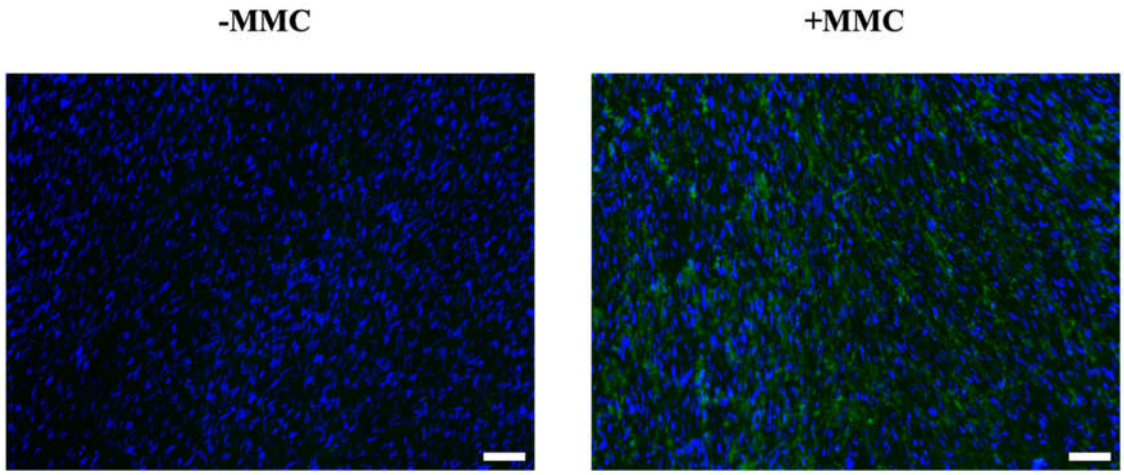


Figure 31. Fluorescent micrographs of WS1 skin fibroblasts after immunofluorescence staining for Col-I 6 days in culture with (50 µg/ml carrageenan) and without the MMC medium. Collagen type I: green. Hoechst 33342 Fluorescent stained nuclei: blue. n = 3. Scale bar: 100 µm.

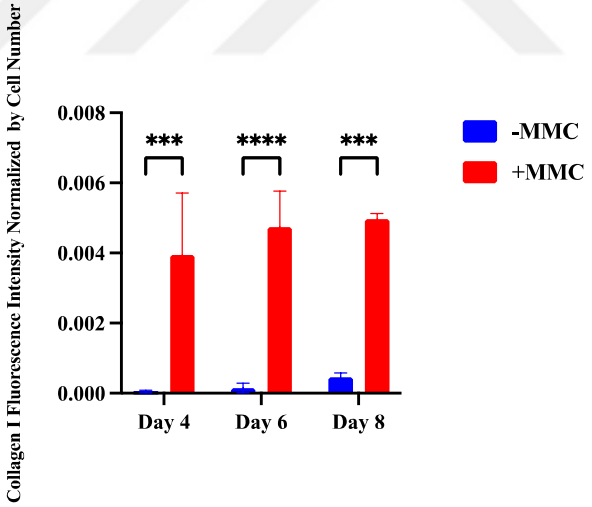


Figure 32. Collagen type I fluorescence intensity analysis normalized to cell number (%) of WS1 cell layers after 4, 6, and 8 days in culture with (50 µg/ml carrageenan) and without the MMC medium. n=3. *** and **** indicate statistically significant differences ($p<0.001$ and $p<0.0001$, respectively) between the groups.

Subsequently, sodium dodecyl sulphate polyacrylamide gel electrophoresis (SDS-PAGE) was performed at certain time points (Day 4, 6 and 8) to quantitatively determine the amount of collagen deposited in both cell groups (Figure 33).

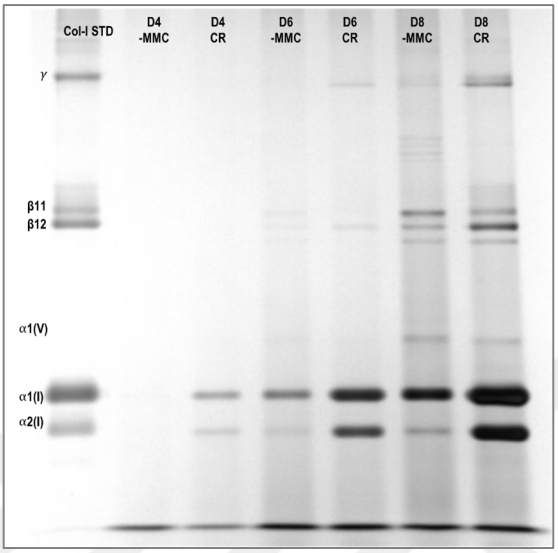


Figure 33. Analysis of collagen content in electrophoresis gels of the WS1 cell layers after 4, 6, and 8 days of culture under -MMC and +MMC conditions. Col-I STD: collagen type I standard. n=3.

Supplementary densitometric analysis unveiled that the Col-I content in the cell layers were significantly ($p<0.05$) higher in +MMC groups at Day 6 and Day 8 compared to non-crowding groups with the exception of Day 4. Furthermore, Col-I accumulation was increased from Day 4 to Day 8 of culture under both -MMC and +MMC conditions (Figure 34).

This study aimed to investigate the effect of the macromolecular crowding method on 2D layers of fibroblast cells. The experiments demonstrated a statistically significant increase in collagen accumulation within these 2D cultures. Subsequently, the application of this technique on 3D spheroid structures and the investigation of its effect on ECM accumulation were carried out.

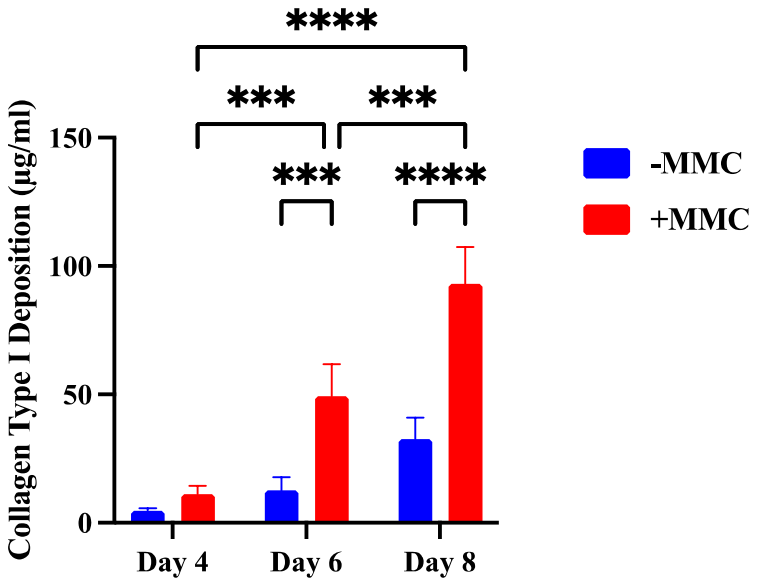


Figure 34. Densitometry analysis of electrophoresis gels of WS1 cell layers after 4, 6, and 8 days of culture in non-crowding and MMC medium. n= 3. *** and **** indicate statistically significant differences ($p<0.001$ and $p<0.0001$, respectively) between the groups.

WS1 cells were cultured for the first time within the magnetic levitation system resulting in the formation of fibroblast spheroids after 24 hours. Subsequently, the spheroids transferred to U-bottom 96 well-plates and the media were renewed every other day. Starting from the third day of culture, we observed that the cells began to spread outward from the center of the spheroids. By the end of the culture time, a comparatively small portion of the original spheroid were intact (Figure 35).

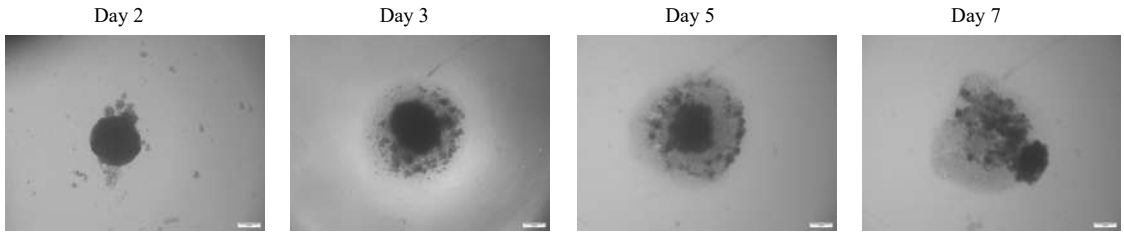


Figure 35. Micrographs of WS1 spheroids after 1,3,5 and 7 days in culture in growth medium. n=3. Scale bar: 100 µm.

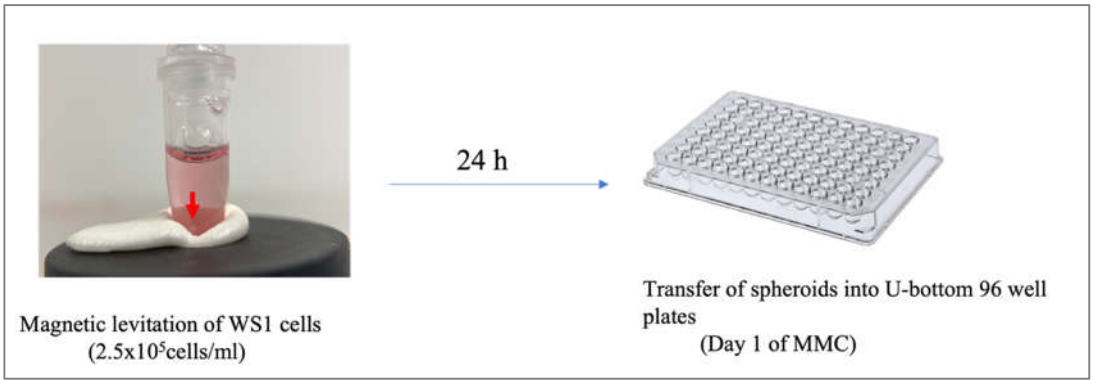


Figure 36. Schematic for the first experimental method. The spheroids were obtained in the magnetic levitation system, and they were transferred to well plates after 24 h for macromolecular crowding.

Following this, to investigate the effect of macromolecular crowding on fibroblast spheroids, two experimental methods were employed. In the first method, cells were cultured in the magnetic levitation system for 24 hours in the paramagnetic medium that contains 150 mM $Gd^{3+}$. After 24 hours of culture, the spheroids were transferred to U-bottom 96-well plates and the magnetic levitation medium was replaced with macromolecular crowding medium. The crowding medium consisted of 50 µg/ml carrageenan and 100 µM L-ascorbic acid 2-phoshpate (AA) in the +MMC groups; and 100 µM L-ascorbic acid 2-phoshpate (AA) alone in control (non-crowing) groups. The culture media were renewed every other day in the absence of $Gd^{3+}$ (Figure 36).

Microscopic analysis revealed that in the control groups, cells within the spheroid structures exhibited outward migration from the center over time (Figure 37). Concomitantly, a significant decrease in the core area of the compact spheroid structures was observed from one day to the next time point (Figure 38), with this reduction become statistically significant from Day 3 ($p<0.05$). In contrast, in the crowding group (+MMC), cell spreading from the center of the spheroids was less pronounced compared to the control groups. Furthermore, the average area of the spheroids in the +MMC group was significantly larger compared to the control group starting from Day 5 ($p<0.05$). Notably, the average spheroid area in the +MMC group did not exhibit any statistically significant changes over time, indicating consistent stability throughout the culture time. This stability can be attributed to the increased collagen production in the +MMC group, which

likely restricted cell spreading and maintained a more compact spheroid structure, mirroring the observations made in the 2D cell layer experiments.

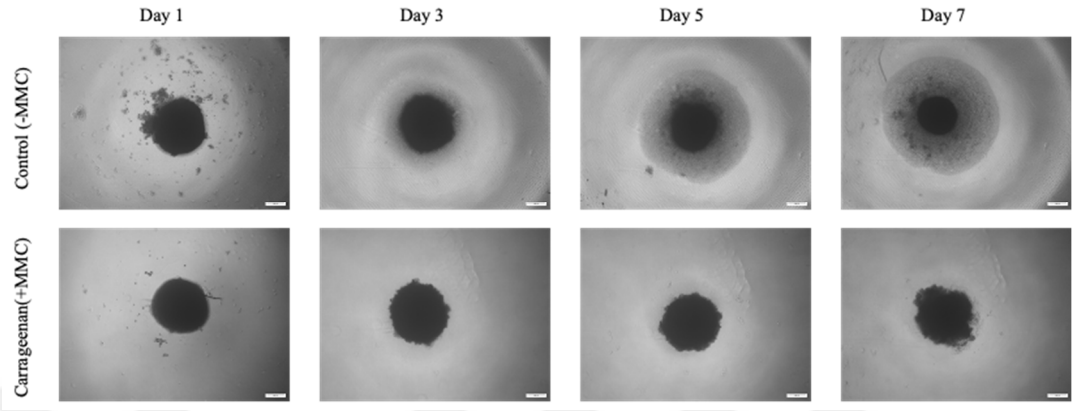


Figure 37. Micrographs of WS1 skin fibroblast spheroids after 1,3,5 and 7 days in culture without (-MMC) and with MMC (Carrageenan at 50 µg/ml). n=3. Scale bar: 100 µm.

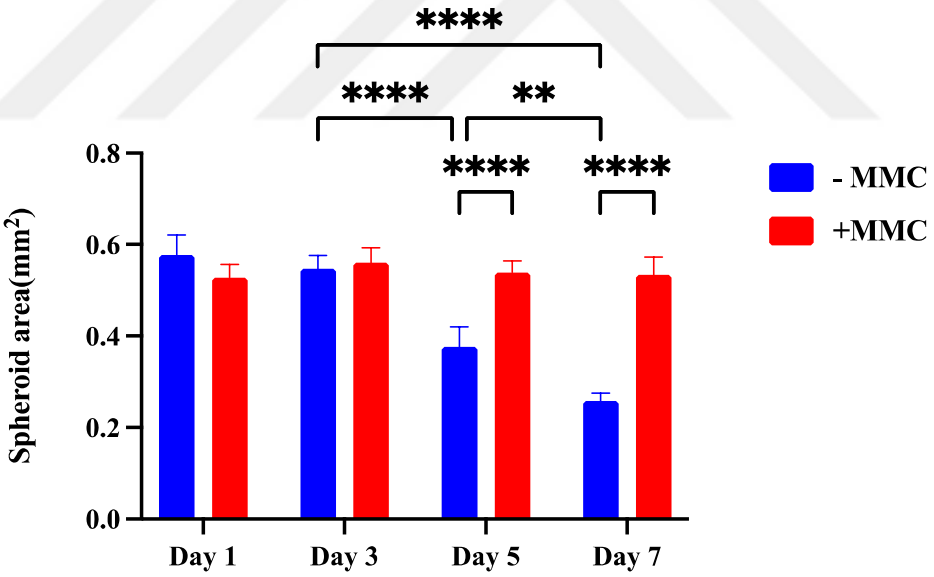


Figure 38. Comparison of the spheroid area over time between the control (-MMC) group and the macromolecular crowding (+MMC) group. Error bars represent the standard error of the mean (SEM). n=3. **and **** indicate statistically significant differences ($p<0.01$and $p<0.0001$, respectively) between the groups.

In the second experimental method, the macromolecular crowding was started in the magnetic levitation system (Figure 39). The cells were cultured in the magnetic levitation system for 24 hours in the paramagnetic medium containing 150 mM paramagnetic agent ($Gd^{3+}$). Three experimental groups were included: 1) a +MMC group containing 50 µg/ml carrageenan (CR) and 100 µM L-ascorbic acid 2-phosphate (AA); 2) a control (non-crowding) group containing only 100 µM L-ascorbic acid 2-phosphate (AA); 3) a carrageenan-only group containing only 50 µg/ml carrageenan (CR) in the medium. After 24 hours of culture, the spheroids were transferred to the U-bottom 96-well plates, and the culture media were refreshed every other day without $Gd^{3+}$.

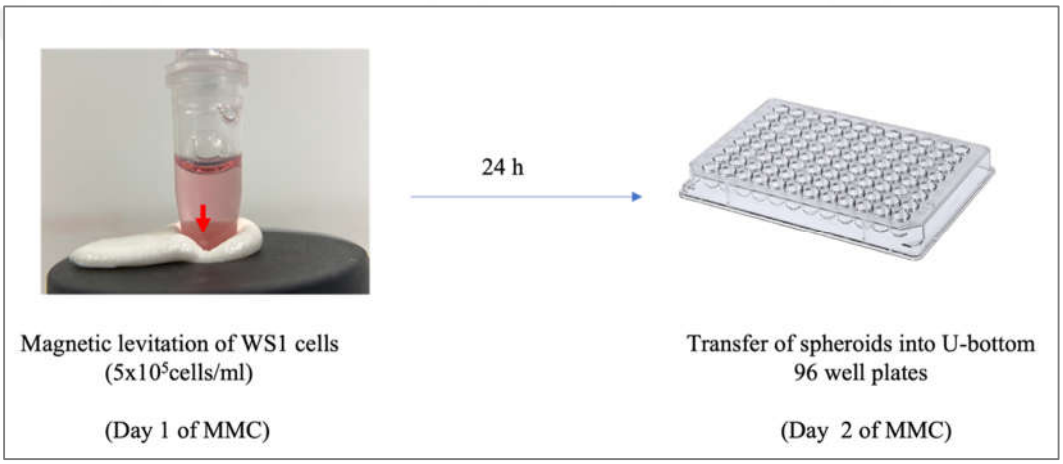


Figure 39. Schematic for the second experimental method where macromolecular crowding starts in the magnetic levitation system.

In the group supplemented with only ascorbic acid (AA) (Figure 40), the observed cell spreading dynamics closely resembled that of WS1 spheroids cultured without the application of macromolecular crowding (Figure 35). Furthermore, no significant differences in the average area of the spheroids were observed among these two groups at any time point ($p>0.05$).

When comparing all three experimental groups, the spheroids cultured in the medium containing both carrageenan and L-ascorbic acid (AA+CR) exhibited the least cell spreading from the spheroid core. These spheroids appeared more intact and bigger than those in other groups at the end of the culture period. In Notably, the average spheroid area in the AA+CR group, the was significantly bigger ($p<0.05$) than in the other

groups at all time points, except for Day 2 for all groups and Day 5 for the CR-only group (Figure 41).

Ascorbic acid is an essential cofactor that plays a crucial role in collagen synthesis in the cells (Pinnell 1985). Carrageenan, a sulfated polysaccharide, is a macromolecule that increases the crowdedness of the extracellular matrix and thus promotes the enhanced assembly and aggregation of collagen fibers (Satyam et al. 2014) . Therefore, it was interpreted that the combination of ascorbic acid and carrageenan in the AA+CR group synergistically enhanced the collagen deposition, leading to the formation of more compact and larger spheroids compared to other experimental groups.

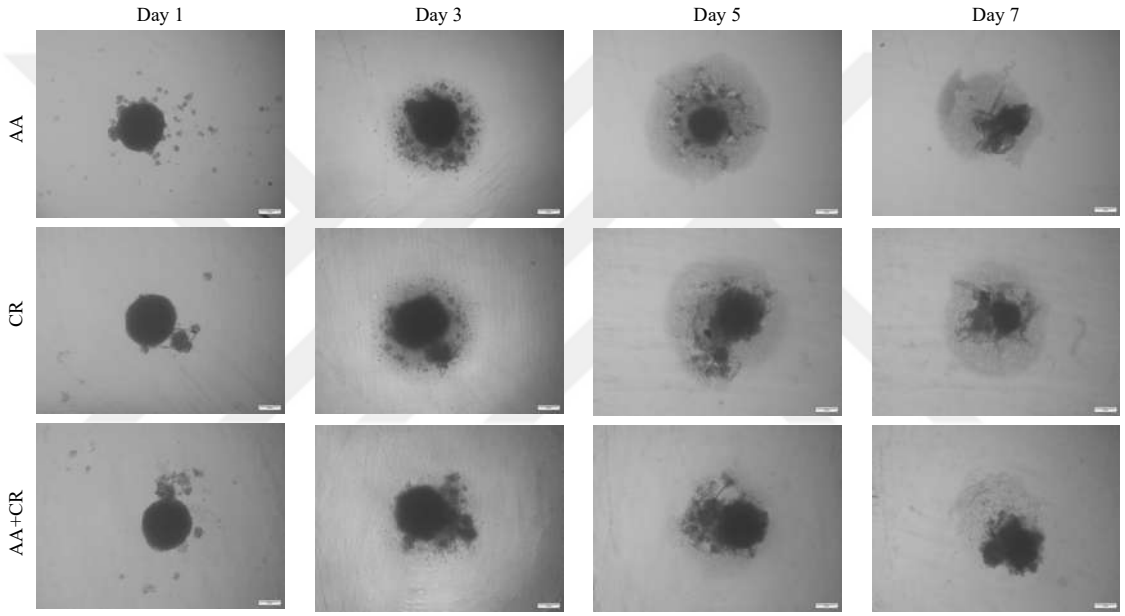


Figure 40. Micrographs of WS1 spheroids, obtained by magnetic levitation in paramagnetic crowding medium, after 1,3,5 and 7 days in culture with only L-ascorbic acid (AA), with only carrageenan (CR), and with L-ascorbic acid and carrageenan (AA+CR). n=3. Scale bar: 100 µm.

In addition, to assess the potential impact of the different additives in the media on the metabolic activity of WS1 spheroids, an alamarBlue assay was performed (Figure 42). No statistically significant differences were observed between the groups. The results suggest that the additives in the crowding media did not exert any significant adverse effects on the metabolic activity of the spheroids.

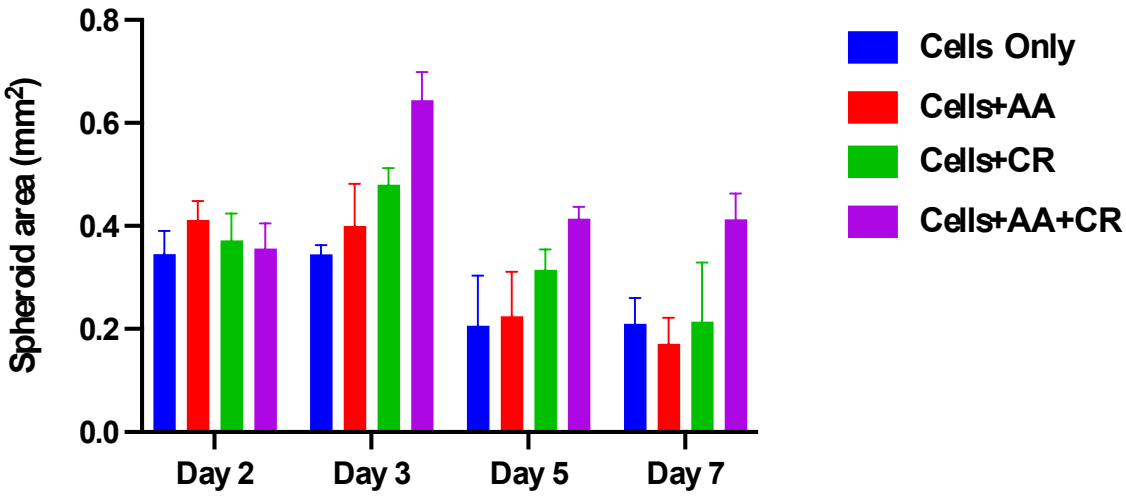


Figure 41. Comparison of the average spheroid area over time between Only Cells, AA, CR, AA+CR groups. n=3.

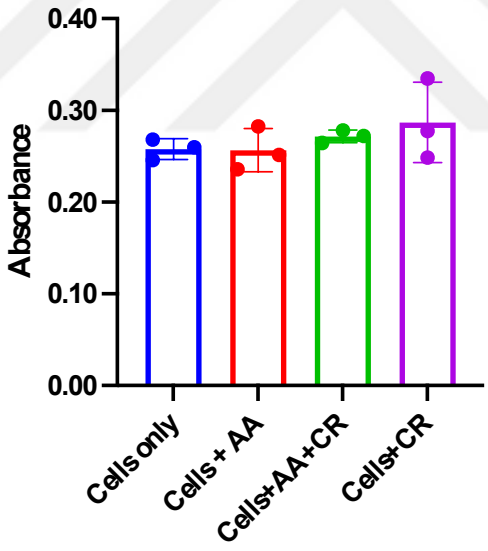


Figure 42. AlamarBlue assay to determine the differences in the metabolic activity of spheroids in different media. n=3.

Building upon the previous experiments, we continued our investigations using human dermal fibroblast (HDFa) cells according to the first experimental method. HDFa cells ($2x10^5$ cells/ml) were magnetically levitated in the single ring magnet-based levitation system in the presence of 150 mM $Gd^{3+}$. After 24 h of culture, the spheroids

were transferred to a U-bottom 96-well plate for macromolecular crowding application. The culture media for both control (-MMC) and + MMC groups were renewed every other day throughout the 7 day of culture period. To further investigate the impact of coculture on collagen accumulation, we levitated the MDA-MB-231$^{dsRed}$ and HDFa cells at a 1:4 cell loading ratio and total cell concentration of $2x10^5$ cells/ml. The same protocol for macromolecular crowding were carried out for the co-culture spheroids (Figure 43).

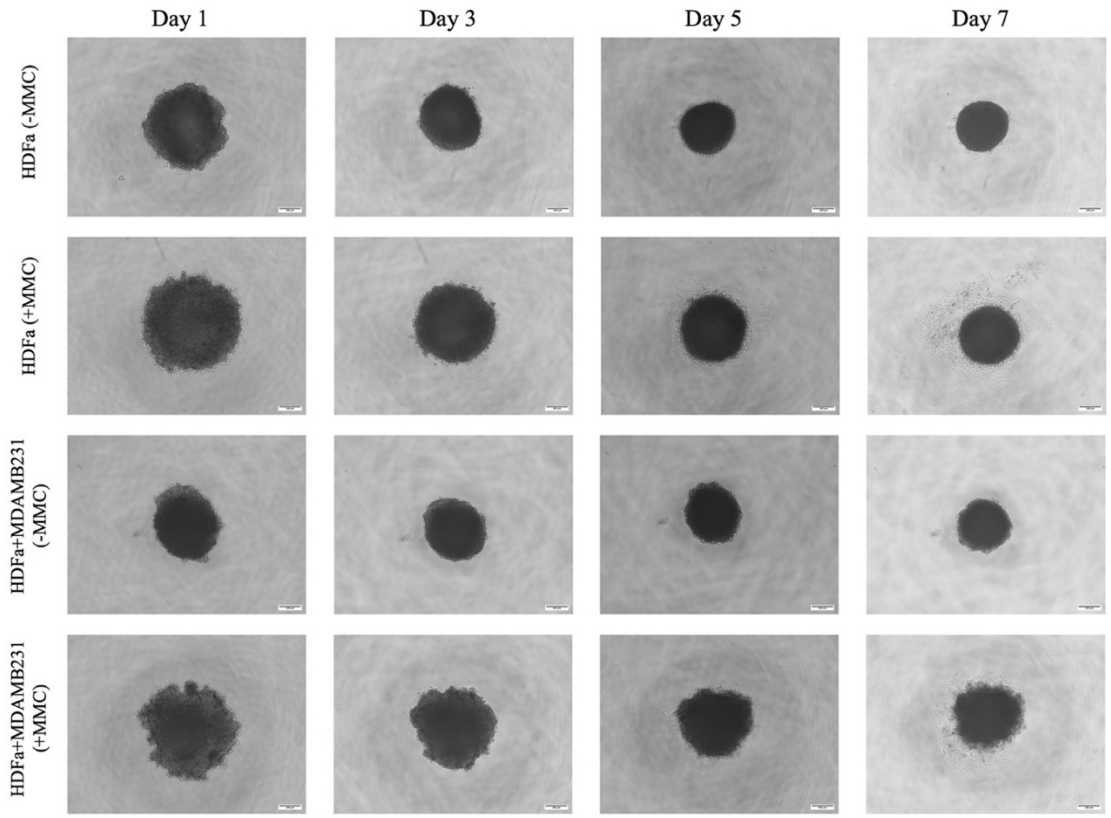


Figure 43. Micrographs of HDFa and co-culture (MDA-MB-231$^{dsRed}$ and HDFa) spheroids after 1,3,5 and 7 days in culture without (-MMC) and with MMC (Carrageenan at 50 µg/ml). n=3. Scale bar: 100 µm.

Microscopic analysis revealed that both HDFa and co-culture exhibited an increase in ECM accumulation around their periphery in the +MMC groups. In contrast, the cells were started to spread to outer regions in control groups as in the experiment with WS1 cells (Figure 36). However, HDFa and co-culture did not exhibit the same behavior with the WS1 cells. Cell spreading from the control spheroids was less

pronounced, and ECM accumulation around the periphery of +MMC spheroids was more evident. The average core area of compact spheroids decreased from over time in all groups (Figure 44). The average spheroid area was generally larger in +MMC groups compared to the control groups at all time points, with the exception of Day 5 for co-culture spheroids. Furthermore, the difference in spheroid area was not statistically significant except for the first day of culture for both HDFa and co-culture spheroids, and the third day of culture for only HDFa spheroids.

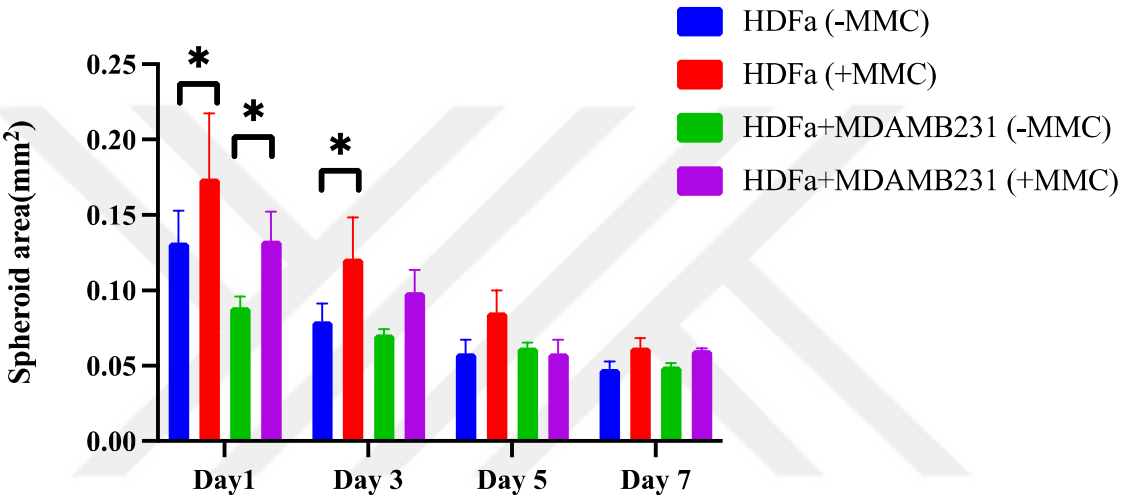


Figure 44. Comparison of average spheroid area over time between HDFa (-MMC), HDFa (+MMC), HDFa +MDA-MB-231$^{dsRed}$ (-MMC) and HDFa +MDA-MB-231$^{dsRed}$ (-MMC) spheroids. n=3. * indicates a statistically significant difference ($p<0.05$) between the groups.

To confirm the identity of the visible accumulation around the spheroids as ECM molecules, Sirius Red staining was performed on the spheroids to quantify the collagen content at the end of the culture period (Figure 45). Comparison of absorbance values between groups, revealed that collagen content was higher in the +MMC groups compared to the control groups. However, this difference was statistically significant only in the HDFa spheroids (Figure 46).

Scaffold-free spheroids are capable of producing ECM molecules with the amount depending on various factors (Rescigno, Ceriotti, and Meloni 2021; Shearier et al. 2016). Although they can produce their own ECM, production is lower compared to scaffold-

based spheroids (Qi et al. 2022). Fibroblast spheroids are one of the cell types that are sensitive to some conditions like scaffold-free growth, such as the need for interaction with their surrounding extracellular matrix to function optimally (Salmenperä et al. 2016). Therefore, incorporating ECM components is crucial, especially in scaffold-free models, to accurately mimic the *in vivo* tissue.

Building upon previous studies on enhancing ECM accumulation in spheroids, our work demonstrates a significant increase in the collagen production in scaffold-free spheroids when employing the MMC method.

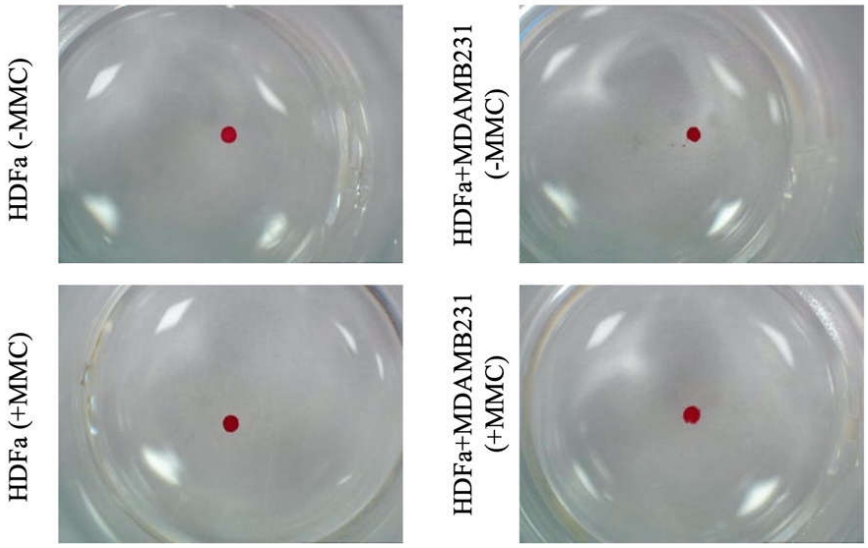


Figure 45. Photographs of the spheroids after staining with Sirius Red.

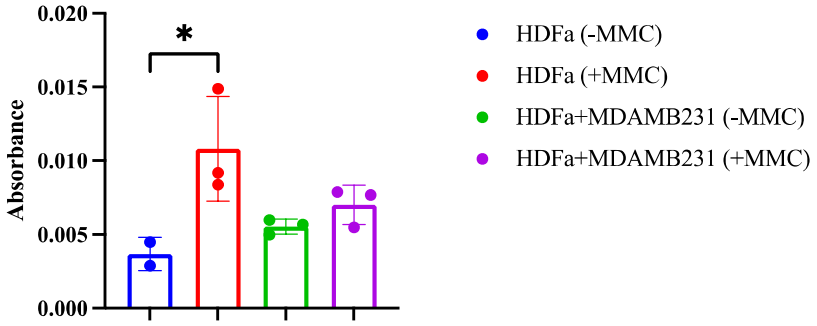


Figure 46. Absorbance values at 405 nm after Sirius Red staining of the spheroids. * indicates a statistically significant difference ($p<0.05$) between the groups.

## 3.5. Conclusions

The macromolecular crowding method was tested on 3D scaffold-free spheroids for the first time with this study. The results demonstrated an increase in collagen accumulation around the peripheral area of spheroids in the macromolecular crowding groups, as evidenced by their larger area and more compact structure time compared to control groups.

ECM production in both scaffold-based and scaffold-free spheroid models is enhanced compared to 2D models. However, scaffold-materials can interfere with the cells and introduce potential drawbacks, such as mechanical stress or immunological responses. Scaffold-free models offer several advantages, including the elimination of the need for long and laborious steps of incorporating scaffold materials into the culture. Furthermore, ECM production in spheroid models can be further augmented through biophysical modulations such as hypoxia or photo biomodulation. However, the macromolecular crowding method offers a unique advantage by increasing ECM accumulation without the need for putting the cells under any pressure.

In this thesis, analysis of collagen content confirmed that macromolecular crowding increased the collagen accumulation within scaffold-free spheroids. Moreover, magnetic levitation, a relatively fast and efficient method for generating 3D spheroids (in less than 3 hours), does not require any complex or expensive equipment or time-consuming experimental procedures. Therefore, the combination of magnetic levitation and macromolecular crowding represents a promising approach for the rapid and efficient creation of 3D cell, tissue or tumor models with physiologically relevant extracellular matrix.

# CHAPTER 4

# UTILIZING THE MAGNETIC LEVITATION AS A DIAGNOSTIC METHOD TO DETECT NEURODEVELOPMENTAL ANOMALIES

Living cells exhibiting diamagnetic properties can be levitated using a paramagnetic medium through a simple and cost-effective protocol that eliminates the need for cell labeling. In this approach, the culture medium containing the cells is made paramagnetic; thus, the weight vectors of the cells are neutralized, and their levitation is achieved by means of two simple magnets (ferromagnets) placed opposite to each other. Within the resulting magnetic field, cells are positioned in a microcapillary channel, that is between the two magnets, according to their volumetric mass densities. This phenomenon enables the separation of different types of cells within heterogenous cell mixtures. Consequently, magnetic levitation technology offers a low-cost and rapid method for cell separation and detection.

## 4.1. Introduction to Neurodevelopmental Anomalies

The nervous system constitutes a complex network of specialized cells spreading to the whole body. Its primary function is to direct and control the physiological processes and events within all organs and systems This system is anatomically categorized as peripheral nervous system (PNS) and central nervous system (CNS); and functionally categorized as somatic and autonomic nervous system. The central nervous system encompasses the brain and spinal cord. Neurons that comprise the peripheral nervous system are originate from the brain and spinal cord and extend through to the organs and limbs (Willerth 2017). Two cell types exist within the nervous system: neurons and glia

(Figure 47). Neurons are the primary cells of the nervous system, responsible for transporting bioelectrical signals throughout the body via action potentials. Glia cells, on the other hand, support the neurons and surround the neuronal microenvironment along with axons and dendrites in both central and peripheral nervous systems (Schmidt and Leach 2003).

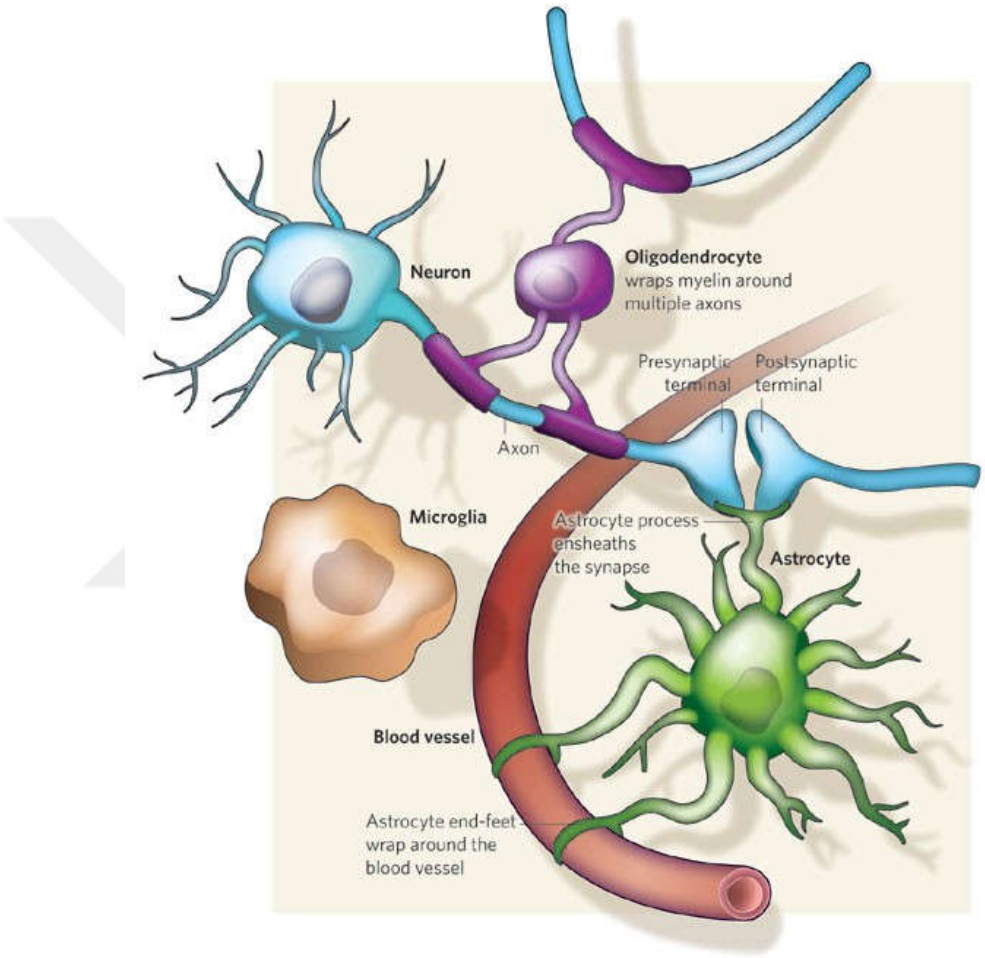


Figure 47. Glia-neuron interactions (Source: Allen and Barres 2009).

Pathological events, such as traumatic injuries, insufficient blood supply to the tissue, genetic mutations or neurodegenerative diseases can lead to a gradual loss of neuron populations, neuronal dysfunction, disruption of axon and dendrite structures, and functional problems in synaptic transmission (Winner and Winkler 2015; Ding and Hammarlund 2019; Conforti, Gilley, and Coleman 2014). Axotomy, defined as complete

physical degeneration of axons following traumatic injury, further exacerbates neuronal damage (Hill, Coleman, and Menon 2016). The potential for neuronal regeneration after injury differs significantly between the peripheral nervous system (PNS) and the central nervous system (CNS). Although the PNS exhibits a greater regenerative capacity compared to the CNS, complete nerve regeneration is rarely achieved (X. Gu, Ding, and Williams 2014). This limited regenerative capacity within the CNS can be attributed to the presence of several inhibitory factors. These inhibitory factors include glial cells that fail to produce neurotrophic factors essential for regeneration, myelin debris, the blood-brain barrier, which impedes macrophage migration to the injury site (Meyer, Ulrich;Handschel, Jörg;Meyer, Thomas;Wiesmann 2009), and certain types of glycoproteins (Curcio and Bradke 2018).

Extensive research efforts have been dedicated to develope diagnostic and therapeutic strategies for neurodegenerative diseases and disorders. However, conventional approaches primarily focus on symptom management, providing physical relief, or slowing disease progression, rather than promoting neuronal regeneration. A gold standard technique in conventional therapies involves the implantation of nerve grafts, fragments of nerve tissue harvested from another part of the body, into the injured or degenerated nerve tissue to bridge the gap between the two ends of a damaged nerve (Sonabend et al. 2012). They can be taken from the same patient (autografts), another person (allografts) or another species (heterografts) (Yildiz 2006). Alternatively, artificial conduits made from different substances have been used to provide axonal growth (Wilkinson and Luxford 2010). Autograft implantation requires an additional surgery to remove the donor nerve from the source and which can potentially lead to unwanted reactions, deformations, or functional loss at the donor site. Moreover, there is a possibility of size incompatibility between the recipient and donor nerves. While autografts present lower immune rejection risk is other graft types face limitations due to limited donor availability (Meyer, Ulrich;Handschel, Jörg;Meyer, Thomas;Wiesmann 2009; Aijie et al. 2018). Despite significant developments in this field, current treatment strategies have not achieved efficient functional recovery in nerve regeneration, even within the PNS.

Together with the knowledge of the ability of an adult organism to renew itself, even within the CNS which has a limited capacity of regeneration, tissue engineering strategies have emerged to develop structures that can repair CNS and PNS damage more effectively than conventional methods. As is known, tissue engineering is a

multidisciplinary field that integrates engineering principles and life sciences knowledge to develop functional materials to restore o replace the damaged cells, tissues, or organs, and to maintain or improve the function of tissues and organs to enhancing the quality of life (Langer, Robert; Vacanti 1993).

Decades of research have focused on restoring tissue function or replacing degenerated tissue or organs across various organ systems, including neural tissue. Neural tissue engineering seeks to identify and develop superior alternatives to conventional methods for nervous system repair, such as surgical interventions (e.g., grafting), or pharmacotherapies aimed at symptom reduction. Neural tissue engineering strategies to enhance the nerve repair can be broadly categorized into four distinct approaches: cell therapies, drug/biomolecular therapies (i.e., neurotrophic factors), axonal guidance therapies (i.e., nerve conduits (Raza et al. 2020)) and electrical stimulation therapies (Schmidt and Leach 2003).

Depending on the situation, various strategies have been developed by using cell therapy for the replacement and functional recovery of degenerated neurons, astrocytes, or glial cells. For example, while the dopaminergic neurons being degenerated in the Parkinson's disease (Poewe et al. 2017), degeneration of the oligodendrocytes is seen in the Multiple sclerosis (MS) disease (Wolswijk 2000). Or neuronal population loss is occurred in the traumatic injuries (Petzold et al. 2011). Therefore, it is necessary to use specific types of neurons for implantation for each pathological condition. Stem cells are undifferentiated cells that are capable of self-renewing and differentiate into multiple types of cells and functioning as repair systems of the body (Lindvall, Kokaia, and Martinez-Serrano 2004).

In the adult brain, neural stem/progenitor cells (NSCs/NPCs) reside in specific brain regions -subventricular zone (SVZ) and subgranular zone (SGZ)- where they continuously differentiate into neurons throughout the life. This process is known as neurogenesis. Once generated, these newly formed neurons integrate into the existing neural network. Based on this knowledge, cell therapy approaches have been explored within the field of neural tissue engineering to increase the neurogenesis in the nervous system. These approaches encompass both i*n vivo* manipulations using neurotrophic factors or therapeutic molecules and transplantation of *in vitro* derived neural stem/progenitor cells into the target tissue (Silva-Vargas, Crouch, and Doetsch 2013; Grochowski, Radzikowska, and Maciejewski 2018).

Numerous studies have investigated *in vitro* neural stem cell cultures for applications in transplantation, or tissue and disease modelling by using scaffolds (Duan et al. 2016; Baiguera et al. 2014), hydrogels (Gonzalez-Perez et al. 2017), 3D printing techniques (W Lee et al. 2009; Q. Gu et al. 2016). Stem cells derived from different sources (Figure 48) have been utilized in neural regeneration studies, including embryonic stem cells (ESCs) (Jones et al. 2018; Zarei-Kheirabadi et al. 2020), mesenchymal stem cells (MSCs) (S. H. Lee et al. 2015; Cooney et al. 2016), human induced pluripotent stem cells (hiPSCs) (Chau, Monica J.;Deveau, Todd C.;Song, Mingke;Gu, Xiaohuan;Chen, Dongdong;Wei 2014; Griffin, Anderson, and Wolfe 2015; Hofrichter et al. 2017; S. Wu et al. 2017; Simão et al. 2018).

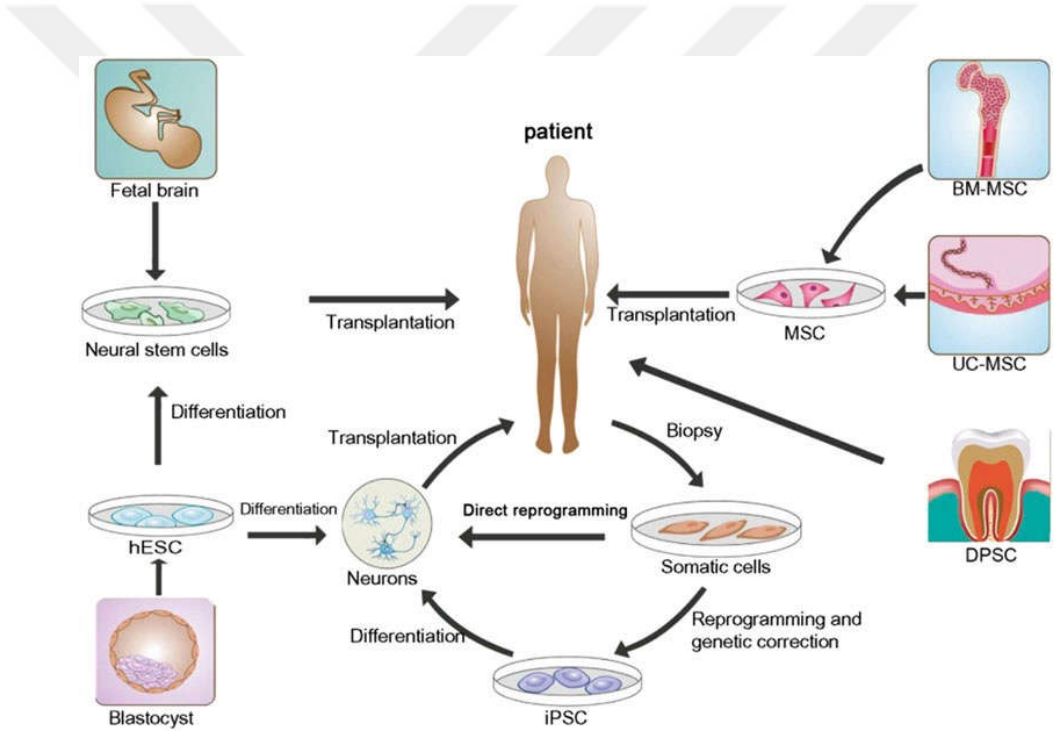


Figure 48. The stem cell sources for transplantation therapy in neurodegenerative diseases: hESCs isolated from the inner cell mass of a blastocyst; neural stem cells from fetal brain tissues; BM-MSC from adult bone marrow; UC-MSC from umbilical cord of the newborn; DPSC isolated from dental pulp tissues of adult or children; and iPSC derived from the reprogrammed somatic cells (Source: Lu and Han 2020).

## 4.2. Potential of Using Magnetic Levitation as a Diagnostic Method for Neurodevelopmental Anomalies

Magnetic force-based cell manipulation is one of the techniques that have been studied on neural cells. These studies include selective purification of neural precursor cells by magnetic bead sorting (Carpenter et al. 2001), directing of neural stem cells towards the neodymium magnet by ferumoxide labeling (M. Song et al. 2010) and by using biocompatible poly(allylamine hydrochloride) stabilized magnetic nanoparticle labeling (Guryanov et al. 2019), enrichment of neural progenitor cells by magnetic activated cell sorting technique (MACS) with an improved yield compared to fluorescence-activated cell sorting (FACS) (Bowles et al. 2019), orientation of the direction of neurite formation by applying magnetic field created with two magnets at both sides of the culture dish (S. Kim et al. 2008), formation of 3D structures utilizing magnetic iron oxide (MIO) nanoparticle incorporated neuronal cells by magnetic levitation technique based on positive magnetophoresis (Souza et al. 2010).

Furthermore, magnetic levitation based on negative magnetophoresis has found applications in various studies including density-based profiling of different types of cancer cells and blood cells, which can be used for the detection of circulating tumor cells in the blood sample (Durmus et al. 2015), density profiling and sorting of lipid accumulating subpopulation during differentiation of hiPSCs into cardiomyocytes (Puluca et al. 2020), density-based detection of adipocytes (Sarigil et al. 2019) and mesenchymal stem cells (Anil-Inevi et al. 2020). However, the potential of this microcapillary-based magnetic levitation setup as a density-based diagnostic tool for neurodevelopmental anomalies remains to be explored.

## 4.3. Magnetic Levitation for Detection of the Single Cell Density Profiles of Neural Cells Derived from Patients with Rare Neurodevelopmental Disorders

Rare neurodevelopmental disorders are caused by variations in single or multiple genes in somatic cells and affect a very low percentage of the world's population. Displayed phenotypes of the patients with the same genetic mutations might differ, or a patient may never exhibit any phenotype at all. Severity levels can vary greatly among individuals with neurodevelopmental disorders. These disorders can manifest with a range of symptoms, including developmental delays, intellectual disability, epilepsy, cerebral palsy, dementia, and autism. In severe cases, these disorders may also be accompanied by other systemic dysfunctions (Niemi et al. 2018; Bain, Ardalan, and Goldman 2021; Sabitha, Shetty, and Upadhya 2021; Q. Q. Huang et al. 2024). The limited availability of suitable models for studying neurodegenerative diseases and developing therapeutic strategies necessitated the development of *in vitro* models. The advent of patient-derived induced pluripotent stem cells (iPSCs) revolutionized this field by enabling the generation of functional neural cells through gene editing techniques. iPSCs are derived from adult human cells, primarily fibroblasts, by a process of direct reprogramming that induces a pluripotent state, similar to embryonic stem cells (ESCs) (Takahashi and Yamanaka 2006). While mesenchymal stem cells (MSCs) are multipotent, capable of differentiating into a limited number of cell types, including neural stem/progenitor cells, ESCs and iPSCs are pluripotent, exhibiting the potential to differentiate into any cell type.Numerous studies have been conducted on iPSCs since its discovery because they eliminate the disadvantages of ESCs including immune rejection risk as they are taken from the same patient, grueling isolation steps and ethical issues. Hence, they have been providing insights into the mechanisms of defective brain functions using 2D and 3D culture models (Sabitha, Shetty, and Upadhya 2021).

This thesis employed microcapillary-based magnetic levitation to investigate the relationship between cellular changes during the differentiation of human-induced pluripotent stem cells (hiPSCs) into neural progenitor cells and their corresponding volumetric mass densities. The study examined hiPSCs derived from fibroblasts of both healthy individuals and patients with a neurodevelopmental disorder caused by a KATNAL-2 gene variant. KATNAL-2 belongs to the katanin protein family, members of

which are responsible for severing microtubules during essential cellular processes such as cell division, migration, and neuronal development. Katanin proteins comprise two subunits: p60, the catalytic subunit, and p80, the regulatory subunit. KATNAL2, a p60-like protein, is highly expressed in the human central nervous system (Hız et al. 2022; Lynn et al. 2021). Previous studies have linked mutations in KATNAL-2 to an increased risk of autism spectrum disorder (Yuen et al. 2015).

In addition to investigating the density profiles of iPSCs differentiating into NPCs, this section of the thesis focused on examining the levitation and volumetric mass density profiles of fibroblasts and neural progenitor cells isolated from both healthy subjects and individuals with a rare neurodevelopmental disorder. These analyses were conducted using microcapillary levitation techniques. The primary objective of this investigation was to explore the potential of this technique as a diagnostic tool for detecting the neurodevelopmental anomaly.

## 4.3.1. Methods

### 4.3.1.1. Isolation of Fibroblasts from Patients

We collaborated with Dr. Yavuz OKTAY and his team at Izmir Biomedicine and Genome Center who provided the iPSCs and NPCs. Primary fibroblast cells were isolated from foreskin of two different healthy subjects. Fibroblasts of two different patients with KATNAL2 and KATNB1 variants are isolated from patients' using a standard protocol (Jacob, Sebastian, and Talley 2024). Cells were cultured in Dulbecco's modified Eagle medium (Gibco) supplemented with 10% fetal bovine serum (FBS) and 1% penicillin/streptomycin (P/S). The cells were incubated in the incubator at 37°C, 5% $CO_2$. The growth mediums were refreshed every other day and the cells were passaged when they reached the 90% confluency by using trypsin-EDTA solution for detaching the cells.

### 4.3.1.2. Cell Culture

Human induced pluripotent stem cells (iPSCs) and neural progenitor cells derived from iPSCs were used throughout this study. Single cell iPSCs culture was prepared by using STEMdiff Neural Induction Medium+SMADi + Y-27632 (Stem Cell Technologies). After that, they were seeded in one Matrigel coated well (one of the 6-well plate) and incubated in a humidified 37 °C incubator with 5% $CO_2$. The culture medium was replaced with Neural Induction Medium that does not contain Y-27632 every day for 6-9 days and they were passaged when the confluency reached 80-90%. When they were ready for 3$^{rd}$ passage, Neural Progenitor Cell Culture protocol was applied. The cells were detached using accutase and they were suspended in Complete STEMdiff Neural Progenitor Medium (Stem Cell Technologies). Then they were seeded onto a Matrigel coated well (one of the 6-well plate) and incubated in a humidified 37 °C incubator with 5% $CO_2$. The morphologies of the cells were observed under an inverted microscope throughout the differentiation process.

### 4.3.1.3. Magnetic Levitation Setup

The magnetic levitation device is composed of two neodymium (NdFeB) permanent magnet (50 mm length, 2 mm width, and 5 mm height) positioned at 1,5 mm distance with same poles facing each other to create magnetic field gradient, a micro-capillary channel (1 mm × 1 mm square cross-section, 50-mm length) between two magnets as a cell culture chamber and two mirrors (12,7 × 12,7 × 3,2 mm) at 45° for real-time imaging of cells. The components of the magnetic levitation device are held together with photoreactive resin (Clear v2 FLGPCL02) printed using 3D printer (Formlabs Form 2) (Figure 1a).

### 4.3.1.4. Magnetic Levitation of Cells

In this system, cells suspended in $Gd^{3+}$ containing 50 $\mu l$ paramagnetic medium were loaded into a microcapillary channel. They were repulsed from the region of high magnetic field (i.e., close to the magnets) to the region of low magnetic field (i.e. middle region of cell culture chamber in the vertical direction) owing to the difference between the magnetic susceptibility of cells and the surrounding medium. Before cells reach equilibrium, fluidic drag ($F_d$), inertial ($F_i$), buoyancy ($F_b$), and magnetic forces ($F_{mag}$) act on them. After about 10 min, at the equilibrium position, the velocity of the cells and thus $F_d$ and $F_i$ become negligible, and only $F_{mag}$ and $F_b$ act on cells in opposite directions, resulting in the levitation of cells (Figure 1b). The cells cultured with magnetic levitation were visualized through 45° mirrors in the device under an inverted microscope (Olympus IX41) and recorded. The density profiles and morphology of the cells were determined by Image J software.

### 4.3.1.5. Statistical Analysis

Results were expressed as mean ± standard deviation for each experiment. Each experiment had at least 3 samples in each repetition. In cases where statistical comparisons need to be made, the differences between groups were measured by ANOVA test, 5% was considered as the significance limit.

## 4.3.2. Results and Discussion

Magnetic levitation was applied to iPSCs and NPCs using a microcapillary-based magnetic levitation system to detect the changes in the single-cell density of the iPSCs and NPCs during the differentiation process. The samples were taken from the cells at different stages of the differentiation process (Figure 49 and 50) with a concentration of

$5x10^3$ cells/capillary, and they were suspended in the paramagnetic medium containing 25 mM $Gd^{3+}$, and they were loaded into the microcapillary channel on the magnetic levitation system. The cell samples were levitated at day 0 (iPSCs), day 6, day 14, day 21 and day 28 (NPCs) of the differentiation process of the iPSCs into the NPCs.

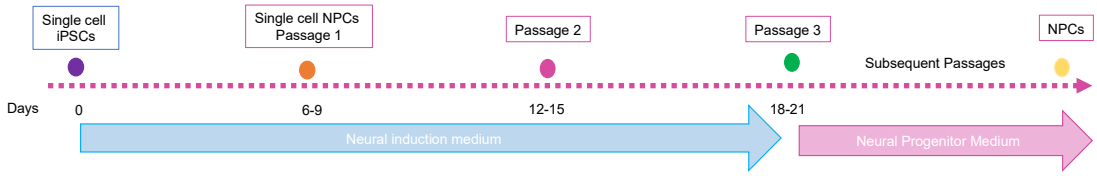


Figure 49. Differentiation steps of hiPSCs into NPCs.

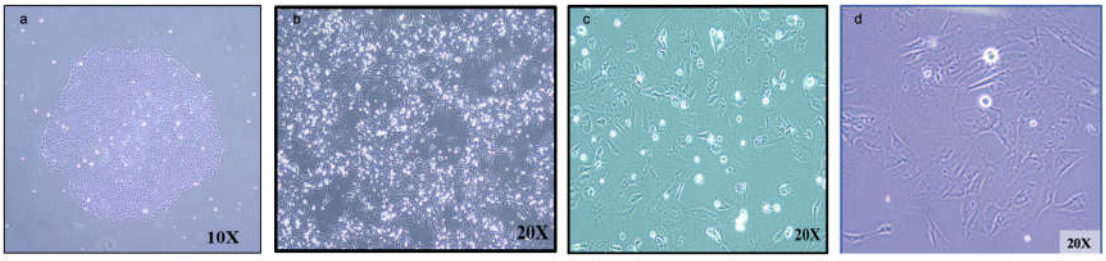


Figure 50. Micrographs of induced pluripotent stem cells (iPSCs) at different steps in the process of differentiation into the neural progenitor cells (NPCs). a) iPSCs b) iPSCs in neural induction medium c) iPSCs in neural progenitor medium d) differentiated NPCs (Source: Burcu Ekinci, Izmir Biomedicine and Genome Center).

To investigate the correlation between cellular morphological and physiological changes during differentiation and cell density, the levitation heights of the cells were analyzed and compared. Levitation height is directly related to the volumetric mass density of the cells. The levitation micrographs are presented in Figure 51. The analysis of levitation heights is summarized graphically and tabularly in Figure 52 and Table 2, respectively.

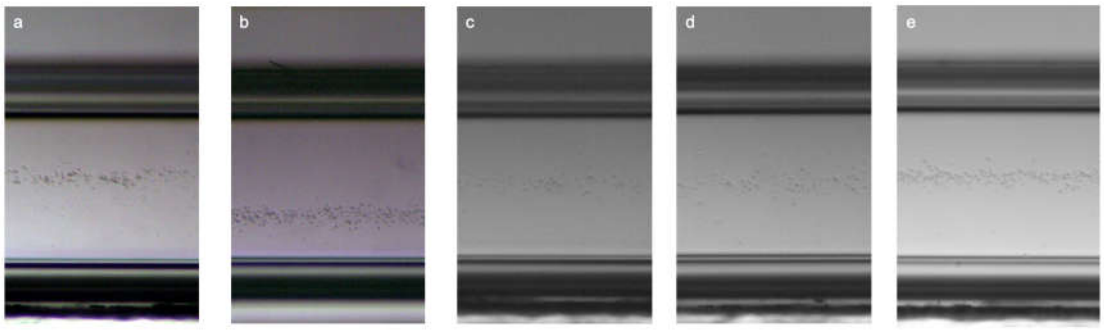


Figure 51. Levitation micrographs of induced pluripotent stem cells (iPSCs) at different steps in the process of differentiation into the neural progenitor cells (NPCs). a) Day 0 b) Day 6 (neural induction medium) c) Day 14 (neural progenitor medium) d) Day 21 (second passage in neural progenitor medium) e) Day 28 (differentiated NPCs).

Statistically significant differences were observed in the average levitation heights of the cells between the first day and the 6th day of the differentiation and the 6th and 14th day of the differentiation. These findings suggest that the average single-cell density increased on day 6, decreased thereafter, and remained relatively stable in the subsequent days. Previous research has demonstrated a dynamic change in the levels of globular actin (G-actin) during the differentiation of induced pluripotent stem cells into neural stem cells. Specifically, an increase in G-actin signals was observed on day 5, followed by a subsequent decrease (Compagnucci et al. 2016). G-actin, the monomeric form of the actin protein, undergoes polymerization to form filamentous F-actin. These two forms exist in a dynamic equilibrium during differentiation and cytoskeletal organization. In line with these previous findings, our results suggest that the observed increase in cell density on day 6 may be attributed to an increase in G-actin monomers, which are utilized for actin polymerization during the early stages of differentiation. As the cells progress towards neuronal differentiation, the abundance of filamentous actin increases, leading to a decrease in the overall cell density.

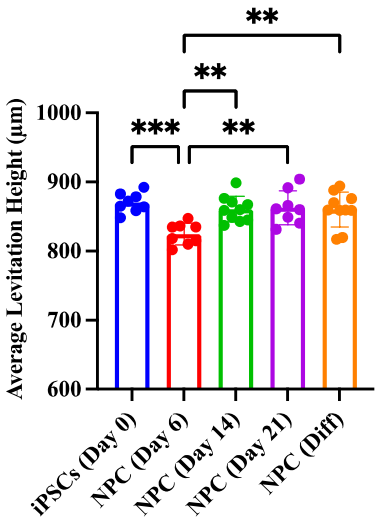


Figure 52. Levitation profiles of iPSCs originated from a healthy subject in the process of differentiation to NPCs in the presence of 25 mM $Gd^{3+}$. ** and *** indicate statistically significant differences ($p<0.01$ and $p<0.001$, respectively) between the groups.

Table 2. Analysis of levitation profiles of iPSCs originated from a healthy subject in the process of differentiation to NPCs in the presence of 25 mM $Gd^{3+}$.

| | Mean | Minimum | Maximum | Range | Std Dev | Skew | CoV(%) |
|---|---|---|---|---|---|---|---|
| iPSC | 870.1 | 848.3 | 892.3 | 43.98 | 14.12 | 0.07177 | 1.62% |
| NPC (Day 6) | 824.7 | 801.7 | 847.2 | 45.51 | 15.71 | -0.07585 | 1.91% |
| NPC (Day 14) | 860.5 | 837.2 | 898.6 | 61.3 | 18.54 | 0.8049 | 2.16% |
| NPC (Day 21) | 862.7 | 831.3 | 903.7 | 72.39 | 24.55 | 0.6068 | 2.85% |
| NPC (Differentiated) | 859.9 | 816.8 | 894 | 77.22 | 25.34 | -0.6834 | 2.95% |

To further elucidate the intracellular mechanisms underlying the observed changes in levitation heights during the differentiation process, it is crucial to quantitatively examine the relationship between cytoskeletal protein dynamics and the volumetric mass density of iPSCs through magnetic levitation. This approach holds the potential to utilize the magnetic levitation system as a diagnostic tool to determine the

stage of neuronal differentiation, thereby eliminating the need for time-consuming, laborious, and expensive experimental procedures.

Furthermore, iPSC samples derived from a patient with a neurodevelopmental anomaly caused by a variant in the KATNAL-2 gene were levitated in a medium containing 25 mM $Gd^{3+}$ at three distinct stages of the differentiation process. The levitation heights and volumetric mass densities of these cells were then compared to those of cells derived from healthy individuals. A significant difference was observed in the average levitation height of differentiated NPCs compared to the preceding two stages of differentiation. These findings suggest a decrease in the average volumetric cell density of the NPCs (Figure 48, Table 3).

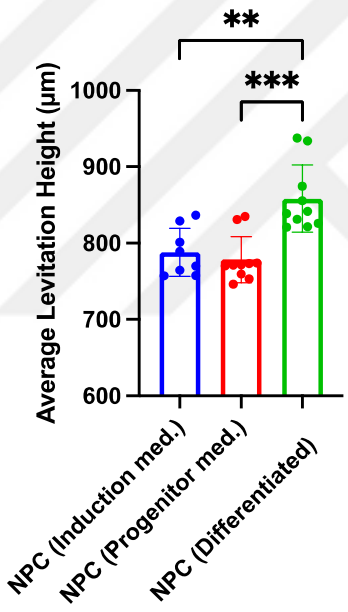


Figure 53. Levitation profiles of iPSCs originated from a patient with the KATNAL-2 variant using 25 mM $Gd^{3+}$ in the process of differentiation to NPCs. ** and *** indicate statistically significant differences ($p<0.01$ and $p<0.001$, respectively) between the groups.

Table 3. Analysis of levitation profiles of iPSCs originated from a patient with KATNAL-2 variant in the process of differentiation to NPCs in the presence of 25 mM $Gd^{3+}$.

| | Mean | Minimum | Maximum | Range | Std Dev | Skew | CoV(%) |
|---|---|---|---|---|---|---|---|
| NPC (Induction med.) | 788.1 | 757.1 | 836.5 | 79.38 | 31.53 | 0.6421 | 4.00% |
| NPC (Progenitor med.) | 778.4 | 746.1 | 834.7 | 88.61 | 30.18 | 1.342 | 3.88% |
| NPC (Differentiated) | 858.1 | 821 | 937.4 | 116.5 | 44.06 | 1.257 | 5.14% |

We compared the levitation height profiles of iPSCs and NPCs, taken from a healthy subject and a patient, at the last three steps of the differentiation process. Statistically significant differences were observed in the average levitation heights, indicating an increase in the volumetric mass density of the differentiated NPCs derived from the patient compared to healthy subjects (Figure 54).

Given the significant time, cost, and labor associated with reprogramming fibroblasts into induced pluripotent stem cells (iPSCs) and subsequently differentiating these iPSCs into neural progenitor cells, we explored the possibility of utilizing primary fibroblast samples to monitor cell density profiles. To this end, primary fibroblast cell samples were isolated from two healthy subjects and two patients with distinct genetic variants (KATNAL-2 and KATNB-1). These samples were then subjected to magnetic levitation analysis to investigate their levitation and density profiles (Figure 55).

A significant difference was observed between the average levitation heights of fibroblasts isolated from the patient with the KATNAL-2 variant and those from both healthy controls (Figure 56, Table 4). This finding suggests a higher volumetric mass density in the fibroblasts from the patient with the KATNAL-2 variant compared to those from healthy subjects. No significant differences were observed between the levitation heights of the two healthy control groups, nor between the patient sample with the KATNB-1 variant and the healthy controls.

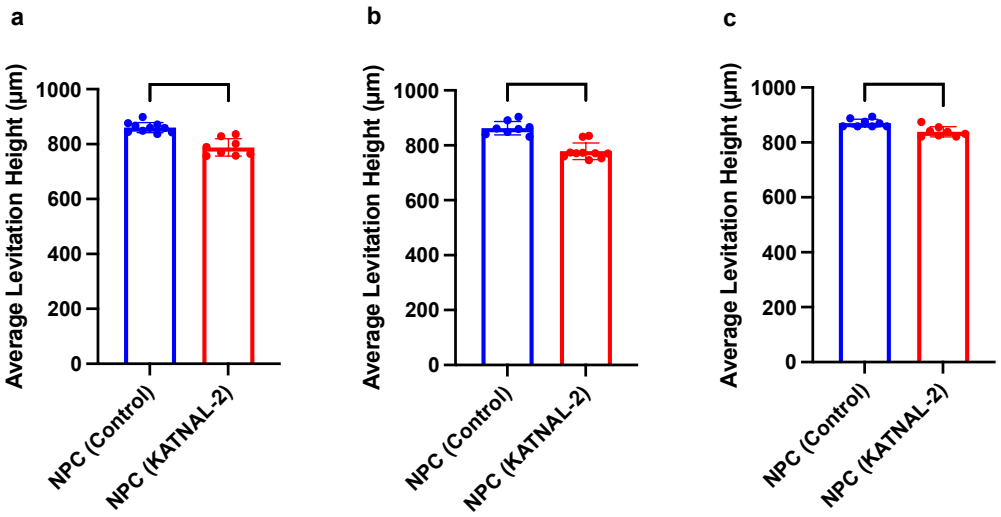


Figure 54. Statistical comparison of levitation profiles of the NPCs, originated from a patient with KATNAL-2 variant and healthy subject, at the last three steps of differentiation a) NPCs in neural induction medium, b) NPCs in neural progenitor medium, c) Differentiated NPCs. ** and **** indicate statistically significant differences ($p<0.01$ and $p<0.0001$, respectively) between the groups.

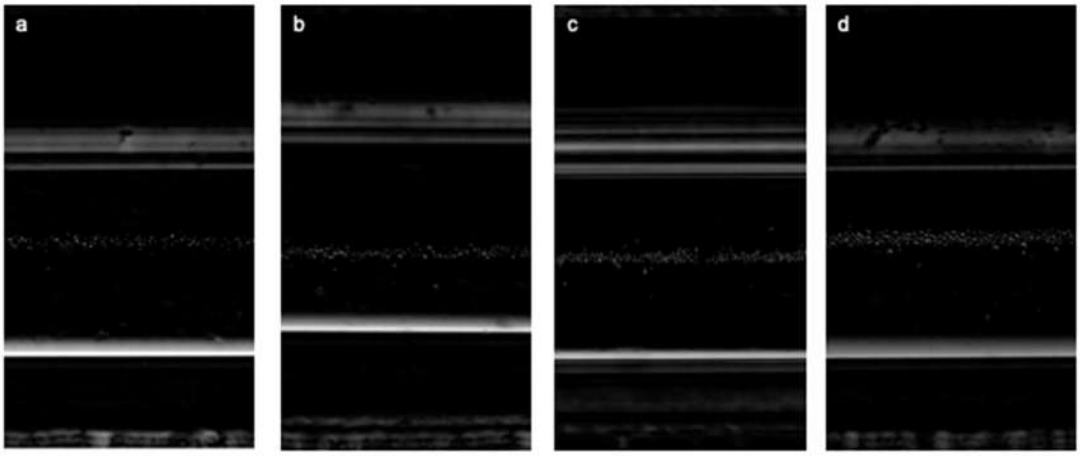


Figure 55. Levitation micrographs of fibroblast samples taken from two healthy subjects (a and b) and two patients with KATNAL-2 (c) and KATNB-1(d) variants, respectively.

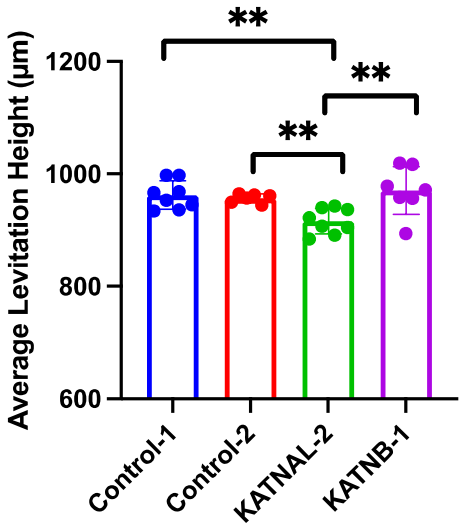


Figure 56. Levitation profiles of primary fibroblast samples isolated from two healthy subjects and two patients with KATNAL-2 and KATNB-1 variants. n=3. ** indicates a statistically significant difference ($p<0.01$) between the groups.

The results indicate that the difference in the average levitation height was specific to the patient with the KATNAL-2 variant. Notably, the difference in the average levitation heights of the fibroblasts isolated from the patient with KATNAL-2 was consistent with the significant difference between the NPCs of the same patient and the control. Both fibroblasts and NPCs had lower average levitation heights compared to controls.

The KATNAL-2 gene encodes the catalytic subunit (p60) of the katanin protein, which is responsible for severing microtubules during the cell division process (Lynn et al. 2021). The observed difference in the volumetric mass density of cells isolated from the patient with the KATNAL-2 variant suggests a potential link to alterations in microtubule structure and abundance compared to healthy controls. In contrast, KATNB-1, the regulatory subunit (p80) of the katanin protein, which modulates the catalytic activity of katanin, appeared to have a less pronounced effect on cellular volumetric mass density compared to the KATNAL-2 variant.

Table 4. Analysis of levitation profiles of primary fibroblasts isolated from a patient with KATNAL-2 variant in the process of differentiation to NPCs in the presence of 25 mM $Gd^{3+}$.

| | Mean | Minimum | Maximum | Range | Std Dev | Skew | CoV(%) |
|---|---|---|---|---|---|---|---|
| Control-1 | 962.4 | 934.1 | 997.9 | 63.85 | 25.16 | 0.496 | 2.61% |
| Control-2 | 956.8 | 944.7 | 964.9 | 20.18 | 7.929 | -0.7648 | 0.83% |
| KATNAL-2 | 916.2 | 884.5 | 943.2 | 58.76 | 22.75 | -0.1177 | 2.48% |
| KATNB-1 | 970.8 | 894 | 1019 | 125.4 | 42.51 | -0.7353 | 4.38% |

Following the differentiation of iPSCs isolated from a patient into NPCs, our collaborators, Yavuz Oktay and his team at the Izmir Biomedicine and Genome Center, investigated a potential therapeutic application for the KATNAL-2 variant. To this end, two groups of NPCs derived from the patient with the KATNAL-2 variant were established. One group served as a control and was transduced with a blank lentivirus. The other group was transduced with a lentivirus carrying the wild-type version of the KATNAL-2 gene to induce overexpression of KATNAL-2. Both groups of NPCs were subjected to magnetic levitation, and their levitation profiles were compared to determine whether cellular volumetric density could be used to distinguish between healthy, diseased, and potentially recovered cells (Figure 57, Table 5).

No significant differences were observed in the average levitation heights between the groups. Notably, the levitation heights of the cells in this experiment were higher compared to those observed for WT and KATNAL-2 cells in previous studies. This discrepancy could potentially be attributed to the space occupied by the lentivirus within the cells. However, due to the limited availability of primary cells from patients with diverse neurodegenerative phenotypes, this experiment could only be conducted once. Furthermore, the lentivirus used for both overexpression and control groups may have inadvertently influenced the volumetric mass density profiles of the cells. Therefore, it is crucial to repeat the experiment using alternative methods (e.g., by using nucleofection method) and analyzing more samples isolated from different patients.

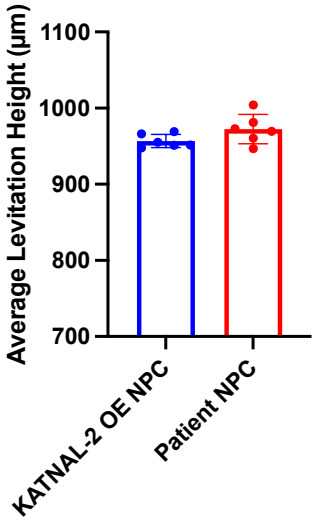


Figure 57. Levitation profiles of KATNAL-2 overexpressed NPCs and patient NPCs.

Table 5. Analysis of levitation profiles of KATNAL-2 overexpressed NPCs and patient NPCs.

| | Mean | Minimum | Maximum | Range | Std Dev | Skew | CoV(%) |
|---|---|---|---|---|---|---|---|
| KATNAL-2 OE NPC | 956.9 | 947.9 | 969.3 | 21.41 | 8.775 | 0.7247 | 0.92% |
| Patient NPC | 972.5 | 946.7 | 1004 | 57.34 | 19.43 | 0.5493 | 2.00% |

Analysis of levitation profiles of fibroblasts were compatible with the levitation profiles of neural progenitor cells that were originated from them. In order to investigate the possibility of the application of magnetic levitation technique as a diagnostic method to detect neurodevelopmental anomalies using either differentiated stem cells or fibroblasts, levitation of the cells originated from different patients will be required.

### 4.3.3. Conclusions

In this part of the thesis, the magnetic levitation technique was utilized for determining the changes in the volumetric mass density of differentiating induced

pluripotent stem cells into neural progenitor cells, which will eventually differentiate into neurons. Induced pluripotent stem cells were reprogrammed from the fibroblasts of healthy subjects and patients with rare neurodevelopmental dysfunctions caused by the KATNAL-2 variant in their genome, which encodes a subunit of the katanin protein. Katanins are microtubule severing enzymes, and they act during cellular processes such as differentiation, neuron growth, axon, dendrite extensions, etc. Therefore, the possible effects of the dysfunction of katanin enzymes in the cells on the single cell density of neuronal cells were evaluated.

A comparison of volumetric density profiles of NPCs originating from a patient and a healthy subject was performed. The differentiated NPCs of two different groups were significantly different from each other. Besides, we conducted an analysis of the levitation profiles of fibroblasts, which served as the source of neural progenitor cells for each individual. The difference between the patient and the controls was significantly different from each other. This difference was in line with the difference in the NPC samples. So, it was concluded that the volumetric density, can be used for distinguishing the patient and healthy samples. In addition, because the discrepancy is evident in the fibroblasts themselves, there is no need to undergo the extensive and expensive process of differentiating these cells into neural progenitor cells (NPCs) to identify this anomaly. This simplifies the approach and reduces both the time and costs associated with the detection. Therefore, it was demonstrated that the microcapillary-based magnetic levitation system could be utilized for the detection of neurodevelopmental anomalies in a rapid cost-effective, and simple manner as a diagnostic method. In addition, overexpression of the wild type KATNAL-2 gene in the NPCs to reverse this anomaly are ongoing. Experiments will be repeated with the samples obtained from these studies to investigate whether there is a change in cell density compared to patient samples and healthy controls. Furthermore, in order to utilize the magnetic levitation technique as a diagnostic method, it is essential to analyze samples from greater number of patients who have rare neurodevelopmental anomalies.

## 4.4. Magnetic Levitation for Detection of the Single Cell Density Profiles of Primary Brain Cells Derived from Mouse Models with Lysosomal Storage Diseases

Lysosomes are organelles responsible for the catabolism of macromolecules within cells through the action of various enzymes. Mutations in lysosomal proteins can lead to a loss of enzymatic activity, resulting in the accumulation of specific substrates within the lysosomes. This accumulation is a hallmark of lysosomal storage diseases (LSDs), which often manifest with neurological and neurometabolic complications. In LSDs, the accumulation of unmetabolized substrates within lysosomes causes cell swelling, functional deterioration, and ultimately, cell death(Tardy et al. 2004).

Furthermore, the accumulation of substrates within lysosomes can trigger various cellular events, including autophagy, oxidative stress, calcium dyshomeostasis, endoplasmic reticulum stress, lipid trafficking abnormalities, and inflammation. Understanding the impact of these cellular events on lysosomal disease pathology has become a major focus of research in recent years. Notably, monogenic LSDs, resulting from single gene deficiencies, have emerged as valuable models for investigating the fundamental biology of these cellular processes.

In lysosomal storage diseases, biomolecules such as glycosphingolipids and glycosaminoglycans accumulate in lysosomes. The resulting lysosomal dysfunction causes cellular pathology and changes in the structure and function of organs or tissues. Most lysosomal storage diseases are fatal diseases with limited lifetime (Platt et al. 2018).Studies are ongoing to develop new diagnostic and treatment methods in the treatment of lysosomal storage diseases, as in all other hereditary diseases. Tay-Sachs disease, an autosomal recessive LSD, serves as a prime example. In this disease, a deficiency in the enzyme β-hexosaminidase A (HexA) prevents the breakdown of the glycolipid GM2 ganglioside, leading to its accumulation within lysosomes. As a result, nerve cells are particularly damaged, and patients die at a very young age due to degeneration of nerve cells. The Hexa-/-Neu3-/- mouse model has been developed as a suitable model to mimic the pathophysiology of Tay-Sachs disease (Seyrantepe et al. 2018).

In research involving lysosomal storage diseases, primary cells isolated from the brains of animal models are frequently utilized. Two commonly employed methods for

isolating neurons and glial cells from neural tissue are fluorescence-activated cell sorting (FACS) and magnetic-activated cell sorting (MACS) (Pan and Wan 2020). FACS relies on labeling cells with fluorescently tagged antibodies for subsequent separation, while MACS utilizes magnetic particles conjugated with cell-specific antibodies. Although these methods can achieve high cell purity, they are often multi-step, laborious, time-consuming, and expensive, requiring significant resources and specialized equipment.

Cells exhibit unique physical properties that are influenced by various factors, including differentiation (Compagnucci et al. 2016; Ravera, Efeoglu, and Byrne 2021), apoptosis (Wlodkowic, Skommer, and Darzynkiewicz 2012), biochemical processes that cause differences in intracellular products, or the cell cycle state (Horbay and Bilyy 2016; Zlotek-Zlotkiewicz et al. 2015). In cell biology and disease mechanism studies, separation and purification processes can be carried out by taking advantage of the different physical properties of cells. One of these properties is the density, which expresses the amount of mass the cell has per unit volume. Cell density varies depending on the cell type or the biological and morphological conditions (Neurohr and Amon 2020). Determining the volumetric mass density of different cell types or separating cells within a heterogeneous population based on their density is crucial for various research applications, including cell biology, drug testing, disease diagnosis, and the development of novel treatments.

While the density profiles of different primary brain tissue subpopulations and the impact of lysosomal storage diseases on cell density have not been extensively studied, this thesis aimed to explore the potential of density-based characterization of primary neural cells and the potential of using density as a marker of changes caused by different cell types of this tissue and lysosomal storage diseases, using magnetic levitation technology. We colloborated with Seyrantepe Lab at the Department Molecular Biology and Genetics at IYTE to obtain primary brain cells from mouse models with lysosomal storage diseases.

### 4.4.1. Methods

#### 4.4.1.1. Mating of Experimental Mice

Neu1+/- and Hexa+/-Neu3+/- mice used were housed in IYTEDEHAM with a work permit from the Ministry of Agriculture. The study was conducted with the approval of the IYTE HADYEK ethics committee. First, they were mated with 4 female (Neu1+/-) and 2 male mice (Neu1+/-). After the mating process of the mice, a 0.5 cm piece of the tails was taken for genotyping purposes, DNA was isolated, and genotyping was completed using appropriate primers. DNA isolation and PCR genotyping were performed in the laboratories of Prof. Dr. Volkan Seyrantepe at the Izmir Institute of Technology. All mating and aging procedures were performed in IYTEDEHAM. At the end of the experiments, only heterozygous male mice were bred in IYTEDEHAM to ensure the continuity of the colony, and mating procedures were continued. During this process, the number of Neu1-/- mice was kept to a minimum. Neu1+/+ mice were used as controls. Hexa+/+ (Normal), and Hexa-/-Neu3-/- mouse colonies were created by mating heterozygotes (Hexa+/-Neu3+/- or Hexa+/-Neu3+/-). For this purpose, 8 female Hexa+/-Neu3+/- mice were mated with 4 male Hexa+/-Neu3+/- mice. Again, genotyping was performed using appropriate primers (Seyrantepe et al. 2018).

#### 4.4.1.2. Isolation of Neural and Glial Cells from Adult Mouse Brains

Adult Brain Dissociation Kit- (MACS Miltenyi Biotec/130-107-677) and cortex tissue were used to obtain nerve cells from the brains of adult (5 months old) control group (Neu1+/+ and Hexa+/+Neu3+/+) and Neu1-/- and Hexa-/-Neu3-/- mice. Care was taken that the brain pieces taken from the upper hemisphere do not exceed 100 mg in total. The pieces were removed, washed in D-PBS solution and removed from the blood. Then the brains were cut into small pieces and placed in a gentleMACS C tube containing 1950 µl enzyme mix 1 (50 µl enzyme P + 1900 µl buffer Z). The C tube was placed in the m_brain_01 program registered in the gentleMACS Dissociator device and was taken

from the gentleMACS Dissociator device and placed in the MACSmic Tube Rotator device and rotated slowly and continuously for 15 minutes at 37°C. At the end of 15 minutes, 30 µl of enzyme mix 2 (20 µl enzyme Y + 10 µl enzyme A) was added and mixed without vortexing and then the C tube was placed in the m_brain_02 program registered in the gentleMACS Dissociator device. The C tube was taken from the gentleMACS Dissociator device and placed in the MACSmic Tube Rotator device and rotated slowly and continuously for a second time for 15 minutes at 37°C. After this process, the C tube was placed in the m_brain_03 program registered in the gentleMACS Dissociator device. It was placed in the MACSmic Tube Rotator device and rotated slowly and continuously for 15 minutes at 37°C. After centrifuging at 300xg at room temperature, the supernatant was removed and the MACS SmartStrainer (70µm) was placed on the 50 ml tube and wetted with D-PBS, the resulting suspension was passed through the MACS SmartStrainer. Then, 10 ml of D-PBS was added quickly. The supernatant was removed after centrifuging at 300xg at room temperature for 10 minutes. 1ml of 1xRBCL was added to the obtained pellet and incubated at +4°C for 15 minutes and then 10ml of DPBS was added and centrifuged at 300xg at +4°C for 10 minutes and the supernatant was removed.

The resulting pellet was dissolved with 1550 µl of cold D-PBS and mixed with 450 µl of debris removal solution. Then, 450 µl of cold D-PBS was slowly added to create a gradient and the resulting solution was centrifuged for 10 minutes at 3000xg at +4°C, and 3 phases were formed. Then, the upper 2 phases were removed, and the remaining phase was transferred to a 15 ml tube, and cold D-PBS was added until it reached 15 ml, and then the solution was centrifuged for 15 minutes at 1000xg at +4°C, and the supernatant was removed. After this, the obtained pellet was dissolved using 500 µl of 1x Red Blood Cell Lysis solution diluted 1:10 and this solution was incubated at +4°C for 10 minutes and then dissolved with 5 ml PB buffer (BSA dissolved in 1x D-PBS at 1:20) and centrifuged at 300xg for 15 minutes at +4°C. The pellet obtained as a result of centrifugation was dissolved in 500 µl DMEM (DMEM and 10% FBS) and seeded into 6-well cell dishes. After this stage, the nerve cell isolation protocol was applied. Cell culture plates were coated with 0.01% Poly-L-lysine overnight at 37°C before the experiment. The next day, they were washed three times with dd$H_2O$ and kept ready for use.

Magnetic labeling step was started with 3 ml of nerve-glia cell mixture and Neuron Isolation Kit (MACS Miltenyi Biotec/130-115-389) was used for nerve cell

isolation. Mouse nerve cells were separated from mouse brain tissue suspension with magnetic labeling system with the kit. After the cell mixture was centrifuged at 300xg for 10 minutes, the supernatant was completely removed. 80 µl of D-PBS solution containing BSA was added to the cell pellet. Then 20 µl of Non-Neuronal Cell Biotin-Antibody Coctail was added to the cell pellet, mixed well, and incubated in the refrigerator for 5 minutes. 1ml of D-PBS solution containing BSA was added and centrifuged at 300xg for 10 minutes and after the supernatant was removed, 80 µl of D-PBS solution containing BSA was added to the cell pellet. Then, 20 µl of AntiBiotin-MicroBeads was added to the cell pellet, mixed well and incubated in the refrigerator for 10 minutes and BSA-containing D-PBS solution was added to a total volume of 500 µl. After this stage, the magnetic separation section was completed. The LS column was placed in the magnetic field, washed with 3 ml of BSA-containing D-PBS solution and the cell mixture were loaded onto the column, and the flowing solution was collected. The column was washed with 2x1 ml of BSA-containing D-PBS solution and combined with the flowing solution from the previous step. The column was separated from the magnetic separator, placed under a 15 ml falcon, 3 ml of BSA-containing D-PBS solution was added, and glial cells were collected with a syringe. In the cell culture stage, cells were grown in special cell culture plates prepared by coating with Poly-L-lysine. 24-well and 6-well cell plates were used. 50 µL of 1 x $10^5$ cells was seeded in the middle of each well and kept in the incubator at 37°C for 30 minutes, and 450 µL of medium was added to each well. 50% of the medium was changed every day to remove dead cells.

### 4.4.1.3. Isolation of Microglia from Adult Mouse Brains

After anesthesia (xylazine, ketamine) was applied to the mice to be used for microglia isolation, the blood in the whole body was drained by cardiac perfusion method using cold PBS. After the removed brain was washed in cold PBS, it was broken into small pieces in disintegration medium (papain, dispase II and DNAase I dissolved in serum-free DMEM). Then, it was mechanically disintegrated in the MACS Dissociator and rotated at a constant and continuous speed for 45 minutes in the MACS Rotator device at 37°C and pipetted every 15 minutes for 45 minutes to ensure better disintegration of the tissue. At the end of 45 minutes, 5 ml of neutralization medium was added for

inactivation of enzymes and centrifuged at 250xg for 5 minutes at room temperature and then the supernatant was removed, and the cell pellet was dissolved in 5 ml of serum-free DMEM. After this step is repeated once more, 3 ml of DMEM containing FBS was added to the obtained cell pellet and dissolved, and passed through 100 µm, 70 µm and 40 µm cell filters, respectively, and centrifuged for 8 minutes at 250xg at room temperature. Then, the supernatant was removed, the cell pellet was dissolved in 5 ml of DMEM containing FBS, and the process was repeated again. After the obtained cell pellet was dissolved in 4 ml of 37% SIP (stock isotonic percoll in PBS), a percoll gradient was created. At this stage, first 4 ml of 70% SIP, then the cell solution in 37% SIP, and then 30% SIP were added to a new 15 ml falcon. It was covered with 2 ml of PBS and centrifuged for 40 minutes at 300xg and 18 degrees. At the top of the gradient formed at the end of the centrifugation, myelin was obtained, and a microglia layer between 37% and 70% was obtained. This microglia layer was taken, dissolved in 6 ml of PBS, and centrifuged for 7 minutes at 500xg and 4 degrees. The cell pellet was dissolved in PBS again and centrifuged for 5 minutes at 800xg and 4 degrees, and this process was repeated 2 more times, and the cell pellet was dissolved in DMEM containing 10% FBS and grown in a 24-well cell plate.

### 4.4.1.4. Magnetic Levitation of Primary Glial Cells

In this system, primary glial cells suspended in 25 mM $Gd^{3+}$ containing 50 µl paramagnetic medium were loaded into a microcapillary channel. They were repulsed from the region of high magnetic field came to an equilibrium point according to their volumetric mass density as explained in the previous section.

### 4.4.1.5. Statistical Analysis

Results were expressed as mean ± standard deviation for each experiment. Each experiment had at least 3 samples in each repetition. In cases where statistical

comparisons need to be made, the differences between groups were measured by ANOVA test, 5% was considered as the significance limit.

### 4.4.2. Results and Discussion

In this section of the thesis, the determination of volumetric cell density with samples isolated from primary brain cells of mice with lysosomal storage diseases using the magnetic levitation system was aimed. We applied the magnetic levitation technique, which can classify different cell groups according to their single-cell densities at separate equilibrium points, that can be utilized for density-based diagnosis of primary neural cells in brain tissue.

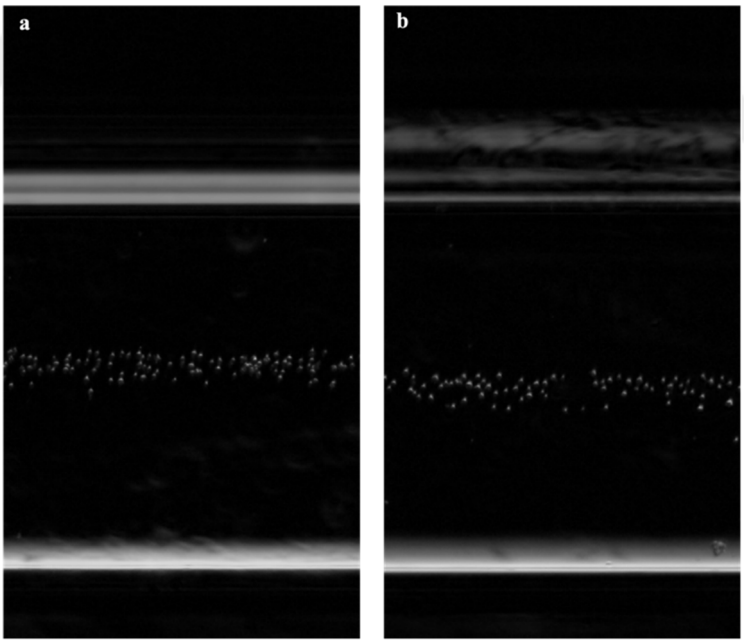


Figure 58. Magnetic levitation images of primary neuroglial cells isolated from wild-type (WT) mouse with Hexa-/-Neu3-/- background (a) and Hexa -/- mouse model (b) in the presence of 25 mM $Gd^3$. n=3.

Primary brain cells were isolated from Hexa-/- and Hexa-/-Neu3-/- mouse models mimicking Tay-Sachs disease and healthy mice (wild-type) using the procedure explained in the methods section. The isolated brain glial cells were levitated in the magnetic levitation system with the determined $Gd^{3+}$ concentration (25 mM). Magnetic levitation images of glial cells isolated from Hexa -/- and wild-type mouse models are shown in Figure 58.

The average levitation heights of the neuroglial cells were determined as 879.5 µm and 914.1 µm, for WT and Hexa-/- models, respectively. The difference between the average levitation heights was found to be statistically significant (Figure 59, Table 6).

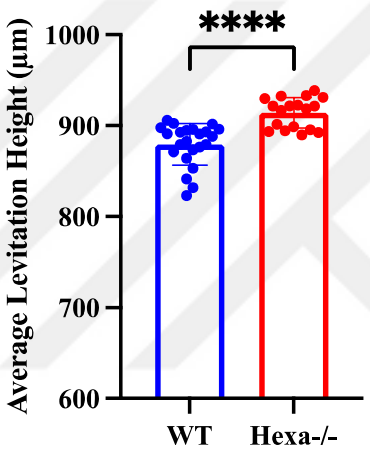


Figure 59. Levitation profiles of primary neuroglial cells isolated from wild-type (WT) mouse with Hexa-/-Neu3-/- background and Hexa-/- mouse model in the presence of 25 mM $Gd^{3+}$. **** indicates a statistically significant difference ($p<0.0001$) between the groups.

Table 6. Analysis of levitation profiles of the neuroglial cells isolated from WT mouse with Hexa-/-Neu3-/- background and Hexa -/- mouse model.

| | Mean | Minimum | Maximum | Range | Std Dev | Skew | CoV(%) |
|---|---|---|---|---|---|---|---|
| WT | 879.5 | 823.1 | 905.7 | 82.65 | 22.86 | -1.231 | 2.60% |
| Hexa-/- | 914.1 | 889.7 | 938.4 | 48.7 | 16.65 | -0.2105 | 1.82% |

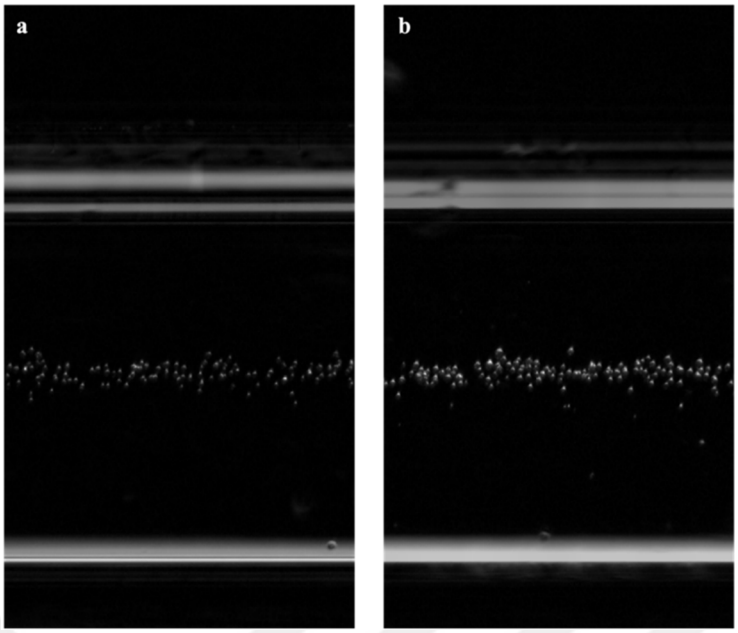


Figure 60. Magnetic levitation images of primary neuroglial cells isolated from wild-type (WT) mouse with Hexa-/-Neu3-/- background (a) and Hexa-/-Neu3-/- mouse model (b) in the presence of 25 mM $Gd^{3+}$. n=3.

Subsequently, primary neuroglial cells isolated from the Hexa-/-Neu3-/- mouse model were levitated (Figure 60). The average levitation heights of the cells were calculated as 879.5 μm and 904.6 μm, respectively, and the difference between the average levitation heights was found to be statistically significant (Figure 61, Table 7).

The observed increase in the levitation heights of neuroglial cells isolated from Hexa-/- and Hexa-/-Neu3-/- models compared to wild-type (WT) cells was expected. In Tay-Sachs disease, lysosomal degradation mechanisms are impaired due to mutations in the gene encoding the β-Hexosaminidase A (HEXA) enzyme. This leads to the accumulation of GM2 gangliosides within lysosomes. GM2 gangliosides are glycosphingolipids that play a role in the biotransformation of complex brain gangliosides. As lipid accumulation is known to decrease volumetric mass density, it consequently increases the levitation heights of the cells (Puluca et al. 2020; Sarigil et al. 2019). The increased levitation heights observed in neuroglial cells from Hexa-/- and Hexa-/-Neu3-/- mouse models compared to wild-type (WT) cells can be attributed to the accumulation of glycosphingolipid molecules within the cells. Similarly, an increase in levitation height was expected in neuroglial cells from the Neu1-/- Sialidosis mouse

model compared to WT, as Sialidosis is characterized by a deficiency in the Neu1 sialidase enzyme, leading to the accumulation of sialyloligosaccharides, sialylglycoproteins, and GD3 gangliosides within cells.

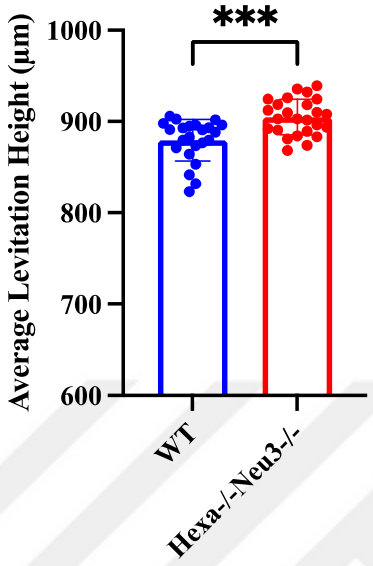


Figure 61. Levitation profiles of primary neuroglial cells isolated from wild-type (WT) mouse with Hexa-/-Neu3-/- background and Hexa-/-Neu3-/- mouse model in the presence of 25 mM $Gd^{3+}$. *** indicates a statistically significant difference ($p<0.001$) between the groups.

Table 7. Analysis of levitation profiles of the neuroglial cells isolated from WT mouse with Hexa-/-Neu3-/- background and Hexa-/-Neu3-/- mouse model.

| | Mean | Minimum | Maximum | Range | Std Dev | Skew | CoV(%) |
|---|---|---|---|---|---|---|---|
| WT | 879.5 | 823.1 | 905.7 | 82.65 | 22.86 | -1.231 | 2.60% |
| Hexa-/-Neu3-/- | 904.6 | 868.3 | 939.3 | 70.92 | 19.51 | 0.01226 | 2.16% |

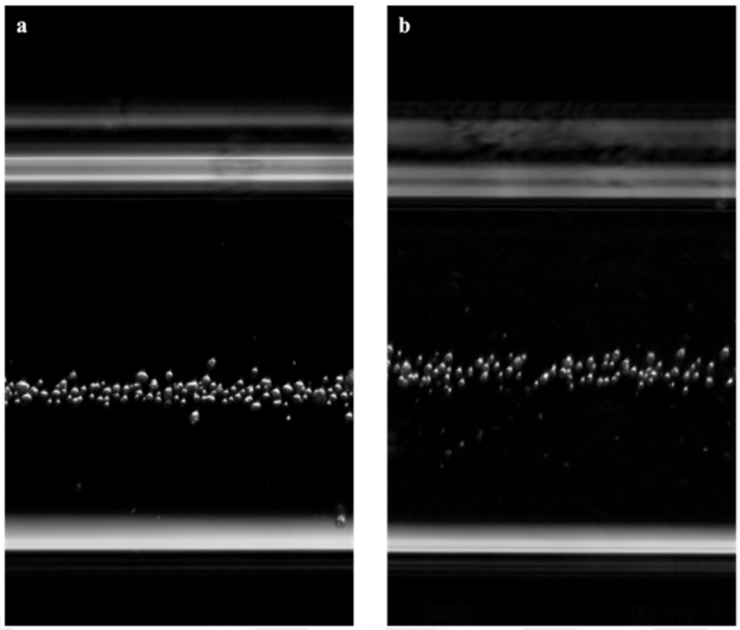


Figure 62. Magnetic levitation images of primary neuroglial cells isolated from wild-type (WT) mouse with Neu1-/- background (a) and Neu1-/- mouse model (b) in the presence of 25 mM $Gd^{3+}$. n=3.

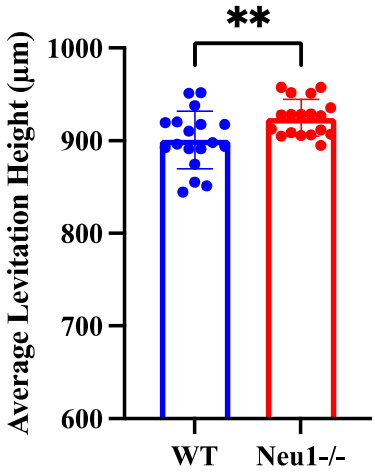


Figure 63. Levitation profiles of primary neuroglial cells isolated from wild-type (WT) mouse with Neu1 -/- background and Neu1 -/- mouse model in the presence of 25 mM $Gd^{3+}$. ** indicates a statistically significant difference ($p<0.01$) between the groups.

Table 8. Analysis of levitation profiles of the neuroglial cells isolated from WT mouse with Neu1-/- background and Neu1-/- mouse model.

| | Mean | Minimum | Maximum | Range | Std Dev | Skew | CoV(%) |
|---|---|---|---|---|---|---|---|
| WT | 900.7 | 844.4 | 951.8 | 107.4 | 31.29 | -0.173 | 3.47% |
| Neu1-/- | 924.6 | 894.7 | 957.6 | 62.87 | 19.8 | 0.4208 | 2.14% |

Indeed, neuroglial cells from the Neu1-/- Sialidosis model exhibited significantly higher levitation heights compared to those from the Hexa-/-Neu3-/- Tay-Sachs model (Figure 64). This finding suggests that higher levitation heights in the Neu1-/- model may indicate a greater accumulation of metabolites within the neuroglial cells. However, further analysis with a larger cohort of samples from both healthy and diseased mice is required to establish a definitive correlation between volumetric mass density, lysosomal metabolite accumulation, and disease state.

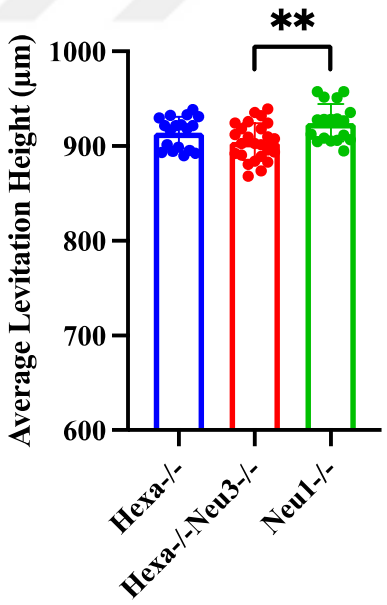


Figure 64. Levitation profiles of primary neuroglial cells isolated from Hexa-/-, Hexa-/-Neu3-/- and Neu1 -/- mouse models in the presence of 25 mM $Gd^{3+}$. ** indicates a statistically significant difference ($p<0.01$) between the groups.

### 4.4.3. Conclusions

The microcapillary-based magnetic levitation system demonstrated the ability to detect differences in the volumetric mass density of cells between healthy and diseased models, as well as between different lysosomal storage disease models. However, it is important to note that primary neuroglial cell isolates from mice are a heterogeneous population comprising oligodendrocytes, astrocytes, and microglia. The relative proportions of these cell types within each isolate are currently unknown, which could potentially influence the average volumetric mass density of the mixture. Therefore, increasing the number of samples isolated from model mice is crucial for accurate interpretation of average levitation heights and volumetric mass density in neuroglial cells associated with different lysosomal storage diseases. Nonetheless, these findings reveal the potential of utilizing the microcapillary-based magnetic levitation system as a diagnostic tool for detecting anomalies in nervous system cells.

# CHAPTER 5

# CONCLUSIONS

Magnetic levitation technique based on negative magnetophoresis principle was used for two purposes in this thesis: For the development of three three-dimensional scaffold and label-free spheroid models to mimic *in vivo* tissue, and for the detection of primary cells isolated from the sources that have neurodevelopmental disorders.

Previous studies have demonstrated the use of axial magnetic levitation, employing a single-ring magnet, for the formation of three-dimensional cellular aggregates. In this thesis, a ring magnet-based magnetic levitation system was utilized to create layered three-dimensional spheroids composed of breast cancer and epithelial cells, resulting in heterogeneous 3D models that mimic the preinvasive stages of breast cancer. Various localization of the cells in heterogenous spheroids were shown via different cell loading methods. Moreover, the macromolecular crowding method was performed on the magnetic levitation spheroids to enhance the accumulation of tissue-specific ECM molecules, leading to the development of improved scaffold-free spheroid models for the first time. Notably, this approach enabled the successful creation of spheroid models through magnetic levitation without the need for mechanical support, within a matter of hours, and in a low magnetic field region. This was achieved without the use of any labeling molecules and without incurring significant costs. Moreover, the configuration of the ring magnet-based levitation system offers several advantages over other magnetic force-based bioprinting methods. These advantages include easy manipulation of the culture medium since it does not contain any upper limits; alterable spheroid dimensions because the system is suitable for various sizes of culture tubes; the self-assembling ability of cells without the use of any nozzles or any other extra forces which eliminates the mechanical force on the cells.

The microcapillary-based magnetic levitation system was previously used to distinguish living or non-living substances based on their volumetric mass density by benefiting the difference between the magnetic susceptibility of the substances and the

paramagnetic medium. The system could detect various cell types without the need to use high-degree magnetic fields. In the context of this thesis, the microcapillary-based magnetic levitation system was employed to analyze the volumetric mass density profiles of neural cells derived from patients or mouse models with neurodevelopmental anomalies. The results demonstrated the successful discrimination of diseased cells from their healthy counterparts based on their distinct volumetric mass densities. Furthermore, the relationship between single-cell density and cellular changes during the differentiation of induced pluripotent cells into neural precursors was investigated. The potential of using magnetic levitation as a method to distinguish cells at different stages of differentiation was also evaluated.

Both magnetic levitation systems employed in this thesis utilize permanent magnets to generate magnetic gradients for cell manipulation. This approach eliminates the need for electrical power, enabling rapid and efficient processing. Furthermore, as labeling is not required, potential negative effects on cell viability are minimized, and the need for time-consuming and labor-intensive labeling steps is eliminated. Both systems are user-friendly and facilitate the handling of living cells. Consequently, they have the potential for widespread application in various fields, including tissue engineering and both diagnostic and therapeutic research for cancer, central nervous system disorders, and numerous other diseases.

# REFERENCES


Abbas, Zaid Nsaif, Ali Z. Al-Saffar, Saba Mahdi Jasim, and Ghassan M. Sulaiman. 2023. "Comparative Analysis between 2D and 3D Colorectal Cancer Culture Models for Insights into Cellular Morphological and Transcriptomic Variations." *Scientific Reports* 13 (1): 18380. https://doi.org/10.1038/s41598-023-45144-w.

Abdel Fattah, Abdel Rahman, Elvira Meleca, Sarah Mishriki, Alina Lelic, Fei Geng, Rakesh P Sahu, Suvojit Ghosh, and Ishwar K Puri. 2016. "In Situ 3D Label-Free Contactless Bioprinting of Cells through Diamagnetophoresis." *ACS Biomaterials Science & Engineering* 2 (12): 2133–38. https://doi.org/10.1021/acsbiomaterials.6b00614.

Abuwatfa, Waad H, William G Pitt, and Ghaleb A Husseini. 2024. "Scaffold-Based 3D Cell Culture Models in Cancer Research." *Journal of Biomedical Science* 31 (1): 7. https://doi.org/10.1186/s12929-024-00994-y.

Aijie, Chen, Lai Xuan, Liang Huimin, Zhang Yanli, Kang Yiyuan, Lin Yuqing, and Shao Longquan. 2018. "Nanoscaffolds in Promoting Regeneration of the Peripheral Nervous System." *Nanomedicine* 13 (9): 1067–85. https://doi.org/10.2217/nnm-2017-0389.

Akiyama, Yoshitake, and Keisuke Morishima. 2011. "Label-Free Cell Aggregate Formation Based on the Magneto-Archimedes Effect." *Applied Physics Letters* 98 (16): 163702. https://doi.org/10.1063/1.3581883.

Allen, Nicola J, and Ben A Barres. 2009. "Glia — More than Just Brain Glue." *Nature* 457 (7230): 675–77. https://doi.org/10.1038/457675a.

Angeloni, Valentina, Nicola Contessi, Cinzia De Marco, Serena Bertoldi, Maria Cristina Tanzi, Maria Grazia Daidone, and Silvia Farè. 2017. "Polyurethane Foam Scaffold as in Vitro Model for Breast Cancer Bone Metastasis." *Acta Biomaterialia* 63 (11): 306–16. https://doi.org/10.1016/j.actbio.2017.09.017.

Anil-Inevi, Muge, Kerem Delikoyun, Gulistan Mese, H. Cumhur Tekin, and Engin Ozcivici. 2021. "Magnetic Levitation Assisted Biofabrication, Culture, and Manipulation of 3D Cellular Structures Using a Ring Magnet Based Setup." *Biotechnology and Bioengineering* 118 (12): 4771–85. https://doi.org/10.1002/bit.27941.

Anil-Inevi, Muge, Ozden Yalcin-Ozuysal, Oyku Sarigil, Gulistan Mese, Engin Ozcivici, Sena Yaman, and H. Cumhur Tekin. 2019. “Biofabrication of Cellular Structures Using Weightlessness as a Biotechnological Tool.” *Proceedings of 9th International Conference on Recent Advances in Space Technologies, RAST 2019* 1 (1): 929–31. https://doi.org/10.1109/RAST.2019.8767431.

Anil-Inevi, Muge, Sena Yaman, Ahu Arslan Yildiz, Gulistan Mese, Ozden Yalcin-Ozuysal, H Cumhur Tekin, and Engin Ozcivici. 2018. “Biofabrication of in Situ Self Assembled 3D Cell Cultures in a Weightlessness Environment Generated Using Magnetic Levitation.” *Scientific Reports* 8 (1): 7239. https://doi.org/10.1038/s41598-018-25718-9.

Anil-Inevi, Muge, Esra Yilmaz, Oyku Sarigil, H. Cumhur Tekin, and Engin Ozcivici. 2020. “Single Cell Densitometry and Weightlessness Culture of Mesenchymal Stem Cells Using Magnetic Levitation.” In *Methods in Molecular Biology*, 2125 (1): 15–25. Humana Press Inc.

Araújo, Taís Bacelar Sacramento de, Raphael Luís Rocha Nogueira, Leonardo de Oliveira Siquara da Rocha, Iasmin Nogueira Bastos, Rosane Borges Dias, Bruno Solano De Freitas Souza, Daniel William Lambert, Ricardo D. Coletta, Viviane Aline Oliveira Silva, and Clarissa A. Gurgel Rocha. 2024. “Enhancing Scaffold-Free Spheroid Models: 3D Cell Bioprinting Method for Metastatic HSC3–Oral Squamous Carcinoma Cell Line.” *SLAS Discovery* 29 (4): 100158. https://doi.org/10.1016/j.slasd.2024.100158.

Armstrong, James P.K., and Molly M. Stevens. 2019. “Emerging Technologies for Tissue Engineering: From Gene Editing to Personalized Medicine.” *Tissue Engineering - Part A* 25 (9–10): 688–92. https://doi.org/10.1089/ten.tea.2019.0026.

Asadi, Khatereh, Nazafarin Samiraninezhad, Amin Reza Akbarizadeh, Abbas Amini, and Ahmad Gholami. 2024. “Stimuli-Responsive Hydrogel Based on Natural Polymers for Breast Cancer.” *Frontiers in Chemistry* 12 (1): 1325204. https://doi.org/10.3389/fchem.2024.1325204.

Assunção, Marisa, Dorsa Dehghan-Baniani, Chi Him Kendrick Yiu, Thomas Später, Sebastian Beyer, and Anna Blocki. 2020. “Cell-Derived Extracellular Matrix for Tissue Engineering and Regenerative Medicine.” *Frontiers in Bioengineering and Biotechnology* 8 (1): 602009. https://doi.org/10.3389/fbioe.2020.602009.

Attiogbe, Emilie, Sébastien Larochelle, Yanis Chaib, Carine Mainzer, Adèle Mauroux, Sylvie Bordes, Brigitte Closs, Caroline Gilbert, and Véronique J. Moulin. 2023. “An in Vitro Autologous, Vascularized, and Immunocompetent Tissue Engineered Skin Model Obtained by the Self-Assembled Approach.” *Acta Biomaterialia* 168 (9): 361–71. https://doi.org/10.1016/j.actbio.2023.06.045.

Augello, Andrea, Roberta Tasso, Simone Maria Negrini, Ranieri Cancedda, and Giuseppina Pennesi. 2007. “Cell Therapy Using Allogeneic Bone Marrow Mesenchymal Stem Cells Prevents Tissue Damage in Collagen-Induced Arthritis.” *Arthritis and Rheumatism* 56 (4): 1175–86. https://doi.org/10.1002/art.22511.

Auvinen, Vili Veli, Arto Merivaara, Jasmi Kiiskinen, Heli Paukkonen, Patrick Laurén, Tiina Hakkarainen, Raili Koivuniemi, et al. 2019. “Effects of Nanofibrillated Cellulose Hydrogels on Adipose Tissue Extract and Hepatocellular Carcinoma Cell Spheroids in Freeze-Drying.” *Cryobiology* 91 (12): 137–45. https://doi.org/10.1016/j.cryobiol.2019.09.005.

Bahcecioglu, Gokhan, Gozde Basara, Bradley W. Ellis, Xiang Ren, and Pinar Zorlutuna. 2020. “Breast Cancer Models: Engineering the Tumor Microenvironment.” *Acta Biomaterialia* 106 (4): 1–21. https://doi.org/10.1016/j.actbio.2020.02.006.

Baiguera, Silvia, Costantino Del Gaudio, Elena Lucatelli, Elena Kuevda, Margherita Boieri, Benedetta Mazzanti, Alessandra Bianco, and Paolo Macchiarini. 2014. “Electrospun Gelatin Scaffolds Incorporating Rat Decellularized Brain Extracellular Matrix for Neural Tissue Engineering.” *Biomaterials* 35 (4): 1205–14. https://doi.org/10.1016/j.biomaterials.2013.10.060.

Bain, Jennifer M., Adel Ardalan, and Sylvie Goldman. 2021. “Deliberate Paradigm Shift in Research in Rare Neurodevelopmental Disorders.” *Orphanet Journal of Rare Diseases* 16 (1): 263. https://doi.org/10.1186/s13023-021-01885-3.

Balkwill, Frances R., Melania Capasso, and Thorsten Hagemann. 2012. “The Tumor Microenvironment at a Glance.” *Journal of Cell Science* 125 (23): 5591–96. https://doi.org/10.1242/jcs.116392.

Barbier, Martin A., Karel Ferland, Henri De Koninck, Emilie J. Doucet, Ludivine Dubourget, Min Joon Kim, Bettina Cattier, et al. 2024. “Cancer Spheroids Embedded in Tissue-Engineered Skin Substitutes: A New Method to Study Tumorigenicity In Vivo.” *International Journal of Molecular Sciences* 25 (3): 1513. https://doi.org/10.3390/ijms25031513.

Barbosa, Mélanie A.G., Cristina P.R. Xavier, Rúben F. Pereira, Vilma Petrikaitė, and M. Helena Vasconcelos. 2022. “3D Cell Culture Models as Recapitulators of the Tumor Microenvironment for the Screening of Anti-Cancer Drugs.” *Cancers* 14 (1): 190. https://doi.org/10.3390/cancers14010190.

Bardini, Roberta, and Stefano Di Carlo. 2024. “Computational Methods for Biofabrication in Tissue Engineering and Regenerative Medicine-a Literature Review.” *Computational and Structural Biotechnology Journal* 23 (1): 601–16. https://doi.org/10.1016/j.csbj.2023.12.035.

Bedir, Tuba, Songul Ulag, Cem Bulent Ustundag, and Oguzhan Gunduz. 2020. “3D Bioprinting Applications in Neural Tissue Engineering for Spinal Cord Injury Repair.” *Materials Science and Engineering: C* 110 (1): 110741. https://doi.org/10.1016/j.msec.2020.110741.

Bowles, Kathryn R., T. C.W. Julia, Lu Qian, Benjamin M. Jadow, and Alison M. Goate. 2019. “Reduced Variability of Neural Progenitor Cells and Improved Purity of Neuronal Cultures Using Magnetic Activated Cell Sorting.” *PLoS ONE* 14 (3): 1–18. https://doi.org/10.1371/journal.pone.0213374.

Braak, Heiko, Eva Braak, Jürgen Bohl, and Walter Lang. 1989. “Alzheimer’s Disease: Amyloid Plaques in the Cerebellum.” *Journal of the Neurological Sciences* 93 (2): 277–87. https://doi.org/10.1016/0022-510X(89)90197-4.

Brancato, Virginia, Valentina Comunanza, Giorgia Imparato, Davide Corà, Francesco Urciuolo, Alessio Noghero, Federico Bussolino, and Paolo A Netti. 2017. “Bioengineered Tumoral Microtissues Recapitulate Desmoplastic Reaction of Pancreatic Cancer.” *Acta Biomaterialia* 49 (1): 152–66. https://doi.org/10.1016/j.actbio.2016.11.072.

Bratt-Leal, Andrés M., Kirsten L. Kepple, Richard L. Carpenedo, Marissa T. Cooke, and Todd C. McDevitt. 2011. “Magnetic Manipulation and Spatial Patterning of Multi-Cellular Stem Cell Aggregates.” *Integrative Biology* 3 (12): 1224–32. https://doi.org/10.1039/c1ib00064k.

Cai, Mao Hua, Xiao Yi Chen, Luo Qin Fu, Wen Lin Du, Xue Yang, Xiao Zhou Mou, and Pei Yang Hu. 2021. “Design and Development of Hybrid Hydrogels for Biomedical Applications: Recent Trends in Anticancer Drug Delivery and Tissue Engineering.” *Frontiers in Bioengineering and Biotechnology* 9 (2): 630943. https://doi.org/10.3389/fbioe.2021.630943.

Campbell, Jonathan J., Anke Husmann, Robert D. Hume, Christine J. Watson, and Ruth E. Cameron. 2017. “Development of Three-Dimensional Collagen Scaffolds with Controlled Architecture for Cell Migration Studies Using Breast Cancer Cell Lines.” *Biomaterials* 114 (1): 34–43. https://doi.org/10.1016/j.biomaterials.2016.10.048.

Capella-Monsonís, Héctor, João Q. Coentro, Valeria Graceffa, Zhuning Wu, and Dimitrios I. Zeugolis. 2018. "An Experimental Toolbox for Characterization of Mammalian Collagen Type i in Biological Specimens." *Nature Protocols* 13 (3): 507–29. https://doi.org/10.1038/nprot.2017.117.

Carpenter, Melissa K., Margaret S. Inokuma, Jerrod Denham, Tahmina Mujtaba, Choy Pik Chiu, and Mahendra S. Rao. 2001. "Enrichment of Neurons and Neural Precursors from Human Embryonic Stem Cells." *Experimental Neurology* 172 (2): 383–97. https://doi.org/10.1006/exnr.2001.7832.

Casey, John, Xiaoshan Yue, Trung Dung Nguyen, Aylin Acun, Victoria R Zellmer, Siyuan Zhang, and Pinar Zorlutuna. 2017. "3D Hydrogel-Based Microwell Arrays as a Tumor Microenvironment Model to Study Breast Cancer Growth." *Biomedical Materials* 12 (2): 025009. https://doi.org/10.1088/1748-605X/aa5d5c.

Chaicharoenaudomrung, Nipha, Phongsakorn Kunhorm, and Parinya Noisa. 2019. "Three-Dimensional Cell Culture Systems as an in Vitro Platform for Cancer and Stem Cell Modeling." *World Journal of Stem Cells* 11 (12): 1065–83. https://doi.org/10.4252/wjsc.v11.i12.1065.

Chau, Monica J.;Deveau, Todd C.;Song, Mingke;Gu, Xiaohuan;Chen, Dongdong;Wei, Ling. 2014. "IPSC Transplantation Increases Regeneration and Functional Recovery After Ischemic Stroke in Neonatal Rats." *Stem Cells Express* 32 (1): 3075–87. https://doi.org/10.1002/stem.1802.

Chaudhary, Shikha, and Eliza Chakraborty. 2022. "Hydrogel Based Tissue Engineering and Its Future Applications in Personalized Disease Modeling and Regenerative Therapy." *Beni-Suef University Journal of Basic and Applied Sciences* 11 (1): 1–15. https://doi.org/10.1186/s43088-021-00172-1.

Chen, Annan, Wanying Wang, Zhengyi Mao, Yunhu He, Shiting Chen, Guo Liu, Jin Su, Pei Feng, Yusheng Shi, and Chunze Yan. 2023. "Multimaterial 3D and 4D Bioprinting of Heterogenous Constructs for Tissue Engineering." *Advanced Materials* 36 (34): 2307686. https://doi.org/10.1002/adma.202307686.

Chiang, Cheng En, Yi Qiao Fang, Chao Ting Ho, Marisa Assunção, Sheng Ju Lin, Yu Chieh Wang, Anna Blocki, and Chieh Cheng Huang. 2021. "Bioactive Decellularized Extracellular Matrix Derived from 3D Stem Cell Spheroids under Macromolecular Crowding Serves as a Scaffold for Tissue Engineering." *Advanced Healthcare Materials* 10 (11): 2100024. https://doi.org/10.1002/adhm.202100024.

Chiou, Pei Yu, Aaron T. Ohta, and Ming C. Wu. 2005. “Massively Parallel Manipulation of Single Cells and Microparticles Using Optical Images.” *Nature* 436 (7049): 370–72. https://doi.org/10.1038/nature03831.

Clémence, Dubois, Dufour Robin, Daumar Pierre, Aubel Corinne, Szczepaniak Claire, Blavignac Christelle, Mounetou Emmanuelle, Penault-Llorca Frédérique, and Mahchid Bamdad. 2017. “Development and Cytotoxic Response of Two Proliferative MDA-MB-231 and Non-Proliferative SUM1315 Three-Dimensional Cell Culture Models of Triple-Negative Basal-like Breast Cancer Cell Lines.” *Oncotarget* 8 (56): 95316–31. https://doi.org/10.18632/oncotarget.20517.

Close, David A, Daniel P Camarco, Feng Shan, Stanton J Kochanek, and Paul A Johnston. 2018. “The Generation of Three-Dimensional Head and Neck Cancer Models for Drug Discovery in 384-Well Ultra-Low Attachment Microplates.” In *High Content Screening: A Powerful Approach to Systems Cell Biology and Phenotypic Drug Discovery*, edited by Paul A Johnston and Oscar J Trask, 2nd ed., 355–69. New York, NY: Springer New York.

Compagnucci, Claudia, Emanuela Piermarini, Antonella Sferra, Rossella Borghi, Alessia Niceforo, Stefania Petrini, Fiorella Piemonte, and Enrico Bertini. 2016. “Cytoskeletal Dynamics during in Vitro Neurogenesis of Induced Pluripotent Stem Cells (IPSCs).” *Molecular and Cellular Neuroscience* 77 (1): 113–24. https://doi.org/10.1016/j.mcn.2016.10.002.

Conforti, Laura, Jonathan Gilley, and Michael P. Coleman. 2014. “Wallerian Degeneration: An Emerging Axon Death Pathway Linking Injury and Disease.” *Nature Reviews Neuroscience* 15 (6): 394–409. https://doi.org/10.1038/nrn3680.

Cooney, Damon S., Eric G. Wimmers, Zuhaib Ibrahim, Johanna Grahammer, Joani M. Christensen, Gabriel A. Brat, Lehao W. Wu, et al. 2016. “Mesenchymal Stem Cells Enhance Nerve Regeneration in a Rat Sciatic Nerve Repair and Hindlimb Transplant Model.” *Scientific Reports* 6 (7): 1–12. https://doi.org/10.1038/srep31306.

Costa, Elisabete C., André F. Moreira, Duarte de Melo-Diogo, Vítor M. Gaspar, Marco P. Carvalho, and Ilídio J. Correia. 2016. “3D Tumor Spheroids: An Overview on the Tools and Techniques Used for Their Analysis.” *Biotechnology Advances* 34 (8): 1427–41. https://doi.org/10.1016/j.biotechadv.2016.11.002.

Cowell, Catherine F., Britta Weigelt, Rita A. Sakr, Charlotte K.Y. Ng, James Hicks, Tari A. King, and Jorge S. Reis-Filho. 2013. “Progression from Ductal Carcinoma in Situ to Invasive Breast Cancer: Revisited.” *Molecular Oncology* 7 (5): 859–69. https://doi.org/10.1016/j.molonc.2013.07.005.

Curcio, Michele, and Frank Bradke. 2018. “Axon Regeneration in the Central Nervous System: Facing the Challenges from the Inside.” *Annual Review of Cell and Developmental Biology* 34 (7): 495–521. https://doi.org/10.1146/annurev-cellbio-100617-062508.

Daquinag, Alexes C, Glauco R Souza, and Mikhail G Kolonin. 2012. “Adipose Tissue Engineering in Three-Dimensional Levitation Tissue Culture System Based on Magnetic Nanoparticles.” *Tissue Engineering Part C: Methods* 19 (5): 336–44. https://doi.org/10.1089/ten.tec.2012.0198.

Davis, John A, David W Inglis, Keith J Morton, David A Lawrence, Lotien R Huang, Stephen Y Chou, James C Sturm, and Robert H Austin. 2006. “Deterministic Hydrodynamics: Taking Blood Apart.” *Proceedings of the National Academy of Sciences* 103 (40): 14779–84. https://doi.org/10.1073/pnas.0605967103.

Demirel, Gamze, Yaprak Donmez Cakıl, Gursel Koltuk, Ranan Gulhan Aktas, and Mahmut Calıskan. 2024. “The Use of Hyaluronic Acid in a 3D Biomimetic Scaffold Supports Spheroid Formation and the Culture of Cancer Stem Cells.” *Scientific Reports* 14 (1): 19560. https://doi.org/10.1038/s41598-024-69047-6.

Dhandapani, Hemavathi, Armaan Siddiqui, Shivam Karadkar, and Prakriti Tayalia. 2023. “In Vitro 3D Spheroid Model Preserves Tumor Microenvironment of Hot and Cold Breast Cancer Subtypes.” *Advanced Healthcare Materials* 12 (21): 2300164. https://doi.org/10.1002/adhm.202300164.

Ding, Chen, and Marc Hammarlund. 2019. “Mechanisms of Injury-Induced Axon Degeneration.” *Current Opinion in Neurobiology* 57 (1):171–78. https://doi.org/10.1016/j.conb.2019.03.006.

Djalali-Cuevas, Adrian, Sergio Garnica-Galvez, Andrea Rampin, Diana Gaspar, Ioannis Skoufos, Athina Tzora, Nikitas Prassinos, Nikolaos Diakakis, and Dimitrios I Zeugolis. 2019. “Preparation and Characterization of Tissue Surrogates Rich in Extracellular Matrix Using the Principles of Macromolecular Crowding.” In *The Extracellular Matrix: Methods and Protocols*, edited by Davide Vigetti and Achilleas D Theocharis, 245–59. New York, NY: Springer New York.

Djalali-Cuevas, Adrian, Mandy Rettel, Frank Stein, Mikhail Savitski, Stephen Kearns, Jack Kelly, Manus Biggs, et al. 2024. “Macromolecular Crowding in Human Tenocyte and Skin Fibroblast Cultures: A Comparative Analysis.” *Materials Today Bio* 25 (4): 100977. https://doi.org/10.1016/j.mtbio.2024.100977.

Doyle, Andrew D., Shayan S. Nazari, and Kenneth M. Yamada. 2022. “Cell-Extracellular Matrix Dynamics.” *Physical Biology* 19 (2): 021002. https://doi.org/10.1088/1478-3975/ac4390.

Duan, Hongmei, Xiaoguang Li, Cong Wang, Peng Hao, Wei Song, Manli Li, Wen Zhao, Yudan Gao, and Zhaoyang Yang. 2016. “Functional Hyaluronate Collagen Scaffolds Induce NSCs Differentiation into Functional Neurons in Repairing the Traumatic Brain Injury.” *Acta Biomaterialia* 45 (1): 182–95. https://doi.org/10.1016/j.actbio.2016.08.043.

Dunne, Lina W, Zhao Huang, Weixu Meng, Xuejun Fan, Ningyan Zhang, Qixu Zhang, and Zhiqiang An. 2014. “Human Decellularized Adipose Tissue Scaffold as a Model for Breast Cancer Cell Growth and Drug Treatments.” *Biomaterials* 35 (18): 4940–49. https://doi.org/10.1016/j.biomaterials.2014.03.003.

Durmus, Naside Gozde, H. Cumhur Tekin, Sinan Guven, Kaushik Sridhar, Ahu Arslan Yildiz, Gizem Calibasi, Ionita Ghiran, Ronald W. Davis, Lars M. Steinmetz, and Utkan Demirci. 2015. “Magnetic Levitation of Single Cells.” *Proceedings of the National Academy of Sciences of the United States of America* 112 (28): E3661–68. https://doi.org/10.1073/pnas.1509250112.

Dvorak, Harold F. 2015. “Tumors: Wounds That Do Not Heal-Redux.” *Cancer Immunology Research* 3 (1): 1–11. https://doi.org/10.1158/2326-6066.CIR-14-0209.

Dzamukova, Maria R., Ekaterina A. Naumenko, Elvira V. Rozhina, Alexander A. Trifonov, and Rawil F. Fakhrullin. 2015. “Cell Surface Engineering with Polyelectrolyte-Stabilized Magnetic Nanoparticles: A Facile Approach for Fabrication of Artificial Multicellular Tissue-Mimicking Clusters.” *Nano Research* 8 (8): 2515–32. https://doi.org/10.1007/s12274-015-0759-1.

Eltom, Abdalla, Gaoyan Zhong, and Ameen Muhammad. 2019. “Scaffold Techniques and Designs in Tissue Engineering Functions and Purposes: A Review.” *Advances in Materials Science and Engineering* 2019 (1): 3429527. https://doi.org/10.1155/2019/3429527.

Fernandes, Hugo, Lorenzo Moroni, Clemens Van Blitterswijk, and Jan De Boer. 2009. “Extracellular Matrix and Tissue Engineering Applications.” *Journal of Materials Chemistry* 19 (31): 5474–84. https://doi.org/10.1039/b822177d.

Ferreira, Luís P., Vítor M. Gaspar, Luís Mendes, Iola F. Duarte, and João F. Mano. 2021. “Organotypic 3D Decellularized Matrix Tumor Spheroids for High-Throughput

Drug Screening." *Biomaterials* 275 (8): 120983. https://doi.org/10.1016/j.biomaterials.2021.120983.

Fonseca, Ana Clotilde, Ferry P W Melchels, Miguel J S Ferreira, Samuel R Moxon, Geoffrey Potjewyd, Tim R Dargaville, Susan J Kimber, and Marco Domingos. 2020. "Emulating Human Tissues and Organs: A Bioprinting Perspective toward Personalized Medicine." *Chemical Reviews* 120 (19): 11093–139. https://doi.org/10.1021/acs.chemrev.0c00342.

Fontoura, Julia C., Christian Viezzer, Fabiana G. dos Santos, Rosane A. Ligabue, Ricardo Weinlich, Renato D. Puga, Dyeison Antonow, Patricia Severino, and Cristina Bonorino. 2020. "Comparison of 2D and 3D Cell Culture Models for Cell Growth, Gene Expression and Drug Resistance." *Materials Science and Engineering C* 107 (2): 110264. https://doi.org/10.1016/j.msec.2019.110264.

Frantz, Christian, Kathleen M. Stewart, and Valerie M. Weaver. 2010. "The Extracellular Matrix at a Glance." *Journal of Cell Science* 123 (24): 4195–4200. https://doi.org/10.1242/jcs.023820.

Gabbiani, G, G B Ryan, and G Majno. 1971. "Presence of Modified Fibroblasts in Granulation Tissue and Their Possible Role in Wound Contraction." *Experientia* 27 (5): 549–50. https://doi.org/10.1007/BF02147594.

Gaitán-Salvatella, Iñigo, Edgar Oliver López-Villegas, Patricia González-Alva, Fernando Susate-Olmos, and Marco Antonio Álvarez-Pérez. 2021. "Case Report: Formation of 3D Osteoblast Spheroid Under Magnetic Levitation for Bone Tissue Engineering." *Frontiers in Molecular Biosciences* 8 (6): 672518. https://doi.org/10.3389/fmolb.2021.672518.

Gangrade, Ankit, and Biman B. Mandal. 2020. "Drug Delivery of Anticancer Drugs from Injectable 3D Porous Silk Scaffold for Prevention of Gastric Cancer Growth and Recurrence." *ACS Biomaterials Science and Engineering* 6 (11): 6195–6206. https://doi.org/10.1021/acsbiomaterials.0c01043.

Ganguli, A, A Mostafa, C Saavedra, Y Kim, P Le, V Faramarzi, R W Feathers, J Berger, K P Ramos-Cruz, and O Adeniba. 2021. "Three-Dimensional Microscale Hanging Drop Arrays with Geometric Control for Drug Screening and Live Tissue Imaging." *Science Advances* 7 (17): eabc1323. https://doi.org/10.1126/sciadv.abc1323.

Garnica-Galvez, Sergio, Stefanie H. Korntner, Ioannis Skoufos, Athina Tzora, Nikolaos Diakakis, Nikitas Prassinos, and Dimitrios I. Zeugolis. 2021. "Hyaluronic Acid as

Macromolecular Crowder in Equine Adipose-Derived Stem Cell Cultures." *Cells* 10 (4): 859. https://doi.org/10.3390/cells10040859.

Gaspar, Diana, Kieran P. Fuller, and Dimitrios I. Zeugolis. 2019. "Polydispersity and Negative Charge Are Key Modulators of Extracellular Matrix Deposition under Macromolecular Crowding Conditions." *Acta Biomaterialia* 88 (4): 197–210. https://doi.org/10.1016/j.actbio.2019.02.050.

Ge, Shencheng, and George M. Whitesides. 2018. "'axial' Magnetic Levitation Using Ring Magnets Enables Simple Density-Based Analysis, Separation, and Manipulation." *Analytical Chemistry* 90 (20): 12239–45. https://doi.org/10.1021/acs.analchem.8b03493.

Gonzalez-Perez, Francisco, Stefano Cobianchi, Claudia Heimann, James B Phillips, Esther Udina, and Xavier Navarro. 2017. "Stabilization, Rolling, and Addition of Other Extracellular Matrix Proteins to Collagen Hydrogels Improve Regeneration in Chitosan Guides for Long Peripheral Nerve Gaps in Rats." *Neurosurgery* 80 (3): 465–74. https://doi.org/10.1093/neuros/nyw068.

Gowrishankar, Swetha, Peng Yuan, Yumei Wu, Matthew Schrag, Summer Paradise, Jaime Grutzendler, Pietro De Camilli, and Shawn M Ferguson. 2015. "Massive Accumulation of Luminal Protease-Deficient Axonal Lysosomes at Alzheimer's Disease Amyloid Plaques." *Proceedings of the National Academy of Sciences* 112 (28): E3699 LP-E3708. https://doi.org/10.1073/pnas.1510329112.

Graceffa, V., and D. I. Zeugolis. 2019. "Carrageenan Enhances Chondrogenesis and Osteogenesis in Human Bone Marrow Stem Cell Culture." *European Cells and Materials* 37 (1): 310–32. https://doi.org/10.22203/ECM.V037A19.

Graham, David M., Mark A. Messerli, and Ronald Pethig. 2012. "Spatial Manipulation of Cells and Organelles Using Single Electrode Dielectrophoresis." *BioTechniques* 52 (1): 39–43. https://doi.org/10.2144/000113802.

Grath, Alexander, and Guohao Dai. 2019. "Direct Cell Reprogramming for Tissue Engineering and Regenerative Medicine." *Journal of Biological Engineering* 13 (1): 14. https://doi.org/10.1186/s13036-019-0144-9.

Griffin, Tagan A., Hayley C. Anderson, and John H. Wolfe. 2015. "Ex Vivo Gene Therapy Using Patient IPSC-Derived NSCs Reverses Pathology in the Brain of a Homologous Mouse Model." *Stem Cell Reports* 4 (5): 835–46. https://doi.org/10.1016/j.stemcr.2015.02.022.

Grochowski, Cezary, Elżbieta Radzikowska, and Ryszard Maciejewski. 2018. “Neural Stem Cell Therapy—Brief Review.” *Clinical Neurology and Neurosurgery* 173 (1): 8–14. https://doi.org/10.1016/j.clineuro.2018.07.013.

Gu, Qi, Eva Tomaskovic-Crook, Rodrigo Lozano, Yu Chen, Robert M Kapsa, Qi Zhou, Gordon G Wallace, and Jeremy M Crook. 2016. “Functional 3D Neural Mini-Tissues from Printed Gel-Based Bioink and Human Neural Stem Cells.” *Advanced Healthcare Materials* 5 (12): 1429–38. https://doi.org/10.1002/adhm.201600095.

Gu, Xiaosong, Fei Ding, and David F. Williams. 2014. “Neural Tissue Engineering Options for Peripheral Nerve Regeneration.” *Biomaterials* 35 (24): 6143–56. https://doi.org/10.1016/j.biomaterials.2014.04.064.

Guo, Xiaoling, Yong Chen, Weiping Ji, Xianwu Chen, Chao Li, and Renshan Ge. 2019. “Enrichment of Cancer Stem Cells by Agarose Multi-Well Dishes and 3D Spheroid Culture.” *Cell and Tissue Research* 375 (2): 397–408. https://doi.org/10.1007/s00441-018-2920-0.

Guryanov, Ivan, Ekaterina Naumenko, Svetlana Konnova, M. Lagarkova, Sergey Kiselev, and R. Fakhrullin. 2019. “Spatial Manipulation of Magnetically-Responsive Nanoparticle Engineered Human Neuronal Progenitor Cells.” *Nanomedicine: Nanotechnology, Biology, and Medicine* 20 (8): 102038. https://doi.org/10.1016/j.nano.2019.102038.

Habanjar, Ola, Mona Diab-Assaf, Florence Caldefie-Chezet, and Laetitia Delort. 2021. “3D Cell Culture Systems: Tumor Application, Advantages, and Disadvantages.” *International Journal of Molecular Sciences* 22 (22): 12200. https://doi.org/10.3390/ijms222212200.

Hansen, N. U.B., F. Genovese, D. J. Leeming, and M. A. Karsdal. 2015. “The Importance of Extracellular Matrix for Cell Function and in Vivo Likeness.” *Experimental and Molecular Pathology* 98 (2): 286–94. https://doi.org/10.1016/j.yexmp.2015.01.006.

Harane, Sanae El, Bochra Zidi, Nadia El Harane, Karl Heinz Krause, Thomas Matthes, and Olivier Preynat-Seauve. 2023. “Cancer Spheroids and Organoids as Novel Tools for Research and Therapy: State of the Art and Challenges to Guide Precision Medicine.” *Cells* 12 (7): 1001. https://doi.org/10.3390/cells12071001.

Hebert, Jess D., Samuel A. Myers, Alexandra Naba, Genevieve Abbruzzese, John M. Lamar, Steven A. Carr, and Richard O. Hynes. 2020. “Proteomic Profiling of the ECM of Xenograft Breast Cancer Metastases in Different Organs Reveals Distinct

Metastatic Niches." *Cancer Research* 80 (7): 1475–85. https://doi.org/10.1158/0008-5472.CAN-19-2961.

Hill, Ciaran S., Michael P. Coleman, and David K. Menon. 2016. "Traumatic Axonal Injury: Mechanisms and Translational Opportunities." *Trends in Neurosciences* 39 (5): 311–24. https://doi.org/10.1016/j.tins.2016.03.002.

Hinz, Boris, Sem H Phan, Victor J Thannickal, Marco Prunotto, Alexis Desmoulière, John Varga, Olivier De Wever, Marc Mareel, and Giulio Gabbiani. 2012. "Recent Developments in Myofibroblast Biology: Paradigms for Connective Tissue Remodeling." *The American Journal of Pathology* 180 (4): 1340–55. https://doi.org/10.1016/j.ajpath.2012.02.004.

Hirota, Noriyuki, Makio Kurashige, Masakazu Iwasaka, Masateru Ikehata, Hiromichi Uetake, Tomohiro Takayama, Hiroyuki Nakamura, Yasuhiro Ikezoe, Shoogo Ueno, and Koichi Kitazawa. 2004. "Magneto-Archimedes Separation and Its Application to the Separation of Biological Materials." *Physica B: Condensed Matter* 346–347 (1): 267–71. https://doi.org/10.1016/j.physb.2004.01.063.

Hız, Ayşe Semra, Ahmet Yaramış, Ece Sönmezler, and Yavuz Oktay. 2022. "The Investigation of the Effects of a Novel Missense Mutation in Katanin-like 2 (KATNAL2) Gene on Microtubule-Related Proteins in Patient Fibroblasts Using a Proteomic Approach." *The Journal of Tepecik Education and Research Hospital* 32 (3): 459–67. https://doi.org/10.4274/terh.galenos.2022.76093.

Ho, Vincent H.B., Wei Mei Guo, Charlotte L. Huang, Shu Fen Ho, Su Yin Chaw, Ern Yu Tan, Kee Woei Ng, and Joachim S.C. Loo. 2013. "Manipulating Magnetic 3D Spheroids in Hanging Drops for Applications in Tissue Engineering and Drug Screening." *Advanced Healthcare Materials* 2 (11): 1430–34. https://doi.org/10.1002/adhm.201200408.

Hockney, Sean, Jessica Parker, Jasmin E. Turner, Xanthea Todd, Stephen Todryk, Roben Ger Gieling, Gerrit Hilgen, Davina Camargo Madeira Simoes, and Deepali Pal. 2023. "Next Generation Organoid Engineering to Replace Animals in Cancer Drug Testing." *Biochemical Pharmacology* 213 (7): 115586. https://doi.org/10.1016/j.bcp.2023.115586.

Hoffman, Tyler, Petar Antovski, Peyton Tebon, Chun Xu, Nureddin Ashammakhi, Samad Ahadian, Leonardo Morsut, and Ali Khademhosseini. 2020. "Synthetic Biology and Tissue Engineering: Toward Fabrication of Complex and Smart Cellular Constructs." *Advanced Functional Materials* 30 (26): 1909882. https://doi.org/10.1002/adfm.201909882.

Hofrichter, Maxi, Laura Nimtz, Julia Tigges, Yaschar Kabiri, Friederike Schröter, Brigitte Royer-Pokora, Barbara Hildebrandt, et al. 2017. "Comparative Performance Analysis of Human IPSC-Derived and Primary Neural Progenitor Cells (NPC) Grown as Neurospheres in Vitro." *Stem Cell Research* 25 (1): 72–82. https://doi.org/10.1016/j.scr.2017.10.013.

Hogan, Catherine, Mihoko Kajita, Kate Lawrenson, and Yasuyuki Fujita. 2011. "Interactions between Normal and Transformed Epithelial Cells: Their Contributions to Tumourigenesis." *The International Journal of Biochemistry & Cell Biology* 43 (4): 496–503. https://doi.org/10.1016/j.biocel.2010.12.019.

Hondroulis, Evangelia, Steven J. Melnick, Xueji Zhang, Ze Zhi Wu, and Chen Zhong Li. 2013. "Electrical Field Manipulation of Cancer Cell Behavior Monitored by Whole Cell Biosensing Device." *Biomedical Microdevices* 15 (4): 657–63. https://doi.org/10.1007/s10544-013-9788-2.

Horbay, Rostyslav, and Rostyslav Bilyy. 2016. "Mitochondrial Dynamics during Cell Cycling." *Apoptosis : An International Journal on Programmed Cell Death* 21 (12): 1327–35. https://doi.org/10.1007/s10495-016-1295-5.

Huang, Jianghong, Jianyi Xiong, Daping Wang, Jun Zhang, Lei Yang, Shuqing Sun, and Yujie Liang. 2021. "3D Bioprinting of Hydrogels for Cartilage Tissue Engineering." *Gels* 7 (3): 144. https://doi.org/10.3390/gels7030144.

Huang, Qin Qin, Emilie M. Wigdor, Daniel S. Malawsky, Patrick Campbell, Kaitlin E. Samocha, V. Kartik Chundru, Petr Danecek, et al. 2024. "Examining the Role of Common Variants in Rare Neurodevelopmental Conditions." *Nature* 636 (11): 404–11. https://doi.org/10.1038/s41586-024-08217-y.

Humphrey, Jay D., Eric R. Dufresne, and Martin A. Schwartz. 2014. "Mechanotransduction and Extracellular Matrix Homeostasis." *Nature Reviews Molecular Cell Biology* 15 (12): 802–12. https://doi.org/10.1038/nrm3896.

Ino, Kosuke, Mina Okochi, and Hiroyuki Honda. 2009. "Application of Magnetic Force-Based Cell Patterning for Controlling Cell-Cell Interactions in Angiogenesis." *Biotechnology and Bioengineering* 102 (3): 882–90. https://doi.org/10.1002/bit.22104.

Irimia, Daniel. 2015. "Manipulating Cells, Techniques." In *Encyclopedia of Microfluidics and Nanofluidics*, edited by Dongqing Li, 1702–5. New York, NY: Springer New York.

Ishikawa, F., K. Ushida, K. Mori, and M. Shibanuma. 2015. “Loss of Anchorage Primarily Induces Non-Apoptotic Cell Death in a Human Mammary Epithelial Cell Line under Atypical Focal Adhesion Kinase Signaling.” *Cell Death and Disease* 6 (1): e1619–e1619. https://doi.org/10.1038/cddis.2014.583.

Jacob, Levitt, Bernardo Sebastian, and Whang Talley. 2024. “How to Perform a Punch Biopsy of the Skin.” *New England Journal of Medicine* 369 (11): e13. https://doi.org/10.1056/NEJMvcm1105849.

Jaganathan, Hamsa, Jacob Gage, Fransisca Leonard, Srimeenakshi Srinivasan, Glauco R. Souza, Bhuvanesh Dave, and Biana Godin. 2014. “Three-Dimensional in Vitro Co-Culture Model of Breast Tumor Using Magnetic Levitation.” *Scientific Reports* 4 (1): 6468. https://doi.org/10.1038/srep06468.

Jin, Qin, Gang Liu, Shubin Li, Haihan Yuan, Zhizhong Yun, Wenqi Zhang, Shu Zhang, Yanfeng Dai, and Yuzhen Ma. 2019. “Decellularized Breast Matrix as Bioactive Microenvironment for in Vitro Three-Dimensional Cancer Culture.” *Journal of Cellular Physiology* 234 (4): 3425–35. https://doi.org/10.1002/jcp.26782.

Jones, Iwan, Liudmila N. Novikova, Lev N. Novikov, Monika Renardy, Andreas Ullrich, Mikael Wiberg, Leif Carlsson, and Paul J. Kingham. 2018. “Regenerative Effects of Human Embryonic Stem Cell-Derived Neural Crest Cells for Treatment of Peripheral Nerve Injury.” *Journal of Tissue Engineering and Regenerative Medicine* 12 (4): e2099–2109. https://doi.org/10.1002/term.2642.

Jubelin, Camille, Javier Muñoz-Garcia, Denis Cochonneau, Emilie Ollivier, François Vallette, Marie Françoise Heymann, Lisa Oliver, and Dominique Heymann. 2023. “Technical Report: Liquid Overlay Technique Allows the Generation of Homogeneous Osteosarcoma, Glioblastoma, Lung and Prostate Adenocarcinoma Spheroids That Can Be Used for Drug Cytotoxicity Measurements.” *Frontiers in Bioengineering and Biotechnology* 11 (1): 1260049. https://doi.org/10.3389/fbioe.2023.1260049.

Jubelin, Camille, Javier Muñoz-Garcia, Laurent Griscom, Denis Cochonneau, Emilie Ollivier, Marie Françoise Heymann, François M. Vallette, Lisa Oliver, and Dominique Heymann. 2022. “Three-Dimensional in Vitro Culture Models in Oncology Research.” *Cell and Bioscience* 12 (1): 155. https://doi.org/10.1186/s13578-022-00887-3.

Jung, Jaeyun, Hyang Sook Seol, and Suhwan Chang. 2017. “The Generation and Application of Patient-Derived Xenograft Model for Cancer Research.” *Crt* 50 (1): 1–10. https://doi.org/10.4143/crt.2017.307.

Kang, Sung Min, Daehan Kim, Ji Hoon Lee, Shuichi Takayama, and Joong Yull Park. 2021. “Engineered Microsystems for Spheroid and Organoid Studies.” *Advanced Healthcare Materials* 10 (2): 2001284. https://doi.org/10.1002/adhm.202001284.

Karamanos, Nikos K., Achilleas D. Theocharis, Zoi Piperigkou, Dimitra Manou, Alberto Passi, Spyros S. Skandalis, Demitrios H. Vynios, et al. 2021. “A Guide to the Composition and Functions of the Extracellular Matrix.” *FEBS Journal* 288 (24): 6850–6912. https://doi.org/10.1111/febs.15776.

Katti, Preeya D., and Haneesh Jasuja. 2024. “Current Advances in the Use of Tissue Engineering for Cancer Metastasis Therapeutics.” *Polymers* 16 (5): 617. https://doi.org/10.3390/polym16050617.

Katz, Rachel R., and Jennifer L. West. 2022. “Reductionist Three-Dimensional Tumor Microenvironment Models in Synthetic Hydrogels.” *Cancers* 14 (5): 1225. https://doi.org/10.3390/cancers14051225.

Kim, Jeong Ah, Jong-Ho Choi, Minsoo Kim, Won Jong Rhee, Boram Son, Hyun-Kyo Jung, and Tai Hyun Park. 2013. “High-Throughput Generation of Spheroids Using Magnetic Nanoparticles for Three-Dimensional Cell Culture.” *Biomaterials* 34 (34): 8555–63. https://doi.org/10.1016/j.biomaterials.2013.07.056.

Kim, Sally A., Chin Yin Tai, Lee Peng Mok, Eric A. Mosser, and Erin M. Schuman. 2011. “Calcium-Dependent Dynamics of Cadherin Interactions at Cell-Cell Junctions.” *Proceedings of the National Academy of Sciences of the United States of America* 108 (24): 9857–62. https://doi.org/10.1073/pnas.1019003108.

Kim, Seungchan, Woo Seok Im, Lami Kang, Soon Tae Lee, Kon Chu, and Byoung In Kim. 2008. “The Application of Magnets Directs the Orientation of Neurite Outgrowth in Cultured Human Neuronal Cells.” *Journal of Neuroscience Methods* 174 (1): 91–96. https://doi.org/10.1016/j.jneumeth.2008.07.005.

Kletzmayr, Anna, Flurina Clement Frey, Miriam Zimmermann, Daniel Eberli, and Christopher Millan. 2020. “An Automatable Hydrogel Culture Platform for Evaluating Efficacy of Antibody-based Therapeutics in Overcoming Chemoresistance.” *Biotechnology Journal* 15 (5): 1900439. https://doi.org/10.1002/biot.201900439.

Kolathupalayam Shanmugam, Balu, Vinoth Murugan, Arumugam Karthik, Suriyaprabha Rangaraj, Karthik Subramani, Surendhiran Srinivasan, Narthana Kandhasamy, Wilhelm K. Aicher, and Venkatachalam Rajendran. 2023. “Silica Incorporated Chitosan-Sodium Alginate Nanocomposite Scaffolds for Tissue Engineering

Applications." *International Journal of Polymeric Materials and Polymeric Biomaterials* 72 (7): 537–49. https://doi.org/10.1080/00914037.2022.2032703.

Kolathupalayam Shanmugam, Balu, Suriyaprabha Rangaraj, Karthik Subramani, Surendhiran Srinivasan, Wilhelm K. Aicher, and Rajendran Venkatachalam. 2020. "Biomimetic TiO2-Chitosan/Sodium Alginate Blended Nanocomposite Scaffolds for Tissue Engineering Applications." *Materials Science and Engineering C* 110 (5): 110710. https://doi.org/10.1016/j.msec.2020.110710.

Kondo, Jumpei, Hiroko Endo, Hiroaki Okuyama, Osamu Ishikawa, Hiroyasu Iishi, Masahiko Tsujii, Masayuki Ohue, and Masahiro Inoue. 2011. "Retaining Cell-Cell Contact Enables Preparation and Culture of Spheroids Composed of Pure Primary Cancer Cells from Colorectal Cancer." *Proceedings of the National Academy of Sciences of the United States of America* 108 (15): 6235–40. https://doi.org/10.1073/pnas.1015938108.

Korntner, Stefanie H., Alessia Di Nubila, Diana Gaspar, and Dimitrios I. Zeugolis. 2023. "Macromolecular Crowding in Animal Component-Free, Xeno-Free and Foetal Bovine Serum Media for Human Bone Marrow Mesenchymal Stromal Cell Expansion and Differentiation." *Frontiers in Bioengineering and Biotechnology* 11 (1): 1136827. https://doi.org/10.3389/fbioe.2023.1136827.

Kose, Ayse R., Birgit Fischer, Leidong Mao, and Hur Koser. 2009. "Label-Free Cellular Manipulation and Sorting via Biocompatible Ferrofluids." *Proceedings of the National Academy of Sciences of the United States of America* 106 (51): 21478–83. https://doi.org/10.1073/pnas.0912138106.

Krebs, Melissa D., Randall M. Erb, Benjamin B. Yellen, Bappaditya Samanta, Avinash Bajaj, Vincent M. Rotello, and Eben Alsberg. 2009. "Formation of Ordered Cellular Structures in Suspension via Label-Free Negative Magnetophoresis." *Nano Letters* 9 (5): 1812–17. https://doi.org/10.1021/nl803757u.

Kumar, Pramod, Abhigyan Satyam, Xingliang Fan, Yury Rochev, Brian J. Rodriguez, Alexander Gorelov, Lokesh Joshi, Michael Raghunath, Abhay Pandit, and Dimitrios I. Zeugolis. 2015. "Accelerated Development of Supramolecular Corneal Stromal-Like Assemblies from Corneal Fibroblasts in the Presence of Macromolecular Crowders." *Tissue Engineering - Part C: Methods* 21 (7): 660–70. https://doi.org/10.1089/ten.tec.2014.0387.

Kuznetsova, Irina M., Boris Y. Zaslavsky, Leonid Breydo, Konstantin K. Turoverov, and Vladimir N. Uversky. 2015. "Beyond the Excluded Volume Effects: Mechanistic Complexity of the Crowded Milieu." *Molecules* 20 (1): 1377–1409. https://doi.org/10.3390/molecules20011377.

Lam, Ethan Hau Yin, Fengqing Yu, Sabrina Zhu, and Zongjie Wang. 2023. "3D Bioprinting for Next-Generation Personalized Medicine." *International Journal of Molecular Sciences* 24 (7): 6357. https://doi.org/10.3390/ijms24076357.

Langer, Robert; Vacanti, Joseph P. 1993. "Tissue Engineering." *Science* 260 (5110): 920–26. https://doi.org/10.1080/00131725009342110.

Le, Minh Chau N., Kailei Xu, Zi Wang, Sean Beverung, Robert L. Steward, and Stephanie J. Florczyk. 2021. "Evaluation of the Effect of 3D Porous Chitosan-Alginate Scaffold Stiffness on Breast Cancer Proliferation and Migration." *Journal of Biomedical Materials Research - Part A* 109 (10): 1990–2000. https://doi.org/10.1002/jbm.a.37191.

Lee, Joanna Y., and Ovijit Chaudhuri. 2021. "Modeling the Tumor Immune Microenvironment for Drug Discovery Using 3D Culture." *APL Bioengineering* 5 (1): 010903. https://doi.org/10.1063/5.0030693.

Lee, Jong Min, Hye In Seo, Jun Hyuk Bae, and Bong Geun Chung. 2017. "Hydrogel Microfluidic Co-Culture Device for Photothermal Therapy and Cancer Migration." *Electrophoresis* 38 (9–10): 1318–24. https://doi.org/10.1002/elps.201600540.

Lee, Meng-Horng, Pei-Hsun Wu, Daniele Gilkes, Ivie Aifuwa, and Denis Wirtz. 2015. "Normal Mammary Epithelial Cells Promote Carcinoma Basement Membrane Invasion by Inducing Microtubule-Rich Protrusions." *Oncotarget* 6 (32): 32634. https://doi.org/10.18632/oncotarget.4728.

Lee, Soo Hyun, Kyung Sil Jin, Oh Young Bang, Byoung Joon Kim, Soo Jin Park, Na Hee Lee, Keon Hee Yoo, Hong Hoe Koo, and Ki Woong Sung. 2015. "Differential Migration of Mesenchymal Stem Cells to Ischemic Regions after Middle Cerebral Artery Occlusion in Rats." *PLoS ONE* 10 (8): 1–11. https://doi.org/10.1371/journal.pone.0134920.

Lee, W, J Pinckney, V Lee, J.-H. Lee, K Fischer, S Polio, J.-K. Park, and S.-S. Yoo. 2009. "Three-Dimensional Bioprinting of Rat Embryonic Neural Cells." *NeuroReport* 20 (8): 798–803. https://doi.org/10.1097/WNR.0b013e32832b8be4.

Lee, Wonhee, Peter Tseng, and Dino Carlo. 2017. *Microtechnology for Cell Manipulation and Sorting*. Cham,Switzerland: Springer International Publishing.

Lee, Woong Ryeol, Kyung Taek Oh, So Young Park, Na Young Yoo, Yong Sik Ahn, Don Haeng Lee, Yu Seok Youn, Deok-Keun Lee, Kyung-Hoi Cha, and Eun Seong Lee. 2011. "Magnetic Levitating Polymeric Nano/Microparticular Substrates for Three-Dimensional Tumor Cell Culture." *Colloids and Surfaces B: Biointerfaces* 85 (2): 379–84. https://doi.org/10.1016/j.colsurfb.2011.02.021.

Lehmann, U., S. Hadjidj, V. K. Parashar, C. Vandevyver, A. Rida, and M. A.M. Gijs. 2006. "Two-Dimensional Magnetic Manipulation of Microdroplets on a Chip as a Platform for Bioanalytical Applications." *Sensors and Actuators, B: Chemical* 117 (2): 457–63. https://doi.org/10.1016/j.snb.2005.12.053.

Lewis, Daniel M., and Sharon Gerecht. 2016. "Microfluidics and Biomaterials to Study Angiogenesis." *Current Opinion in Chemical Engineering* 11 (2): 114–22. https://doi.org/10.1016/j.coche.2016.02.005.

Li, Wenfang, Xueyan Hu, Shuping Wang, Yan Xing, Hai Wang, Yi Nie, Tianqing Liu, and Kedong Song. 2019. "Multiple Comparisons of Three Different Sources of Biomaterials in the Application of Tumor Tissue Engineering in Vitro and in Vivo." *International Journal of Biological Macromolecules* 130 (6): 166–76. https://doi.org/10.1016/j.ijbiomac.2019.02.136.

Lindvall, Olle, Zaal Kokaia, and Alberto Martinez-Serrano. 2004. "Stem Cell Therapy for Human Neurodegenerative Disorders-How to Make It Work." *Nature Medicine* 10 (7): 42–50. https://doi.org/10.1038/nm1064.

Liu, Allen P, Eric A Appel, Paul D Ashby, Brendon M Baker, Elisa Franco, Luo Gu, Karmella Haynes, Neel S Joshi, April M Kloxin, and Paul H J Kouwer. 2022. "The Living Interface between Synthetic Biology and Biomaterial Design." *Nature Materials* 21 (4): 390–97. https://doi.org/10.1038/s41563-022-01231-3.

Livingston, Megan K., Molly M. Morgan, William T. Daly, William L. Murphy, Brian P. Johnson, David J. Beebe, and MarÍa Virumbrales-Muñoz. 2019. "Evaluation of PEG-Based Hydrogel Influence on Estrogen-Receptor-Driven Responses in MCF7 Breast Cancer Cells." *ACS Biomaterials Science and Engineering* 5 (11): 6089–98. https://doi.org/10.1021/acsbiomaterials.9b00480.

Lombardo, Maria Elena, Francesco Carfì Pavia, Ilenia Vitrano, Giulio Ghersi, Valerio Brucato, Federico Rosei, and Vincenzo La Carrubba. 2019. "PLLA Scaffolds with Controlled Architecture as Potential Microenvironment for in Vitro Tumor Model." *Tissue and Cell* 58 (6): 33–41. https://doi.org/10.1016/j.tice.2019.04.004.

Lu, Paul, and Fabin Han. 2020. “Introduction for Stem Cell–Based Therapy for Neurodegenerative Diseases.” In *Stem Cell-Based Therapy for Neurodegenerative Diseases*, edited by Paul Lu and Fabin Han, 1266 (1): 1–8. Singapore: Springer Singapore.

Lv, Yonggang, Hongjun Wang, Gui Li, and Boyuan Zhao. 2021. “Three-Dimensional Decellularized Tumor Extracellular Matrices with Different Stiffness as Bioengineered Tumor Scaffolds.” *Bioactive Materials* 6 (9): 2767–82. https://doi.org/10.1016/j.bioactmat.2021.02.004.

Lynn, Nicole A., Emily Martinez, Hieu Nguyen, and Jorge Z. Torres. 2021. “The Mammalian Family of Katanin Microtubule-Severing Enzymes.” *Frontiers in Cell and Developmental Biology* 9 (8): 1–18. https://doi.org/10.3389/fcell.2021.692040.

Mahmoodi, Mozaffar, Somayeh Ebrahimi– Barough, Shaghayegh Kamian, Mahmoud Azami, Mozhgan Mehri, Mohammad Abdi, and Jafar Ai. 2022. “Fabrication and Characterization of a Three-Dimensional Fibrin Gel Model to Evaluate Anti-Proliferative Effects of Astragalus Hamosus Plant Extract on Breast Cancer Cells.” *Asian Pacific Journal of Cancer Prevention* 23 (2): 731–41. https://doi.org/10.31557/APJCP.2022.23.2.731.

Manavitehrani, Iman, Thi Y.L. Le, Sean Daly, Yiwei Wang, Peter K. Maitz, Aaron Schindeler, and Fariba Dehghani. 2019. “Formation of Porous Biodegradable Scaffolds Based on Poly(Propylene Carbonate) Using Gas Foaming Technology.” *Materials Science and Engineering C* 96 (3): 824–30. https://doi.org/10.1016/j.msec.2018.11.088.

Manduca, Nicoletta, Ester Maccafeo, Ruggero De Maria, Antonella Sistigu, and Martina Musella. 2023. “3D Cancer Models: One Step Closer to in Vitro Human Studies.” *Frontiers in Immunology* 14 (1): 1175503. https://doi.org/10.3389/fimmu.2023.1175503.

Maresca, Jamie A, Derek C DeMel, Grayson A Wagner, Colin Haase, and John P Geibel. 2023. “Three-Dimensional Bioprinting Applications for Bone Tissue Engineering.” *Cells* 12 (9): 1230. https://doi.org/10.3390/cells12091230.

Maric, Dragan, Irina Maric, and Jeffery L. Barker. 1998. “Buoyant Density Gradient Fractionatian and Flow Cytometric Analysis of Embryonic Rat Cortical Neurons and Progenitor Cells.” *Methods: A Companion to Methods in Enzymology* 16 (3): 247–59. https://doi.org/10.1006/meth.1998.0682.

Marques, Joana Rita Oliveira Faria, Patricia González-Alva, Ruby Yu-Tong Lin, Beatriz Ferreira Fernandes, Akhilanand Chaurasia, and Nileshkumar Dubey. 2023. "Advances in Tissue Engineering of Cancer Microenvironment-from Three-Dimensional Culture to Three-Dimensional Printing." *SLAS Technology* 28 (3): 152–64. https://doi.org/10.1016/j.slast.2023.03.005.

Martinez-Pacheco, Sarai, and Lorraine O'driscoll. 2021. "Pre-Clinical in Vitro Models Used in Cancer Research: Results of a Worldwide Survey." *Cancers* 13 (23): 6033. https://doi.org/10.3390/cancers13236033.

Massaro, Maria Stefania, Richard Pálek, Jáchym Rosendorf, Lenka Červenková, Václav Liška, and Vladimíra Moulisová. 2021. "Decellularized Xenogeneic Scaffolds in Transplantation and Tissue Engineering: Immunogenicity versus Positive Cell Stimulation." *Materials Science and Engineering C* 127 (8): 112203. https://doi.org/10.1016/j.msec.2021.112203.

Maughan, Elizabeth F., Robert E. Hynds, Toby J. Proctor, Sam M. Janes, Martin Elliott, Martin A. Birchall, Mark W. Lowdell, and Paolo De Coppi. 2017. "Autologous Cell Seeding in Tracheal Tissue Engineering." *Current Stem Cell Reports* 3 (4): 279–89. https://doi.org/10.1007/s40778-017-0108-2.

Mejía-Cruz, Claudia Camila, Emilia Barreto-Durán, María Alejandra Pardo-Pérez, María Camila Jimenez, Julieth Rincón, Karen Vanegas, Jorge Luis Rodríguez, et al. 2019. "Generation of Organotypic Multicellular Spheres by Magnetic Levitation: Model for the Study of Human Hematopoietic Stem Cells Microenvironment." *Ijsc* 12 (1): 51–62. https://doi.org/10.15283/ijsc18061.

Meyer, Ulrich;Handschel, Jörg;Meyer, Thomas;Wiesmann, Hans Peter. 2009. *Fundamentals of Tissue Engineering and Regenerative Medicine*. 1st ed. Springer Berlin, Heidelberg.

Mi, Xuelian, Zhi Su, Xiaokun Yue, Ya Ren, Xue Yang, Lei Qiang, Weiqing Kong, Zhenjiang Ma, Changru Zhang, and Jinwu Wang. 2023. "3D Bioprinting Tumor Models Mimic the Tumor Microenvironment for Drug Screening." *Biomaterials Science* 11 (11): 3813–27. https://doi.org/10.1039/D3BM00159H.

Minton, Allen P. 2006. "Macromolecular Crowding." *Current Biology* 16 (8): R269–71. https://doi.org/10.1016/j.cub.2006.03.047.

Mishriki, S., A. R. Abdel Fattah, T. Kammann, R. P. Sahu, F. Geng, and I. K. Puri. 2019. "Rapid Magnetic 3D Printing of Cellular Structures with MCF-7 Cell Inks." *Research* 2019 (1): 1-13. https://doi.org/10.34133/2019/9854593.

Moncal, Kazim Kerim, Sena Yaman, and Naside Gozde Durmus. 2022. “Levitational 3D Bioassembly and Density-Based Spatial Coding of Levitoids.” *Advanced Functional Materials* 32 (50): 2204092. https://doi.org/10.1002/adfm.202204092.

Mosquera, Matthew J, Sungwoong Kim, Rohan Bareja, Zhou Fang, Shuangyi Cai, Heng Pan, Muhammad Asad, Maria Laura Martin, Michael Sigouros, and Florencia M Rowdo. 2022. “Extracellular Matrix in Synthetic Hydrogel-based Prostate Cancer Organoids Regulate Therapeutic Response to EZH2 and DRD2 Inhibitors.” *Advanced Materials* 34 (2): 2100096. https://doi.org/10.1002/adma.202100096.

Munaz, Ahmed, Muhammad J.A. Shiddiky, and Nam Trung Nguyen. 2018. “Recent Advances and Current Challenges in Magnetophoresis Based Micro Magnetofluidics.” *Biomicrofluidics* 12 (3): 031501. https://doi.org/10.1063/1.5035388.

Nelson, Mark Tyler, Aaron Short, Sara L. Cole, Amy C. Gross, Jessica Winter, Tim D. Eubank, and John J. Lannutti. 2014. “Preferential, Enhanced Breast Cancer Cell Migration on Biomimetic Electrospun Nanofiber ‘Cell Highways.’” *BMC Cancer* 14 (1): 1–16. https://doi.org/10.1186/1471-2407-14-825.

Neurohr, Gabriel E, and Angelika Amon. 2020. “Relevance and Regulation of Cell Density.” *Trends in Cell Biology* 30 (3): 213–25. https://doi.org/10.1016/j.tcb.2019.12.006.

Niemi, Mari E.K., Hilary C. Martin, Daniel L. Rice, Giuseppe Gallone, Scott Gordon, Martin Kelemen, Kerrie McAloney, et al. 2018. “Common Genetic Variants Contribute to Risk of Rare Severe Neurodevelopmental Disorders.” *Nature* 562 (7726): 268–71. https://doi.org/10.1038/s41586-018-0566-4.

Obayemi, J. D., S. M. Jusu, A. A. Salifu, S. Ghahremani, M. Tadesse, V. O. Uzonwanne, and W. O. Soboyejo. 2020. “Degradable Porous Drug-Loaded Polymer Scaffolds for Localized Cancer Drug Delivery and Breast Cell/Tissue Growth.” *Materials Science and Engineering C* 112 (7): 110794. https://doi.org/10.1016/j.msec.2020.110794.

Okochi, Mina, Sho Takano, Yayoi Isaji, Takeshi Senga, Michinari Hamaguchi, and Hiroyuki Honda. 2009. “Three-Dimensional Cell Culture Array Using Magnetic Force-Based Cell Patterning for Analysis of Invasive Capacity of BALB/3T3/v-Src.” *Lab on a Chip* 9 (23): 3378–84. https://doi.org/10.1039/b909304d.

Onbas, Rabia, and Ahu Arslan Yildiz. 2021. “Fabrication of Tunable 3D Cellular Structures in High Volume Using Magnetic Levitation Guided Assembly.” *ACS*

*Applied Bio Materials* 4 (2): 1794–1802. https://doi.org/10.1021/acsabm.0c01523.

Palamà, Ilaria E., Valentina Arcadio, Stefania D'Amone, Mariano Biasiucci, Giuseppe Gigli, and Barbara Cortese. 2017. "Therapeutic PCL Scaffold for Reparation of Resected Osteosarcoma Defect." *Scientific Reports* 7 (1): 12672. https://doi.org/10.1038/s41598-017-12824-3.

Pamme, Nicole, and Claire Wilhelm. 2006. "Continuous Sorting of Magnetic Cells via On-Chip Free-Flow Magnetophoresis." *Lab on a Chip* 6 (8): 974–80. https://doi.org/10.1039/b604542a.

Pan, Jie, and Jun Wan. 2020. "Methodological Comparison of FACS and MACS Isolation of Enriched Microglia and Astrocytes from Mouse Brain." *Journal of Immunological Methods* 486 (8): 112834. https://doi.org/10.1016/j.jim.2020.112834.

Parfenov, Vladislav A, Yusef D Khesuani, Stanislav V Petrov, Pavel A Karalkin, Elizaveta V Koudan, Elizaveta K Nezhurina, Frederico D A S Pereira, Alisa A Krokhmal, Anna A Gryadunova, and Elena A Bulanova. 2020. "Magnetic Levitational Bioassembly of 3D Tissue Construct in Space." *Science Advances* 6 (29): eaba4174. https://doi.org/10.1126/sciadv.aba4174.

Parfenov, Vladislav A, Elizaveta V Koudan, Elena A Bulanova, Pavel A Karalkin, Frederico DAS Pereira, Nikita E Norkin, Alisa D Knyazeva, et al. 2018. "Scaffold-Free, Label-Free and Nozzle-Free Biofabrication Technology Using Magnetic Levitational Assembly." *Biofabrication* 10 (3): 034104. https://doi.org/10.1088/1758-5090/aac900.

Pathak, Amit, and Sanjay Kumar. 2012. "Independent Regulation of Tumor Cell Migration by Matrix Stiffness and Confinement." *Proceedings of the National Academy of Sciences* 109 (26): 10334–39. https://doi.org/10.1073/pnas.1118073109.

Peretti, Giuseppe M, Mark A Randolph, Mark T Villa, Michele S Buragas, and Michael J Yaremchuk. 2000. "Cell-Based Tissue-Engineered Allogeneic Implant for Cartilage Repair." *Tissue Engineering* 6 (5): 567–76. https://doi.org/10.1089/107632700750022206.

Peter, Mathew, Archana Singh, Kumaravel Mohankumar, Rajeev Jeenger, Puja Arun Joge, Madhumanjiri Mukulesh Gatne, and Prakriti Tayalia. 2019. "Gelatin-Based Matrices as a Tunable Platform to Study in Vitro and in Vivo 3D Cell Invasion."

*ACS Applied Bio Materials* 2 (2): 916–29. https://doi.org/10.1021/acsabm.8b00767.

Petersson, Filip, Lena Åberg, Ann-Margret Swärd-Nilsson, and Thomas Laurell. 2007. "Free Flow Acoustophoresis: Microfluidic-Based Mode of Particle and Cell Separation." *Analytical Chemistry* 79 (14): 5117–23. https://doi.org/10.1021/ac070444e.

Petzold, Axel, Martin M Tisdall, Armand R Girbes, Lillian Martinian, Maria Thom, Neil Kitchen, and Martin Smith. 2011. "In Vivo Monitoring of Neuronal Loss in Traumatic Brain Injury: A Microdialysis Study." *Brain* 134 (2): 464–83. https://doi.org/10.1093/brain/awq360.

Pinnell, Sheldon R. 1985. "Regulation of Collagen Biosynthesis by Ascorbic Acid: A Review." *The Yale Journal of Biology and Medicine* 58: 553–59.

Platt, Frances M., Alessandra d'Azzo, Beverly L. Davidson, Elizabeth F. Neufeld, and Cynthia J. Tifft. 2018. "Lysosomal Storage Diseases." *Nature Reviews Disease Primers* 4 (1): 27. https://doi.org/10.1038/s41572-018-0025-4.

Plikus, Maksim V., Xiaojie Wang, Sarthak Sinha, Elvira Forte, Sean M. Thompson, Erica L. Herzog, Ryan R. Driskell, Nadia Rosenthal, Jeff Biernaskie, and Valerie Horsley. 2021. "Fibroblasts: Origins, Definitions, and Functions in Health and Disease." *Cell* 184 (15): 3852–72. https://doi.org/10.1016/j.cell.2021.06.024.

Poewe, Werner, Klaus Seppi, Caroline M Tanner, Glenda M Halliday, Patrik Brundin, Jens Volkmann, Anette-Eleonore Schrag, and Anthony E Lang. 2017. "Parkinson Disease." *Nature Reviews Disease Primers* 3 (1): 17013. https://doi.org/10.1038/nrdp.2017.13.

Post, Janine N, Sandra Loerakker, Roeland M H Merks, and Aurélie Carlier. 2022. "Implementing Computational Modeling in Tissue Engineering: Where Disciplines Meet." *Tissue Engineering Part A* 28 (11–12): 542–54. https://doi.org/10.1089/ten.tea.2021.021.

Pradhan, Shantanu, Jacob M Clary, Dror Seliktar, and Elizabeth A Lipke. 2017. "A Three-Dimensional Spheroidal Cancer Model Based on PEG-Fibrinogen Hydrogel Microspheres." *Biomaterials* 115 (1): 141–54. https://doi.org/10.1016/j.biomaterials.2016.10.052.

Puluca, Nazan, Naside Gözde Durmus, Soah Lee, Nadjet Belbachir, Francisco X. Galdos, Mehmet Giray Ogut, Rakhi Gupta, et al. 2020. "Levitating Cells to Sort the Fit and the Fat." *Advanced Biosystems* 4 (6): 1900300. https://doi.org/10.1002/adbi.201900300.

Qi, Xiaoli, Alexandra V. Prokhorova, Alexander V. Mezentsev, Ningfei Shen, Alexander V. Trofimenko, Gleb I. Filkov, Rushan A. Sulimanov, Vladimir A. Makarov, and Mikhail O. Durymanov. 2022. "Comparison of EMT-Related and Multi-Drug Resistant Gene Expression, Extracellular Matrix Production, and Drug Sensitivity in NSCLC Spheroids Generated by Scaffold-Free and Scaffold-Based Methods." *International Journal of Molecular Sciences* 23 (21): 13306. https://doi.org/10.3390/ijms232113306.

Qian, A. R., D. C. Yin, P. F. Yang, Y. Lv, Z. C. Tian, and P. Shang. 2013. "Application of Diamagnetic Levitation Technology in Biological Sciences Research." *IEEE Transactions on Applied Superconductivity* 23 (1): 3600305–3600305. https://doi.org/10.1109/TASC.2012.2232919.

Quereda, Victor, Shurong Hou, Franck Madoux, Louis Scampavia, Timothy P. Spicer, and Derek Duckett. 2018. "A Cytotoxic Three-Dimensional-Spheroid, High-Throughput Assay Using Patient-Derived Glioma Stem Cells." *SLAS Discovery* 23 (8): 842–49. https://doi.org/10.1177/2472555218775055.

Quint, Clay, Melissa Arief, Akihito Muto, Alan Dardik, and Laura E. Niklason. 2012. "Allogeneic Human Tissue-Engineered Blood Vessel." *Journal of Vascular Surgery* 55 (3): 790–98. https://doi.org/10.1016/j.jvs.2011.07.098.

Qureshi-Baig, Komal, Pit Ullmann, Fabien Rodriguez, Sónia Frasquilho, Petr V. Nazarov, Serge Haan, and Elisabeth Letellier. 2016. "What Do We Learn from Spheroid Culture Systems? Insights from Tumorspheres Derived from Primary Colon Cancer Tissue." *PLoS ONE* 11 (1): e0146052. https://doi.org/10.1371/journal.pone.0146052.

Rabionet, Marc, Teresa Puig, and Joaquim Ciurana. 2020. "Manufacture of PCL Scaffolds through Electrospinning Technology to Accommodate Triple Negative Breast Cancer Cells Culture." In *Procedia CIRP*, 89 (1): 98–103. Elsevier B.V. https://doi.org/10.1016/j.procir.2020.05.124.

Rabionet, Marc, Marc Yeste, Teresa Puig, and Joaquim Ciurana. 2017. "Electrospinning PCL Scaffolds Manufacture for Three-Dimensional Breast Cancer Cell Culture." *Polymers* 9 (8): 328. https://doi.org/10.3390/polym9080328.

Raghavan, Shreya, Pooja Mehta, Maria R. Ward, Michael E. Bregenzer, Elyse M.A. Fleck, Lijun Tan, Karen McLean, Ronald J. Buckanovich, and Geeta Mehta. 2017. "Personalized Medicine–Based Approach to Model Patterns of Chemoresistance and Tumor Recurrence Using Ovarian Cancer Stem Cell Spheroids." *Clinical Cancer Research* 23 (22): 6934–45. https://doi.org/10.1158/1078-0432.CCR-17-0133.

Rakib Hasan Khan, Md, Raj Shankar Hazra, Gauthami Nair, Jiyan Mohammad, Long Jiang, Katie Reindl, Mohammad Khalid Jawed, Sabha Ganai, and Mohiuddin Quadir. 2022. “Cellulose Nanofibers as Scaffold-Forming Materials for Thin Film Drug Delivery Systems.” *International Journal of Pharmaceutics* 627 (11): 122189. https://doi.org/10.1016/j.ijpharm.2022.122189.

Ralston, G B. 1990. “Effects of" Crowding" in Protein Solutions.” *Journal of Chemical Education* 67 (10): 857. https://doi.org/10.1021/ed067p857.

Rampin, Andrea, Ioannis Skoufos, Michael Raghunath, Athina Tzora, Nikolaos Diakakis, Nikitas Prassinos, and Dimitrios I. Zeugolis. 2022. “Allogeneic Serum and Macromolecular Crowding Maintain Native Equine Tenocyte Function in Culture.” *Cells* 11 (9): 1562. https://doi.org/10.3390/cells11091562.

Ranjbarnejad, Fatemeh, Mozafar Khazaei, Alireza Shahryari, Fatemeh Khazaei, and Leila Rezakhani. 2022. “Recent Advances in Gene Therapy for Bone Tissue Engineering.” *Journal of Tissue Engineering and Regenerative Medicine* 16 (12): 1121–37. https://doi.org/10.1002/term.3363.

Ravera, Francesca, Esen Efeoglu, and Hugh J Byrne. 2021. “Monitoring Stem Cell Differentiation Using Raman Microspectroscopy: Chondrogenic Differentiation, towards Cartilage Formation.” *The Analyst* 146 (1): 322–37. https://doi.org/10.1039/d0an01983f.

Raza, Chand, Hasib Aamir Riaz, Rabia Anjum, and Noor ul Ain Shakeel. 2020. “Repair Strategies for Injured Peripheral Nerve: Review.” *Life Sciences* 243 (10): 117308. https://doi.org/10.1016/j.lfs.2020.117308.

Redmond, John, Helen McCarthy, Paul Buchanan, Tanya J. Levingstone, and Nicholas J. Dunne. 2021. “Advances in Biofabrication Techniques for Collagen-Based 3D in Vitro Culture Models for Breast Cancer Research.” *Materials Science and Engineering C* 122 (3): 111944. https://doi.org/10.1016/j.msec.2021.111944.

Rescigno, Francesca, Laura Ceriotti, and Marisa Meloni. 2021. “Extra Cellular Matrix Deposition and Assembly in Dermis Spheroids.” *Clinical, Cosmetic and Investigational Dermatology* 14 (1): 935–43. https://doi.org/10.2147/CCID.S316707.

Ricci, Claudio, Bahareh Azimi, Luca Panariello, Benedetta Antognoli, Beatrice Cecchini, Roberta Rovelli, Meruyert Rustembek, et al. 2023. “Assessment of Electrospun Poly(ε-Caprolactone) and Poly(Lactic Acid) Fiber Scaffolds to Generate 3D In

Vitro Models of Colorectal Adenocarcinoma: A Preliminary Study." *International Journal of Molecular Sciences* 24 (11): 9443. https://doi.org/10.3390/ijms24119443.

Robert, Damien, Nicole Pamme, Hélène Conjeaud, Florence Gazeau, Alexander Iles, and Claire Wilhelm. 2011. "Cell Sorting by Endocytotic Capacity in a Microfluidic Magnetophoresis Device." *Lab on a Chip* 11 (11): 1902–10. https://doi.org/10.1039/c0lc00656d.

Roy, Vincent, Brice Magne, Maude Vaillancourt-Audet, Mathieu Blais, Stéphane Chabaud, Emil Grammond, Leó Piquet, et al. 2020. "Human Organ-Specific 3D Cancer Models Produced by the Stromal Self-Assembly Method of Tissue Engineering for the Study of Solid Tumors." *BioMed Research International* 2020 (1): 6051210. https://doi.org/10.1155/2020/6051210.

Rozario, Tania, and Douglas W. DeSimone. 2010. "The Extracellular Matrix in Development and Morphogenesis: A Dynamic View." *Developmental Biology* 341 (1): 126–40. https://doi.org/10.1016/j.ydbio.2009.10.026.

Ryan, Christina N.M., Eugenia Pugliese, Naledi Shologu, Diana Gaspar, Peadar Rooney, Md Nahidul Islam, Alan O'Riordan, Manus J. Biggs, Matthew D. Griffin, and Dimitrios I. Zeugolis. 2023. "The Synergistic Effect of Physicochemical in Vitro Microenvironment Modulators in Human Bone Marrow Stem Cell Cultures." *Biomaterials Advances* 144 (1): 213196. https://doi.org/10.1016/j.bioadv.2022.213196.

Sabitha, K. R., Ashok K. Shetty, and Dinesh Upadhya. 2021. "Patient-Derived IPSC Modeling of Rare Neurodevelopmental Disorders: Molecular Pathophysiology and Prospective Therapies." *Neuroscience and Biobehavioral Reviews* 121 (2): 201–19. https://doi.org/10.1016/j.neubiorev.2020.12.025.

Sadeghi, Moslem, Farzaneh Falahi, Shiva Akbari-Birgani, and Nasser Nikfarjam. 2023. "Trilayer Tubular Scaffold to Mimic Ductal Carcinoma Breast Cancer for the Study of Chemo-Photothermal Therapy." *ACS Applied Polymer Materials* 5 (4): 2394–2407. https://doi.org/10.1021/acsapm.2c02087.

Salmenperä, Pertteli, Piia Riitta Karhemo, Kati Räsänen, Pirjo Laakkonen, and Antti Vaheri. 2016. "Fibroblast Spheroids as a Model to Study Sustained Fibroblast Quiescence and Their Crosstalk with Tumor Cells." *Experimental Cell Research* 345 (1): 17–24. https://doi.org/10.1016/j.yexcr.2016.05.005.

Santini, Maria Teresa, Gabriella Rainaldi, and Pietro Luigi Indovina. 2000. "Apoptosis, Cell Adhesion and the Extracellular Matrix in the Three-Dimensional Growth of

Multicellular Tumor Spheroids." *Critical Reviews in Oncology/Hematology* 36 (2–3): 75–87. https://doi.org/10.1016/S1040-8428(00)00078-0.

Sarigil, Oyku, Muge Anil-Inevi, Burcu Firatligil-Yildirir, Yagmur Ceren Unal, Ozden Yalcin-Ozuysal, Gulistan Mese, H. Cumhur Tekin, and Engin Ozcivici. 2021. "Scaffold-Free Biofabrication of Adipocyte Structures with Magnetic Levitation." *Biotechnology and Bioengineering* 118 (3): 1127–40. https://doi.org/10.1002/bit.27631.

Sarigil, Oyku, Muge Anil-Inevi, Esra Yilmaz, Gulistan Mese, H. Cumhur Tekin, and Engin Ozcivici. 2019. "Label-Free Density-Based Detection of Adipocytes of Bone Marrow Origin Using Magnetic Levitation." *The Analyst* 144 (9): 2942–53. https://doi.org/10.1039/c8an02503g.

Satyam, Abhigyan, Pramod Kumar, Xingliang Fan, Alexander Gorelov, Yury Rochev, Lokesh Joshi, Héctor Peinado, et al. 2014. "Macromolecular Crowding Meets Tissue Engineering by Self-Assembly: A Paradigm Shift in Regenerative Medicine." *Advanced Materials* 26 (19): 3024–34. https://doi.org/10.1002/adma.201304428.

Schmidt, Christine E., and Jennie Baier Leach. 2003. "Neural Tissue Engineering: Strategies for Repair and Regeneration." *Annual Review of Biomedical Engineering* 5 (1): 293–347. https://doi.org/10.1146/annurev.bioeng.5.011303.120731.

Sepantafar, Mohammadmajid, Reihan Maheronnaghsh, Hossein Mohammadi, Fatemeh Radmanesh, Mohammad Mahdi Hasani-sadrabadi, Marzieh Ebrahimi, and Hossein Baharvand. 2017. "Engineered Hydrogels in Cancer Therapy and Diagnosis." *Trends in Biotechnology* 35 (11): 1074–87. https://doi.org/10.1016/j.tibtech.2017.06.015.

Seyrantepe, Volkan, Nurselin Ates, Melike Can, Tugce Sengul, and Secil Akyildiz Demir. 2018. "Abnormal GM2 Accumulation Alters the Function of the Autophagic Pathway in Early-Onset Tay-Sachs Disease Mouse Model." *Molecular Genetics and Metabolism* 123 (2): S129–30. https://doi.org/10.1016/j.ymgme.2017.12.353.

Sharp, Kim A. 2015. "Analysis of the Size Dependence of Macromolecular Crowding Shows That Smaller Is Better." *Proceedings of the National Academy of Sciences of the United States of America* 112 (26): 7990–95. https://doi.org/10.1073/pnas.1505396112.

Shearier, Emily, Qi Xing, Zichen Qian, and Feng Zhao. 2016. “Physiologically Low Oxygen Enhances Biomolecule Production and Stemness of Mesenchymal Stem Cell Spheroids.” *Tissue Engineering - Part C: Methods* 22 (4): 360–69. https://doi.org/10.1089/ten.tec.2015.0465.

Shologu, Naledi, Mehmet Gurdal, Eva Szegezdi, Una FitzGerald, and Dimitrios I. Zeugolis. 2022. “Macromolecular Crowding in the Development of a Three-Dimensional Organotypic Human Breast Cancer Model.” *Biomaterials* 287 (8): 121642. https://doi.org/10.1016/j.biomaterials.2022.121642.

Shopova, Dobromira, Antoniya Yaneva, Desislava Bakova, Anna Mihaylova, Petya Kasnakova, Maria Hristozova, Yordan Sbirkov, Victoria Sarafian, and Mariya Semerdzhieva. 2023. “(Bio) Printing in Personalized Medicine—Opportunities and Potential Benefits.” *Bioengineering* 10 (3): 287. https://doi.org/10.3390/bioengineering10030287.

Shu, Yan, Bing Li, Hailin Ma, Jiaqi Liu, Yuen Yee Cheng, Xiangqin Li, Tianqing Liu, Chuwei Yang, Xiao Ma, and Kedong Song. 2024. “Three-dimensional breast cancer tumor models based on natural hydrogels: a review” *Journal of Zhejiang University. Science. B* 25 (9): 736–55. https://doi.org/10.1631/jzus.B2300840.

Shukla, Priyanshu, Sriya Yeleswarapu, Marcel A. Heinrich, Jai Prakash, and Falguni Pati. 2022. “Mimicking Tumor Microenvironment by 3D Bioprinting: 3D Cancer Modeling.” *Biofabrication* 14 (3): 032002. https://doi.org/10.1088/1758-5090/ac6d11.

Sievers, Jana, Vaibhav Mahajan, Petra B. Welzel, Carsten Werner, and Anna Taubenberger. 2023. “Precision Hydrogels for the Study of Cancer Cell Mechanobiology.” *Advanced Healthcare Materials* 12 (14): 2202514. https://doi.org/10.1002/adhm.202202514.

Silva-Vargas, Violeta, Elizabeth E. Crouch, and Fiona Doetsch. 2013. “Adult Neural Stem Cells and Their Niche: A Dynamic Duo during Homeostasis, Regeneration, and Aging.” *Current Opinion in Neurobiology* 23 (6): 935–42. https://doi.org/10.1016/j.conb.2013.09.004.

Simão, Daniel, Marta M. Silva, Ana P. Terrasso, Francisca Arez, Marcos F.Q. Sousa, Narges Z. Mehrjardi, Tomo Šarić, et al. 2018. “Recapitulation of Human Neural Microenvironment Signatures in IPSC-Derived NPC 3D Differentiation.” *Stem Cell Reports* 11 (2): 552–64. https://doi.org/10.1016/j.stemcr.2018.06.020.

Solarte David, Víctor Alfonso, Viviana Raquel Güiza-Argüello, Martha L. Arango-Rodríguez, Claudia L. Sossa, and Silvia M. Becerra-Bayona. 2022. “Decellularized Tissues for Wound Healing: Towards Closing the Gap Between Scaffold Design and Effective Extracellular Matrix Remodeling.” *Frontiers in*

*Bioengineering and Biotechnology* 10 (2): 821852. https://doi.org/10.3389/fbioe.2022.821852.

Sonabend, Adam M., Patricia Smith, Jason H. Huang, and Christopher Winfree. 2012. *Peripheral Nerve Injury*. *Schmidek and Sweet Operative Neurosurgical Techniques: Indications, Methods, and Results: Sixth Edition*. Sixth Edit. Vol. 2. Elsevier.

Song, Miyeoun, Young Ju Kim, Yoon Ha Kim, Jina Roh, Seung U. Kim, and Byung Woo Yoon. 2010. "Using a Neodymium Magnet to Target Delivery of Ferumoxide-Labeled Human Neural Stem Cells in a Rat Model of Focal Cerebral Ischemia." *Human Gene Therapy* 21 (5): 603–10. https://doi.org/10.1089/hum.2009.144.

Song, Taiyu, Hui Zhang, Zhiqiang Luo, Luoran Shang, and Yuanjin Zhao. 2023. "Primary Human Pancreatic Cancer Cells Cultivation in Microfluidic Hydrogel Microcapsules for Drug Evaluation." *Advanced Science* 10 (12): 2206004. https://doi.org/10.1002/advs.202206004.

Souza, Glauco R., Jennifer R. Molina, Robert M. Raphael, Michael G. Ozawa, Daniel J. Stark, Carly S. Levin, Lawrence F. Bronk, et al. 2010. "Three-Dimensional Tissue Culture Based on Magnetic Cell Levitation." *Nature Nanotechnology* 5 (4): 291–96. https://doi.org/10.1038/nnano.2010.23.

Spink, Barbara C, Richard W Cole, Barbara H Katz, John F Gierthy, Laurie M Bradley, and David C Spink. 2006. "Inhibition of MCF-7 Breast Cancer Cell Proliferation by MCF-10A Breast Epithelial Cells in Coculture." *Cell Biology International* 30 (3): 227–38. https://doi.org/10.1016/j.cellbi.2005.11.006.

Sun, Yan, Dong Xiao, Xing-Hua Pan, Ruo-Shuang Zhang, Guang-Hui Cui, and Xi-Gu Chen. 2007. "Generation of Human/Rat Xenograft Animal Model for the Study of Human Donor Stem Cell Behaviors in Vivo." *World J Gastroenterol* 13 (1): 2707–16. https://doi.org/10.3748/wjg.v13.i19.2707.

Suo, Aili, Weijun Xu, Yaping Wang, Tiantian Sun, Lijie Ji, and Junmin Qian. 2019. "Dual-Degradable and Injectable Hyaluronic Acid Hydrogel Mimicking Extracellular Matrix for 3D Culture of Breast Cancer MCF-7 Cells." *Carbohydrate Polymers* 211 (5): 336–48. https://doi.org/10.1016/j.carbpol.2019.01.115.

Takahashi, Kazutoshi, and Shinya Yamanaka. 2006. "Induction of Pluripotent Stem Cells from Mouse Embryonic and Adult Fibroblast Cultures by Defined Factors." *Cell* 126 (4): 663–76. https://doi.org/10.1016/j.cell.2006.07.024.

Tamayo-Angorrilla, Marta, Julia López de Andrés, Gema Jiménez, and Juan Antonio Marchal. 2022. “The Biomimetic Extracellular Matrix: A Therapeutic Tool for Breast Cancer Research.” *Translational Research* 247 (9): 117–36. https://doi.org/10.1016/j.trsl.2021.11.008.

Tan, Matthew L., Lu Ling, and Claudia Fischbach. 2021. “Engineering Strategies to Capture the Biological and Biophysical Tumor Microenvironment in Vitro.” *Advanced Drug Delivery Reviews* 176 (9): 113852. https://doi.org/10.1016/j.addr.2021.113852.

Tardy, Claudine, Nathalie Andrieu-abadie, Robert Salvayre, and Thierry Levade. 2004. “Lysosomal Storage Diseases : Is Impaired Apoptosis a Pathogenic Mechanism?” *Neurochemical Research* 29 (5): 871–80. https://doi.org/10.1023/B:NERE.0000021232.05175.38.

Tasoglu, Savas, Joseph A. Khoory, Huseyin C. Tekin, Clemence Thomas, Antoine E. Karnoub, Ionita C. Ghiran, and Utkan Demirci. 2015. “Levitational Image Cytometry with Temporal Resolution.” *Advanced Materials* 27 (26): 3901–8. https://doi.org/10.1002/adma.201405660.

Tevlek, Atakan, Seren Kecili, Ozge S. Ozcelik, Haluk Kulah, and H. Cumhur Tekin. 2023. “Spheroid Engineering in Microfluidic Devices.” *ACS Omega* 8 (4): 3630–49. https://doi.org/10.1021/acsomega.2c06052.

Tocchio, Alessandro, Naside Gozde Durmus, Kaushik Sridhar, Vigneshwaran Mani, Bukre Coskun, Rami El Assal, and Utkan Demirci. 2018. “Magnetically Guided Self-Assembly and Coding of 3D Living Architectures.” *Advanced Materials* 30 (4): 1705030. https://doi.org/10.1002/adma.201705034.

Truffi, Marta, Luca Sorrentino, and Fabio Corsi. 2020. “Fibroblasts in the Tumor Microenvironment.” In *Tumor Microenvironment: Non-Hematopoietic Cells*, edited by Alexander Birbrair, 1234 (1): 15–29. Cham: Springer International Publishing. https://doi.org/10.1007/978-3-030-37184-5_2.

Tsiapalis, Dimitrios, Stephen Kearns, Jack L. Kelly, and Dimitrios I. Zeugolis. 2021. “Growth Factor and Macromolecular Crowding Supplementation in Human Tenocyte Culture.” *Biomaterials and Biosystems* 1 (3): 100009. https://doi.org/10.1016/j.bbiosy.2021.100009.

Tsiapalis, Dimitrios, and Dimitrios I. Zeugolis. 2021. “It Is Time to Crowd Your Cell Culture Media – Physicochemical Considerations with Biological

Consequences." *Biomaterials* 275 (8): 120943. https://doi.org/10.1016/j.biomaterials.2021.120943.

Türker, Esra, Nida Demirçak, and Ahu Arslan-Yildiz. 2018. "Scaffold-Free Three-Dimensional Cell Culturing Using Magnetic Levitation." *Biomaterials Science* 6 (7): 1745–53. https://doi.org/10.1039/C8BM00122G.

Urciuolo, F, A Garziano, G Imparato, V Panzetta, S Fusco, C Casale, and P A Netti. 2016. "Biophysical Properties of Dermal Building-Blocks Affect Extra Cellular Matrix Assembly in 3D Endogenous Macrotissue." *Biofabrication* 8 (1): 015010. https://doi.org/10.1088/1758-5090/8/1/015010.

Urciuolo, F., G. Imparato, and P. A. Netti. 2023. "In Vitro Strategies for Mimicking Dynamic Cell–ECM Reciprocity in 3D Culture Models." *Frontiers in Bioengineering and Biotechnology* 11 (1): 1197075. https://doi.org/10.3389/fbioe.2023.1197075.

Vapniarsky, Natalia, Boaz Arzi, Jerry C. Hu, Jan A. Nolta, and Kyriacos A. Athanasiou. 2015. "Concise Review: Human Dermis as an Autologous Source of Stem Cells for Tissue Engineering and Regenerative Medicine." *Stem Cells Translational Medicine* 4 (10): 1187–98. https://doi.org/10.5966/sctm.2015-0084.

Verbridge, Scott S, Emily M Chandler, and Claudia Fischbach. 2010. "Tissue-Engineered Three-Dimensional Tumor Models to Study Tumor Angiogenesis." *Tissue Engineering Part A* 16 (7): 2147–57. https://doi.org/10.1089/ten.tea.2009.0668.

Wang, Mark M., Eugene Tu, Daniel E. Raymond, Joon Mo Yang, Haichuan Zhang, Norbert Hagen, Bob Dees, et al. 2005. "Microfluidic Sorting of Mammalian Cells by Optical Force Switching." *Nature Biotechnology* 23 (1): 83–87. https://doi.org/10.1038/nbt1050.

Wang, Xiaolin, Shuxun Chen, Marco Kong, Zuankai Wang, Kevin D Costa, Ronald A Li, and Dong Sun. 2011. "Enhanced Cell Sorting and Manipulation with Combined Optical Tweezer and Microfluidic Chip Technologies." *Lab Chip* 11 (21): 3656–62. https://doi.org/10.1039/C1LC20653B.

Wang, Yaping, Junmin Qian, Ting Liu, Weijun Xu, Na Zhao, and Aili Suo. 2017. "Electrospun PBLG/PLA Nanofiber Membrane for Constructing in Vitro 3D Model of Melanoma." *Materials Science and Engineering C* 76 (7): 313–18. https://doi.org/10.1016/j.msec.2017.03.098.

Wang, Zihan, Qinzhou Ye, Sheng Yu, and Behnam Akhavan. 2023. "Poly Ethylene Glycol (PEG)-Based Hydrogels for Drug Delivery in Cancer Therapy: A

Comprehensive Review." *Advanced Healthcare Materials* 12 (18): 2300105. https://doi.org/10.1002/adhm.202300105.

Weiswald, Louis Bastien, Dominique Bellet, and Virginie Dangles-Marie. 2015. "Spherical Cancer Models in Tumor Biology." *Neoplasia (United States)* 17 (1): 1–15. https://doi.org/10.1016/j.neo.2014.12.004.

Wilkinson, Eric P., and William M. Luxford. 2010. *Hypoglossal Facial Anastomosis*. *Otologic Surgery*. 3rd ed. Elsevier.

Willerth, Stephanie. 2017. "Chapter 2-Introduction to the Nervous System." In *Engineering Neural Tissue from Stem Cells*, 17–38. Elsevier.

Winner, Beate, and Jürgen Winkler. 2015. "Adult Neurogenesis in Neurodegenerative Diseases." *Cold Spring Harbor Perspectives in Biology* 7 (4): a021287. https://doi.org/10.1101/cshperspect.a021287.

Wlodkowic, D, J Skommer, and Z Darzynkiewicz. 2012. "Cytometry of Apoptosis. Historical Perspective and New Advances." *Experimental Oncology* 34 (3): 255–62.

Wojdyla, Michal, Saurabh Raj, and Dmitri Petrov. 2012. "Absorption Spectroscopy of Single Red Blood Cells in the Presence of Mechanical Deformations Induced by Optical Traps." *Journal of Biomedical Optics* 17 (9): 0970061. https://doi.org/10.1117/1.jbo.17.9.097006.

Wolswijk, Guus. 2000. "Oligodendrocyte Survival, Loss and Birth in Lesions of Chronic-Stage Multiple Sclerosis." *Brain* 123 (1): 105–15. https://doi.org/10.1093/brain/123.1.105.

World Health Organization (WHO). 2024. "Global Cancer Burden Growing, amidst Mounting Need for Services." World Health Organization Official Website. February 1, 2024. https://www.who.int/news/item/01-02-2024-global-cancer-burden-growing--amidst-mounting-need-for-services.

Worthington, Peter, Darrin J. Pochan, and Sigrid A. Langhans. 2015. "Peptide Hydrogels - Versatile Matrices for 3D Cell Culture in Cancer Medicine." *Frontiers in Oncology* 5 (4): 92. https://doi.org/10.3389/fonc.2015.00092.

Wu, Shaohua, Ranjie Xu, Bin Duan, and Peng Jiang. 2017. "Three-Dimensional Hyaluronic Acid Hydrogel-Based Models for in Vitro Human IPSC-Derived NPC Culture and Differentiation." *Journal of Materials Chemistry B* 5 (21): 3870–78. https://doi.org/10.1039/c7tb00721c.

Wu, Yenan, Haiwei Liang, Aiping Luo, Yong Li, Zhiqiang Liu, Xin Li, Wenxin Li, et al. 2023. "Gelatin-Based 3D Biomimetic Scaffolds Platform Potentiates Culture of Cancer Stem Cells in Esophageal Squamous Cell Carcinoma." *Biomaterials* 302 (11): 122323. https://doi.org/10.1016/j.biomaterials.2023.122323.

Wyllie, A H, and R G Morris. 1982. "Hormone-Induced Cell Death. Purification Ad Properties of Thymocytes Undergoing Apoptosis after Glucocorticoid Treatment." *The American Journal of Pathology* 109 (1): 78–87.

Xie, Renjian, Vaibhav Pal, Yanrong Yu, Xiaolu Lu, Mengwei Gao, Shijie Liang, Miao Huang, Weijie Peng, and Ibrahim T. Ozbolat. 2024. "A Comprehensive Review on 3D Tissue Models: Biofabrication Technologies and Preclinical Applications." *Biomaterials* 304 (1): 122408. https://doi.org/10.1016/j.biomaterials.2023.122408.

Xu, Kailei, K. Ganapathy, Thomas Andl, Zi Wang, John A. Copland, R. Chakrabarti, and Stephen J. Florczyk. 2019. "3D Porous Chitosan-Alginate Scaffold Stiffness Promotes Differential Responses in Prostate Cancer Cell Lines." *Biomaterials* 217 (10): 119311. https://doi.org/10.1016/j.biomaterials.2019.119311.

Yaman, Sena, Muge Anil-Inevi, Engin Ozcivici, and H. Cumhur Tekin. 2018. "Magnetic Force-Based Microfluidic Techniques for Cellular and Tissue Bioengineering." *Frontiers in Bioengineering and Biotechnology* 6 (12): 192. https://doi.org/10.3389/fbioe.2018.00192.

Yildiz, Nilufer. 2006. "Nerve Implants." In *Medical Textiles and Biomaterials for Healthcare*, 441–47. Woodhead Publishing.

Yong, Insung, Seung Won Oh, and Pilnam Kim. 2020. "Re-Engineered Cell-Derived Extracellular Matrix as a New Approach to Clarify the Role of Native ECM." In *Methods in Cell Biology*, 156 (1): 205–31. Academic Press Inc. https://doi.org/10.1016/bs.mcb.2019.12.007.

Yuen, Ryan K.C., Bhooma Thiruvahindrapuram, Daniele Merico, Susan Walker, Kristiina Tammimies, Ny Hoang, Christina Chrysler, et al. 2015. "Whole-Genome Sequencing of Quartet Families with Autism Spectrum Disorder." *Nature Medicine* 21 (2): 185–91. https://doi.org/10.1038/nm.3792.

Zarei-Kheirabadi, Masoumeh, Hoda Sadrosadat, Atiyeh Mohammadshirazi, Razieh Jaberi, Farzaneh Sorouri, Fahimeh Khayyatan, and Sahar Kiani. 2020. "Human Embryonic Stem Cell-Derived Neural Stem Cells Encapsulated in Hyaluronic Acid Promotes Regeneration in a Contusion Spinal Cord Injured Rat."

*International Journal of Biological Macromolecules* 148 (1): 1118–29. https://doi.org/10.1016/j.ijbiomac.2020.01.219.

Zborowski, Maciej, and Jeffrey J Chalmers. 2015. "Magnetophoresis: Fundamentals and Applications." *Wiley Encyclopedia of Electrical and Electronics Engineering* 1(1): 1–23. https://doi.org/10.1002/047134608X.W8236.

Zhang, Chengqian, Peng Zhao, Daofan Tang, Neng Xia, Xuechun Zhang, Jing Nie, Fu Gu, Huamin Zhou, and Jianzhong Fu. 2020. "Axial Magnetic Levitation: A High-Sensitive and Maneuverable Density-Based Analysis Device." *Sensors and Actuators, B: Chemical* 304 (1): 127362. https://doi.org/10.1016/j.snb.2019.127362.

Zhang, Lei, Yubin Hou, Zhiyuan Li, Xinmiao Ji, Ze Wang, Huizhen Wang, Xiaofei Tian, Fazhi Yu, Zhenye Yang, and Li Pi. 2017. "27 T Ultra-High Static Magnetic Field Changes Orientation and Morphology of Mitotic Spindles in Human Cells." Elife 6 (1): e22911. https://doi.org/10.7554/eLife.22911.

Zlotek-Zlotkiewicz, Ewa, Sylvain Monnier, Giovanni Cappello, Mael Le Berre, and Matthieu Piel. 2015. "Optical Volume and Mass Measurements Show That Mammalian Cells Swell During Mitosis." *The Journal of Cell Biology* 211 (4): 765–74. https://doi.org/10.1083/jcb.201505056.

# APPENDIX A

# PRINCIPLES OF MAGNETIC LEVITATION

Magnetic manipulation of cells can be achieved in the presence of three elements: a magnetic field, a magnetic field gradient and magnetic susceptibility difference between the cells and their medium. In magnetic levitation technique using negative magnetophoresis, cells migrate to the lower magnetic field regions. During this process, the cells are exposed to resultant of 3 forces ($F_{NET}$) which are magnetic ($F_M$), buoyancy ($F_G$) and drag force ($F_D$) till the cells come to an equilibrium point (Equation 1). Because of the low Reynolds number of the system the inertial force ($F_i$) can be neglected. Another force to be neglected is the the Brownian force ($F_B$) because it only has an effect on the motion of the small particles in nanometer scale (approx. ≤ 10 nm). Cells stop at some point where the magnetic and buoyancy forces come to an equilibrium state, where the net force acting on every single cell ($F_{NET}$) becomes zero and cells are positioned at a stable point and become levitated (Tasoglu et al. 2015). If:

$$\vec{F}_{NET} = \vec{F}_M + \vec{F}_G + \vec{F}_D$$

and

$$ma = \vec{F}_M + \vec{F}_G + \vec{F}_D;$$

$$m\frac{\overrightarrow{dv_p}}{dt} = \vec{F}_M + \vec{F}_G + \vec{F}_D \qquad (1)$$

$F_M$ acting on a particle depends on; B: magnetic flux density (Tesla, T), ∇: del operator, $\vec{m}$ : the magnetic dipole values (Equation 2). B decreases as it moves away from the surface of the magnet. From here, the magnetic dipole produced in a low magnetic field in a paramagnetic salt solution or in a ferrofluid can be reached (Equation 3).

$$\vec{F}_M = (\overrightarrow{m}.\ \nabla)\ \vec{B} \qquad (2)$$

and

$$\overrightarrow{m} = \frac{V.\Delta_\chi}{\mu_o}\ \vec{B} \qquad (3)$$

In this equation; V: volume of the particle can be arranged as; $\mu_o$: permeability of the gap ($1.2566 \times 10^{-6}$ kg m $A^{-2}$ $s^{-2}$), Δχ: magnetic susceptibility difference ($\mathcal{X}_\rho - \mathcal{X}_m$) between the particle and the surrounding medium and the $F_M$ value can be expressed (Equation 4).

$$\vec{\mathrm{F}}_\mathrm{M} = \frac{\mathrm{V}.(\mathcal{X}_\rho - \mathcal{X}_\mathrm{m})}{\mu_\mathrm{o}}\ \left(\vec{\mathrm{B}}.\nabla\right)\vec{\mathrm{B}} \qquad (4)$$

When $\left(\vec{B}.\nabla\right)\vec{B}$ expanded in the Cartesian coordinate system:

$$\left(\vec{B}.\ \nabla\right)\overrightarrow{B} = \begin{pmatrix} B_x\ \frac{\partial B_X}{\partial_x} + B_y\ \frac{\partial B_X}{\partial_x} + B_z\ \frac{\partial B_X}{\partial_x} \\ B_x\ \frac{\partial B_Y}{\partial_x} + B_y\ \frac{\partial B_Y}{\partial_x} + B_z\ \frac{\partial B_Y}{\partial_x} \\ B_x\ \frac{\partial B_Z}{\partial_x} + B_y\ \frac{\partial B_Z}{\partial_x} + B_z\ \frac{\partial B_Z}{\partial_x} \end{pmatrix} \qquad (5)$$

magnetic flux values can be reached in three dimensions. Another force acting on a spherical particle under the specified conditions, the liquid drag force $F_D$, will vary depending on R (diameter of the particle), η(dynamic viscosity), $f_d$ (drag coefficient) and $\nu_p$ (velocity of the particle) (Equation 6).

$$\overrightarrow{F_D} = 6\pi R\eta f_d(v_p) \qquad (6)$$

The other force, $F_G$, acting on the particle can be calculated depending on V: volume of the particle, Δρ: volumetric density difference between the particle and the surrounding medium ($\rho_p$-$\rho_m$), g: gravitational acceleration (9.8 m·s$^{-2}$) (Equation 7).

$$\overrightarrow{F_G} = V\Delta_\rho g \qquad (7)$$

In this case, the force acting on the particle until it reaches the equilibrium point is regulated (Equation 8), and since the particle's velocity will be zero when the equilibrium point is reached ($F_D = 0$), $F_{NET}$ can be regulated according to the equilibrium state of the spherical particle (Equation 9).

$$\vec{F}_{NET} = \frac{V.(\chi_\rho - \chi_m)}{\mu_o}\left(\vec{B}.\nabla\right)\vec{B} + 6\pi R\eta f_d\left(v_p\right) + V.(\rho_P - \rho_M)g \qquad (8)$$

and

$$\vec{F}_{NET} = \frac{V.(\chi_\rho - \chi_m)}{\mu_o}\left(\vec{B}.\nabla\right)\vec{B} + V.(\rho_P - \rho_M)g \qquad (9)$$

When a magnetic field is applied to diamagnetic particles such as cells, a magnetic dipole is formed that is aligned antiparallel to the magnetic field. Therefore, a magnetic force is generated towards the area where the magnetic field is minimum. This magnetic dipole varies according to the magnetic susceptibility value of the particle and the surrounding medium.

In this doctoral thesis, by utilizing the physical events explained in detail above, the magnetic force acting in the opposite direction to gravity increased the magnetic susceptibility value ($\chi_m$) of the culture medium and levitation of the cells was provided with microcapillary based magnetic levitation system depending on their volumetric mass densities (Figure 65). The magnetic susceptibility value of the medium surrounding the cells was obtained by adding different concentrations of $Gd^{3+}$ (Gadavist) to the culture medium.

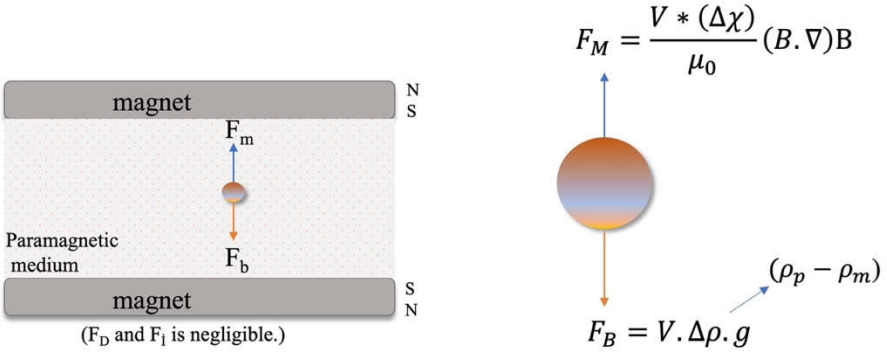


Figure 65. Schematic representation of the forces act on each individual cell within microcapillary based magnetic levitation system.

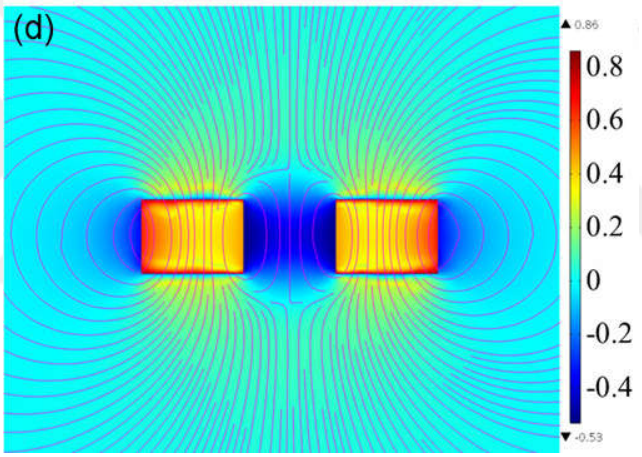


Figure 66. Simulation of z component ($B_Z$) of magnetic flux density around the ring magnet via finite element methodology. Total magnetic induction ($B_Z + B_X$) is presented as streamlines (Source: Anil-Inevi et al. 2021) .

The ring magnet-based levitation system is composed of a single, ring shaped magnet with a with a hole in the center, a culture tube and an apparatus made from photoactive resin to fix the culture tube within the hole in the magnet. In this system, magnetic and buoyancy forces balance each other and levitation of the cells in the culture tube is provided by the difference in the magnetic susceptibility difference ($\chi_\rho - \chi_m$) between the cells ($\chi_\rho$)and the paramagnetic culture medium($\chi_m$)(Equation 9). The medium is magnetized through the use of Gadolinium ($Gd^{3+}$) paramagnetic agent. The

value of the magnetic susceptibility of paramagnetic agent is significantly higher than that of diamagnetic cells, so $\chi_p$can be neglected. The magnetic forces that act on the cells in the x-direction make the cells move to the center of the hole in the center of the magnet and form cellular aggregates (Figure 66).

# VITA

## İLAYDA ÖZKAN

### Education:

**Ph.D.,** Bioengineering (GPA: 3.75/4.00) | Izmir Institute of Technology | İzmir –Turkey, 2025, Thesis: "Magnetic Levitation of Cells for Tissue Engineering and Diagnostic Applications"
**BSc,** Bioengineering (GPA: 3.04/4.00) | Ege University | İzmir –Turkey, 2016

### Professional & Research Experience and Scholarship:

2018 – Present: Research Assistant in Bioengineering, Izmir Institute of Technology
2024 TUBITAK, "2214/A International Research Fellowship Programme for PhD Students "

### List of selected publications:

Tarim, E. Alperay, Muge Anil Inevi, Ilayda Ozkan, Seren Kecili, Eyup Bilgi, M. Semih Baslar, Engin Ozcivici, Ceyda Oksel Karakus, and H. Cumhur Tekin. 2023. "Microfluidic-Based Technologies for Diagnosis, Prevention, and Treatment of COVID-19: Recent Advances and Future Directions." *Biomedical Microdevices* 25 (2): 10. https://doi.org/10.1007/s10544-023-00649-z.